HETEROGENEOUS INTEGRATION OF MICROWAVE AND MILLIMETER-WAVE DIODES ON SILICON AND FLEX SUBSTRATES

By

Amanpreet Kaur

A DISSERTATION

Submitted to
Michigan State University
in partial fulfillment of the requirements
for the degree of

Electrical Engineering - Doctor of Philosophy

2016

ABSTRACT

HETEROGENEOUS INTEGRATION OF MICROWAVE AND MILLIMETER-WAVE DIODES ON SILICON AND FLEX SUBSTRATES

By

Amanpreet Kaur

Millimeter waves (MMW) are electromagnetic (EM) signal between microwave and far infrared, i.e., frequencies between 30GHz (10mm wavelength) and 300 GHz (1mm wavelength). It has applications in future high-speed communications, automotive collision avoidance and navigation, homeland security, and high speed chip interconnects. To make commercial MMW integrated circuits a reality, low cost approaches for wafer level integration of all components (actives, passives, back end CMOS) is critically needed. The current state of art MMW circuits utilizes expensive compound semiconductors (CS) for active devices. To meet the future need, there is growing interest in heterogeneous integration of CS and other non-Si materials (novel materials) on large area, low-cost substrates such as Si, glass and flexible substrates. Integration compatibility with flexible substrate is of special interest for applications such as wearable medical and communication devices. Diodes are of particular interest for high-frequency applications such as rectification, frequency mixing and multiplication. So, there is a need for heterogeneous integration compatible diodes for MMW circuits. Key focus of this thesis is to demonstrate carefully engineered high frequency diodes that allow higher levels of integration on existing silicon ICs and on other lower cost materials such as flex polymer substrates. This work focuses on three types of diodes: Graphene based diodes and Metal-Insulator-Metal (MIM) tunneling diode for low power applications and excimer laser synthesized Silicon Carbide/ Silicon (SiC/Si) heterojunction diodes for high power devices.

Graphene is a good candidate for flexible GHz circuits as it possesses excellent electronic and mechanical properties. In its natural state, graphene does not have a band gap which limits its use in the design of diodes. In this thesis, graphene based diodes have been demonstrated by first opening its band gap through chemical modification. The modified graphene or reduced graphene oxide (r-GO) based diodes are fabricated on flexible substrates. The r-GO diodes show strong non-linearity with current in the micro-Amp range. This diodes also work well as microwave rectifiers up to 22 GHz as well as frequency multiplier and mixer over a wide frequency range. In parallel, a non-semiconductor alternative technique, i.e., MIM diodes, is also demonstrated for low power GHz circuits on flex substrates. Their high speed and frequency response in comparison to III-V Schottky diodes and compatibility with variety of substrates (flexible substrate, SiO_2, on top of existing CMOS circuitry) makes them a good choice for MMW integrated circuits. Two different types of insulators (TiO_2 and NiO) with different dielectric constants are used here. The diodes were also characterized for rectification, multiplication and mixing circuit applications.

Diodes for high power MMW applications require wide band gap materials such as Silicon Carbide (SiC) or Gallium Nitride (GaN). Integration of these materials with Si using conventional techniques is very challenging. This thesis presents a new technique for local growth of SiC on Si using high power KrF excimer laser under ambient air conditions. The fabricated diodes show high breakdown voltage (>200 V), high rectification ratio and low leakage current densities. The diode also works efficiently as high power microwave rectifier and as frequency doubler.

To my husband Vikram Saini, loving son Viraaj
and
my Parents

ACKNOWLEDGEMENTS

I am grateful to all the people who supported me during my Ph.D. program. Firstly, I would like to express my special thanks to my advisor, Dr. Premjeet Chahal. It was a great experience for me to work in his Lab at Michigan State University. As the academic advisor, he has given me helpful suggestions and a great guidance during my graduate study. Also I would like to thank my committee members, Dr. Lawrence Drzal, Dr. Virgina Ayres and Dr. Timothy P. Hogan for their valuable suggestions and feedback on my work.

I appreciate all the support from my colleagues. Dr. Yang and Dr. Park who has contributed to my Ph.D. work. I would also express my thanks to Tesla group members: Jennifer Byford, Dr. J.Myers, Ifwat Ghazali and Saran Karuppaswami.

I am grateful to Dr. Hogan for providing me access to his lab for fabrication of SiC device. I would also like to thank Dr. Per Askeland from composite center for sharing his expertise on material science and helping me in material characterization.

Finally, special thanks go to my lovely family for their unconditional love and support throughout my years of Ph.D. Especially, my husband Vikram Saini who has always encouraged and supported me with his endless love and helped me to successfully complete my study. Also thanks to my parents, and my loving son Viraaj. Thank you.

TABLE OF CONTENTS

LIST OF TABLES

LIST OF FIGURES

CHAPTER 1: INTRODUCTION

1.1 Motivation

The rapid increase in the number of wireless devices worldwide and the growing demand for high data rates is increasing the pressure on mobile industry and the research community to come up with innovative solutions to meet this challenge. Recently, Cisco forecasted that there will be 1.5 mobile devices per capita by 2020 and the demand for bandwidth is growing exponentially [1]. Moving up to Millimeter wave (MMW) range (30-300 GHz) is a promising solution to meet the demand of large bandwidth, as the available bandwidth scales with frequency. Recent allocation of 7GHz bandwidth of un-channelized spectrum by FCC (Federal Communication commission) for license-free operation between 57-64 GHz (also referred as 60 GHz band) is a big driver for MMW communications. The 60 GHz band offers several advantages such as high data rate, realization of integrated antennas due to smaller wavelengths, and less co-channel interference for secure wireless communication [2-5]. Millimeter wave technology has many other interesting applications such as long (76–77 GHz) and short (77–81 GHz) range automotive radars, medical treatments, high speed chip interconnects and wireless backhaul [6-8]. Millimeter wave signals can penetrate many materials including building materials, clothing, and are robust to all weather conditions (day and night, low-visibly condition such as fog, haze and cloud) and thus making it attractive for imaging applications such as all-weather driving, airplane landing [9].

The state of arts MMW circuits are based on expensive compound semiconductor (CS) materials as they provide higher saturated electron velocity, high mobility and high breakdown in comparison to silicon. Until now space and military applications have been the major driving force behind the advancement in MMW integrated circuit technology. However, to make MMW circuits a commercial reality, integration of MMW device technology with silicon is necessary. For the design of any MMW system, integration of low frequency circuits, mixed signal and digital circuits are needed on a common platform. Silicon based CMOS technology is the workhorse of most of low frequency and mixed signal circuits. Furthermore, with the growth of wearable low cost electronics, there is a growing trend towards integration of these technologies on a low-cost flexible (polymer, thin glass, thin silicon, papers, etc.) substrates. Recent advances in the area of nanomaterials and devices provide required electrical and mechanical properties such as high mobility, high thermal conductivity, high mechanical flexibility and can easily be attained with nanomaterials. Thus, this opens up opportunities of directly fabricating electronic devices on flexible substrates. Heterogeneous integration of different materials and devices on a common substrate will enable designers to mix and match technologies to design novel mixed signal and high frequency circuits that cannot be attained using a single material or device technology. However, there are many challenges that need to be solved to make such a technology realizable. To better understand the challenges, sections below provides a brief background on the applications and needs of microwave and millimeter wave circuit technologies.

1.2 Application of Millimeter waves

MMW are electromagnetic (EM) signal between microwave and far infrared frequencies, i.e. between 30GHz (10mm wavelength) and 300 GHz (1mm wavelength). They are longer than terahertz and infrared signal, but shorter than radio waves (Figure 1.1). Historically, millimeter-wave bands have been used exclusively for government and non-consumer products due to the FCC regulations and high cost barrier of CS technologies like Gallium Arsenide (GaAs) and Indium Phosphide (InP) that could operate at such high frequencies [2,3]. However, the maturation of silicon technologies and introduction of novel materials has created the possibility for volume production for low cost consumer applications. Another interesting aspect of mm-wave systems is the small antenna size (small wavelength) thus allowing integration of multiple antenna elements on a chip.

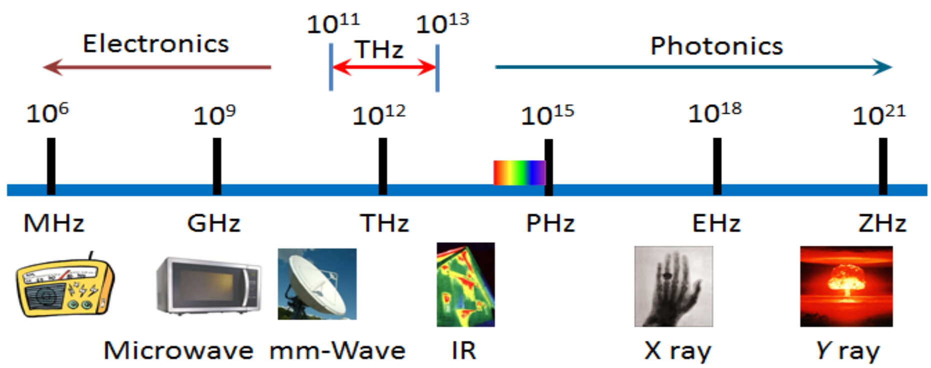

Figure 1.1 Electromagnetic spectrum showing MMW

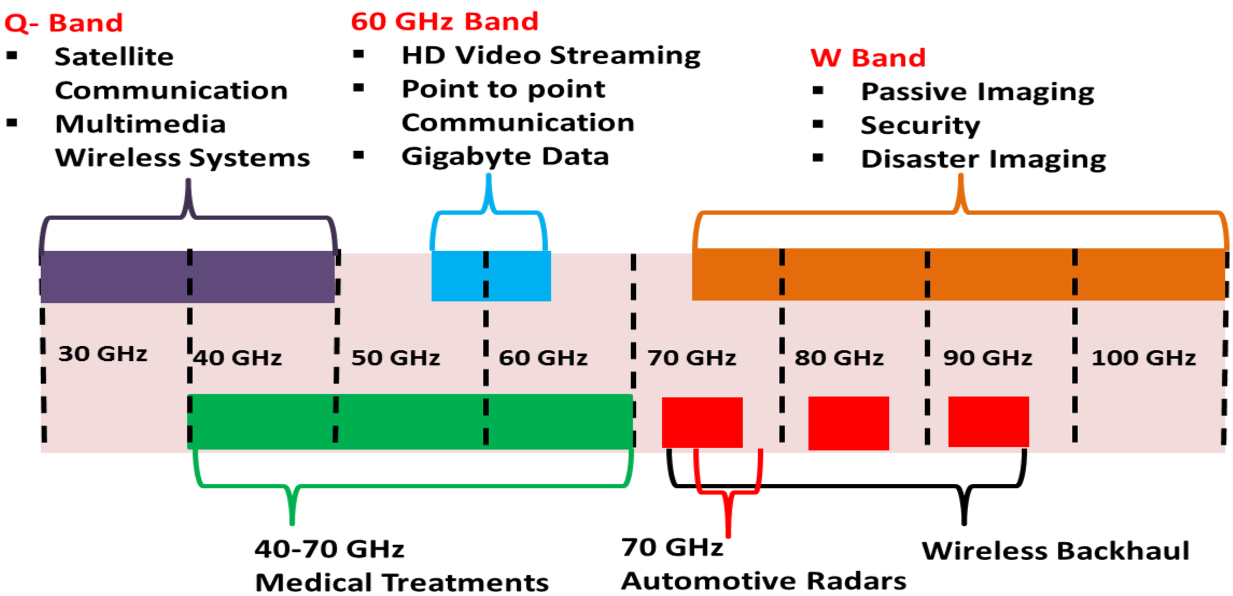

Figure 1.2 Applications in MMW spectrum

However, the maturation of silicon technologies and introduction of novel materials has created the possibility for volume production for low cost consumer applications. Another interesting aspect of mm-wave systems is the small antenna size (small wavelength) thus allowing integration of multiple antenna elements on a chip. Similarly, other passive elements such as resistors, capacitors and inductors occupy smaller footprint. Thus, making the circuits smaller and requiring less material. The following sections will introduce some of the applications of MMW applications, as shown in Figure. 1.2.

1.2.1 60-GHz Band for Multi-Gigabit Wireless Communications

The rapid increase in high- definition (HD) digital multimedia content along with the higher data storage capabilities on mobile devices drives the need for wireless connection with higher data rates (Gbps connectivity). This is not feasible with the existing communication standards. Moving to higher frequencies with larger bandwidth allocations can conquer these limitations and also serve the rapidly increasing number of internet and mobile users [4]. To solve this problem, governments worldwide have made spectral allocations in MMW spectrum to support unlicensed multi-gigabit wireless communications (Figure.1.3).

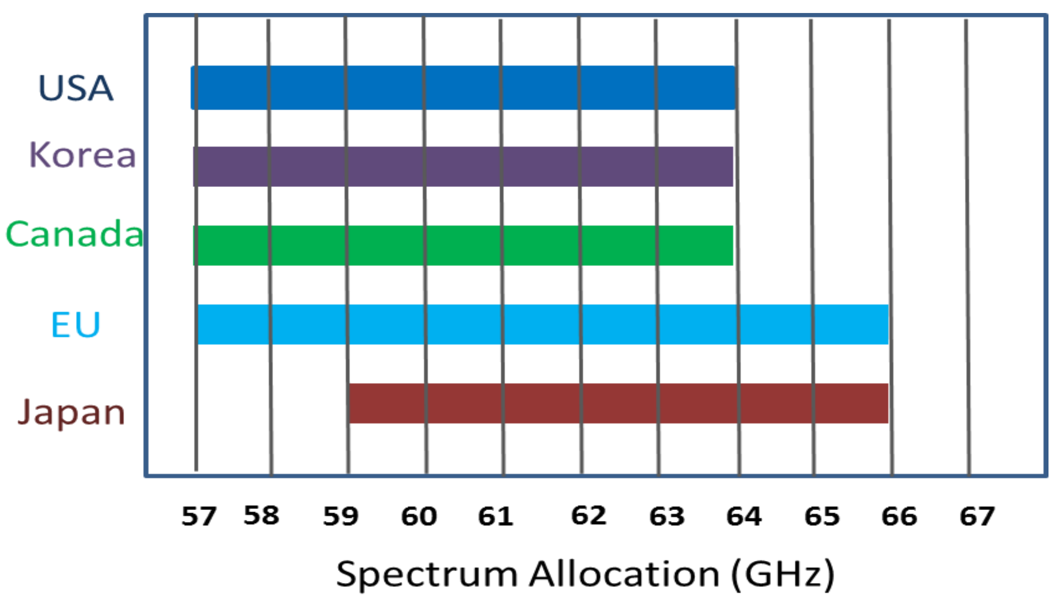

Figure 1.3 Worldwide spectrum allocations in 60 GHz band

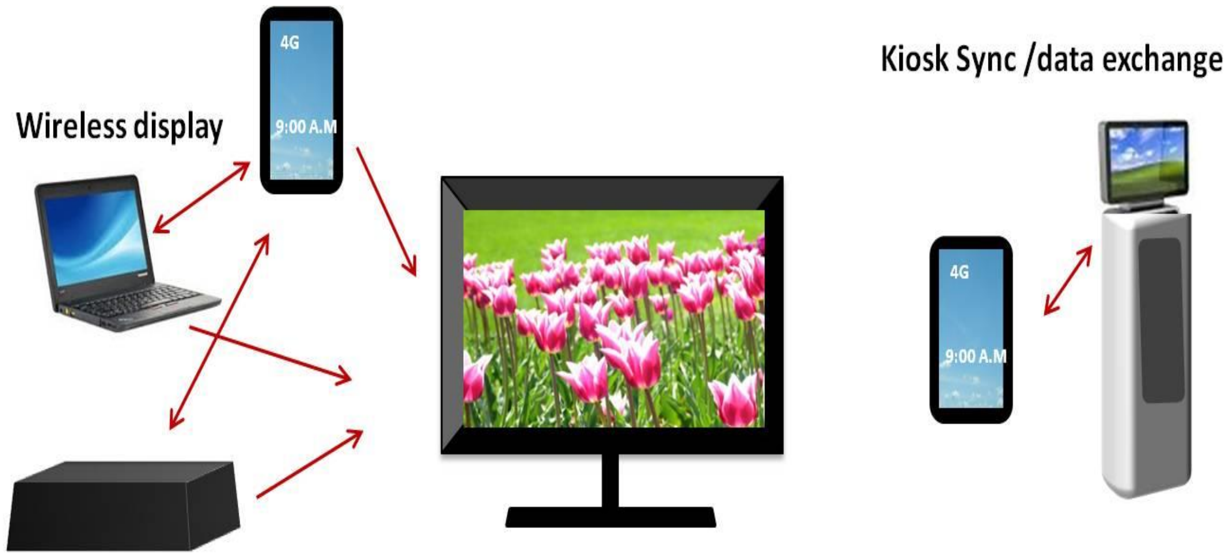

Figure 1.4 Example of Gbps connectivity in 60 GHz band

The 60-GHz band has number of characteristics that make it attractive for short-range wireless communications [5]. The 60-GHz band enables wireless HD multimedia streaming, multi Gbps connectivity, high speed Wireless Personal Area Network (WPAN) and Wireless Sensor Network (WSN). It has the ability to cut cost for data centers by replacing the existing interconnects by MMW communication links. There are three types of interconnects in data centers: shelf-to-shelf, chip-to-chip and rack-to-rack. At present, data centers employ wired connections for all types of communication. The biggest problem is shelf-to-shelf or rack-to-rack communication which is implemented using electrical copper connections. There is need to switch to other technologies as the signal loss in metal wire increases with increasing frequency. The 60 GHz communication is a good alternative and offers lower cost, lower power consumption and greater flexibility.

The 60 GHz band will also allow future application like fifth generation (5G) broadband cellular communication, wireless backhaul connections, and in-vehicular communications. Figure.1.4 shows some of the application of Gbps connectivity in 60 GHz band such as point-to-point connection between a multimedia terminal (kiosk) and a mobile phone, connection between a HD television and a HD video source, rapid download (multi Gbps) of huge video files.

1.2.2 High speed On-chip wireless Interconnects

The integrated antennas used to link individual 60 GHz devices may also be adapted to link different components on a single chip or within a package. There is great interest in on-chip wireless interconnects using highly integrated antennas as the bandwidth and conductivity of on-chip copper interconnects is an important issue. The bandwidth of copper interconnects decreases at higher frequencies due to the higher resistance caused by skin effect losses. An on-chip or in-package antenna can help reduce the overall length of metal wire interconnects and serve future applications requiring very high data rates within a chip, package or a board.

1.2.3 Automotive RADAR

Another important application of MMW is in commercial automotive radars [6]. The 77-GHz band allows long- and mid-range functionality, enabling implementation of features such as adaptive cruise control, front- and rear-object detection for collision avoidance, headway alert, and blind-spot monitoring (Figure 1.5). So far the automotive radar systems have been adopted largely in high-end car market. However, with availability of the low cost MMW systems, they will soon be affordable for the mid-range automobile market and help provide safety across the consumer spectrum. Other vehicular applications of MMW include vehicle-to-vehicle communication and vehicle-to-infrastructure communication. Millimeter wave spectrum is especially attractive for vehicle-to-vehicle communication for the exchange of traffic information and for use in collision avoidance systems due to its inability to interfere with other vehicular networks.

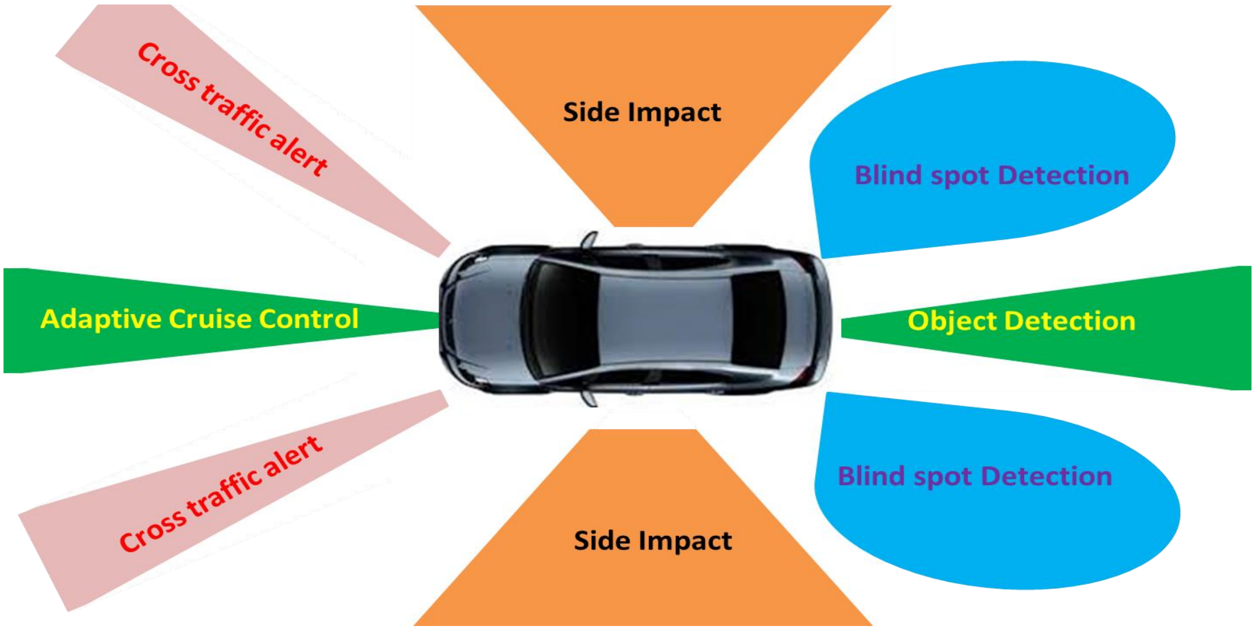

Figure 1.5 Automotive RADAR system for commercial vehicles.

1.2.4 Imaging

A heated object will emit black body radiation that includes optical, infrared and millimeter wave frequencies. Most optically opaque materials, such as cardboard and clothes are transparent in the MMW frequency region. Also, in comparison to optical spectrum, MMW have low atmospheric absorption and thus well suited for imaging applications such as homeland security, law enforcement, and body detection in low or zero-visibility [9]. In the MMW regime, the atmospheric propagation windows are at 35, 94, 140, and 220 GHz, with relatively modest attenuation in both clear and foggy conditions. Even though the blackbody radiation is higher in IR and visible frequency ranges, the strongest signal under fog conditions is maximum for MMW signal which is a big advantage for MMW imaging [10]. Also, the wavelength at MMW is small to achieve good imaging resolution.

1.2.5 Medical Treatments

Low-level MMW energy has a number of medical benefits. Potential areas of application include treatment of cardiovascular disease, tissue re-generation stimulus, and mitigation of chronic pain such as arthritis [7,8]. Typical treatments used at hospitals use large and expensive machines. However, with the ability of low cost technology to generate MMW energy, inexpensive in-home treatment options can be made feasible in the near future. Furthermore, MMW based medical imaging is gaining significant attention as some of the cancerous tissues can readily be identified using MMW images as compared to optical images. In comparison to X-rays, MMW is non-ionizing and thus can be used for imaging without any adverse effects.

1.3 Research Overview

All of the above discussed application requires solid state MMW circuits, especially the transceiver (transmit and receive) circuits. MMW systems and circuits are composed of both active and passive components. Some of the common active components are synthesizers, detectors, mixers, amplifiers, multipliers and oscillators. The commonly used passive components are interconnects, waveguides, filters, couplers and antennas. In addition, all complex high frequency circuits required complementary metal oxide semiconductor (CMOS) circuitry for providing data conditioning and signal processing functions. So, there is need for wafer level integration of both MMW active and passive components along with backend CMOS circuitry (Figure 1.6). This research work demonstrates various approaches to achieve active and passive element that are compatible with large-area and low-temperature fabrication. In particular, the focus of this research is on two terminal high frequency actives, diodes, which can readily be integrated on low cost large area substrate such as polymer (flexible) and Si. The ultimate goal is envisioned to be fully integrated systems with Antennas, RF, and Digital components on a common substrate (Figure 1.6). At higher frequencies the availability of suitable materials with low loss and low cost is limited, and most of these materials are incompatible with direct deposition on Si (CMOS technology) and low-cost flexible substrates.

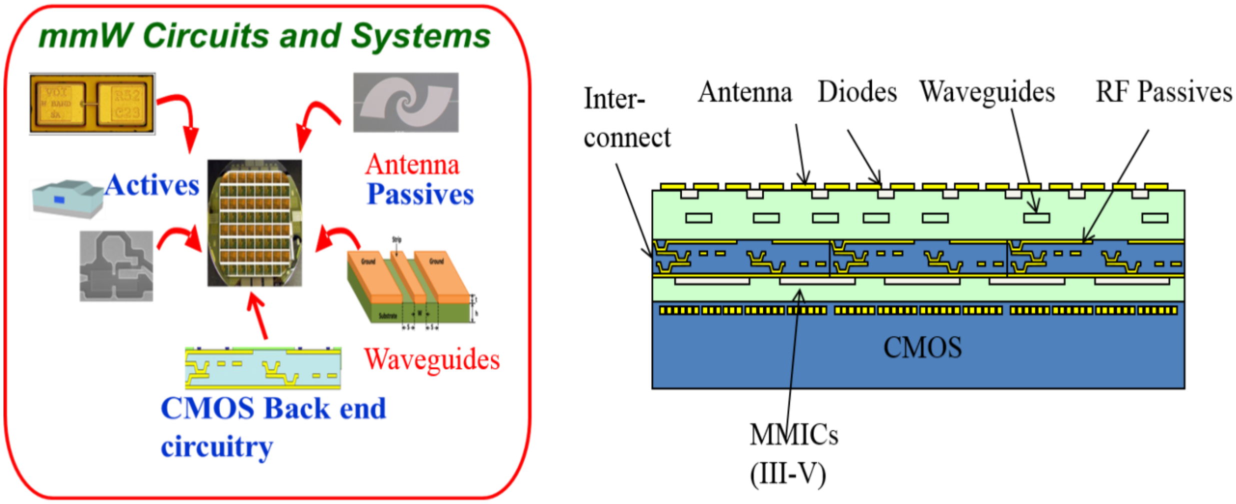

Figure 1.6 Research goal is to demonstrate fabrication of MMW active and passive elements that can be integrated on a common substrate

The success of these materials is due to their superior electrical properties compared to silicon. Recently, extensive work has been done to improve SiGe (silicon germanium) technology and Si CMOS technology in order to potentially improve their performance at MMW frequencies and to enable mass production for commercial applications. However, significant progress needs to be made to make this into reality. Based on the needs and challenges it is clear that the future of MMW electronics depends not on replacing Si, but rather on heterogeneous integration of CS with Si [14, 15]. Many high speed applications require assembly of passive and active components, where most of the area (> 90%) is covered by large passive components such as antennas, waveguides, matching circuitries and filters. For example, a MMW/THz imaging system is made of large array (100×100 elements) of GaAs diode (detectors) coupled with antenna elements (Figure 1.7). If the whole circuit (active + passive+ CMOS) is built on CS wafer technology, the cost will be extremely high. Thus there is need to find active devices (diodes) that can be easily integrated with different material techniques such as Si CMOS, flex or plastic. Implementation of carefully engineered diodes in thin film electronics has the potential to allow higher levels of integration. The goal of this work is to potentially reduce cost, size, and improve the performance for applications associated.

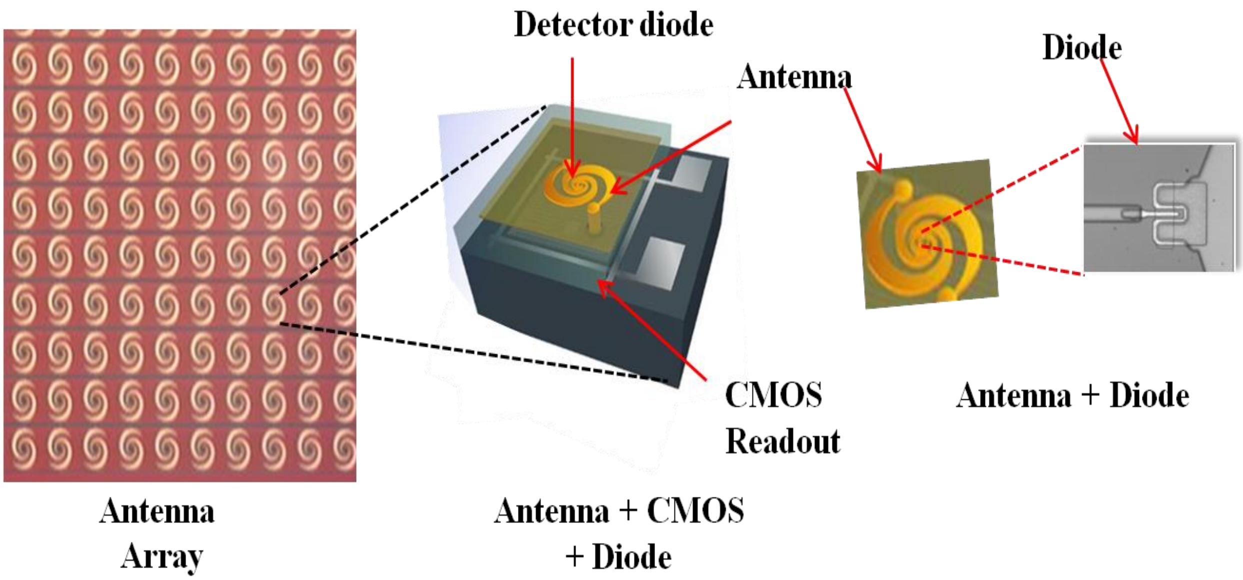

Figure 1.7 Schematic image of a Schottky diode based MMW/THz imaging arrays showing the area occupied by diode in comparison to passive devices (antenna)

MMW applications require both high power and low power devices. For example, low power flexible GHz circuits are required for the future wearable communication and health monitoring system and high power microwave/MMW circuits are needed for base station transceiver systems, frequency synthesizers, and automotive collision avoidance. The goal of this thesis is to investigate new heterogeneous compatible diodes for both low power flexible GHz circuits and affordable high power circuits. This work focus on three major types of diodes: Reduced oxide graphene based diodes, Metal-Insulator-Metal (MIM) tunneling diode for low power flexible GHz circuits and excimer laser synthesized SiC/Si heterojunction diodes for high power microwave/MMW circuits, see outline in Figure 1.8.

For low power MW circuits on flex, novel materials like carbon nanonotubes (CNTs) and graphene are of great interest and can surpass the traditional CS in terms of high frequency performance. These materials have excellent properties such as high mobility, high thermal conductivity, high mechanical flexibility and can readily be integrated on a host of substrates such as glass, Si, quartz, flexible/polymer [16-17]. The ease of integration is of special interest for flexible GHz electronics due to emerging applications in wearable communication devices, wireless sensors, health monitoring, and large area radar systems for remote sensing and security [18, 19]. MIM technology is also of great interest for low power flexible GHz circuits as they are ultra-fast, compatible with many substrates and can be processed at low-temperatures. They provide a non-semiconductor solution and therefore not limited by band conduction process [20, 21]. In this thesis graphene based diodes and Metal-Insulator-Metal tunneling diodes are investigated for low power diodes for flexible GHz circuits.

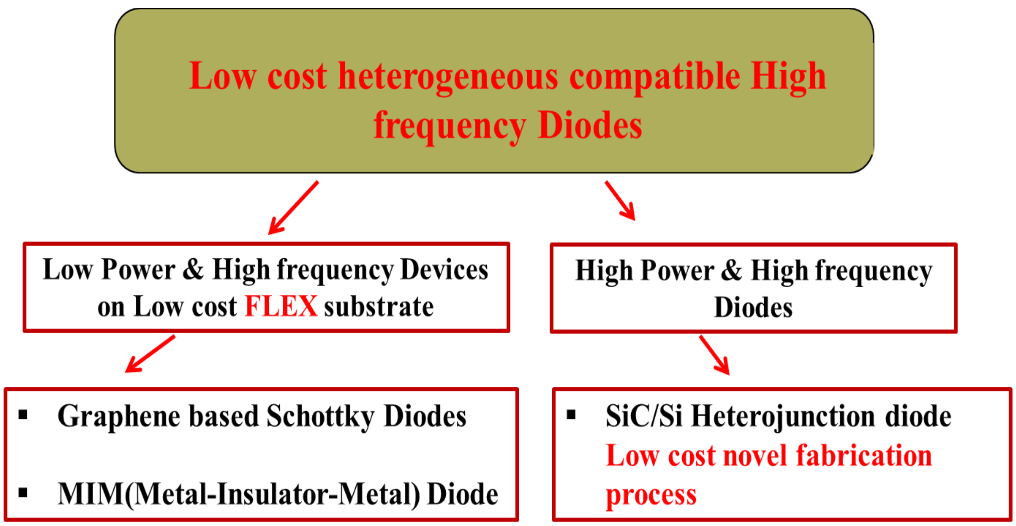

Figure 1.8 Research flow of the thesis

However, there are many applications that require high power microwave devices. Operation at frequencies up to 100 GHz with high RF output power requires semiconductor materials with high electron velocity, high electric field strength and high thermal conductivity, such as GaN and SiC [13, 22, 23]. Integration of these materials with Si is very important for commercial millimeter-wave applications in order design complex mixed signal circuits which includes digital, analog and RF circuits. However, integrating these materials with Si using traditional or conventional techniques is very challenging. Heterogeneous integration of CS with silicon has been explored in past decades but its main practical implementation today is through the use of multi-chip modules and epitaxy on Si. The performances of these multi-chip modules have been limited by parasitic effects between chips and by device variability issues. However, the most challenging part for direct epitaxy is thermal expansion coefficient mismatch and lattice mismatch between Si and the epitaxy material. So, there is a need to develop new technique for heterogeneous integration of high power material (CS) with silicon or Si CMOS substrates. The objective here is investigating a process to synthesize high power microwave diode, in particular SiC/Si diodes, to enable mass production of low cost, high power devices for commercial millimeter-wave applications. In this thesis, a novel process is developed and demonstrated to selectively grow SiC on Si wafer using high power KrF excimer laser.

1.4 Microwave and MMW Diodes for Low Power GHz circuits on Flexible Substrates

For future mobile communications, low power devices are required for battery powered mobile devices for large bandwidth data transfer (multi Gbps, e.g., video files). For applications using Wireless Sensor Network (WSN) for surveillance and health monitoring [18, 24] self-powered sensors (either use batteries or harvest energy from the environment) are required and their lifetime depends on the circuit's power consumption, which has to be very low. Besides low power and high data rate, a third requirement is ultra-low fabrication or manufacturing costs. The use of polymer substrate allows low power consumption, very high data rate, and low cost circuits. The advantages of using flexible material for high frequency circuits are light weight and large area process compatibility. This provides a low-cost avenue to fabrication of wearable electronics. Also, the demand for flexible and wearable wireless systems is growing exponentially. Therefore, there is need to investigate new semiconductor device technologies for next generation flexible GHz electronics.

1.4.1 Background

Microwave circuits on flexible substrates have applications in Radio frequency identification systems (RFID), personal Wi-Fi devices, wearable radios, medical equipments, and compact hand-held systems. Flexible electronics have potential advantages over conventional system as they enable roll to roll fabrication, low temperature processing, light weight and large area processing [25-27]. While fabrication of passive components such as resistors, capacitors, inductors, antennas on flexible substrates is a matured technology; however, the incorporation of active elements such as diodes and transistors onto flexible substrate is still a major challenge [28-30]. As discussed earlier, many applications require assembly of passive and active components. In most circuit designs, most of the area is occupied by passive components (Fig. 1.7) which need not be fabricated on a high quality semiconducting wafer. Thus, it is advantageous to use low cost plastic substrates for these applications.

Over the last decade organic materials have been studied for flexible circuits due to their mechanical resilience [27]. Flexible organic field effect transistors (FETs) and diodes with extreme bending stability have been presented; however, their low charge mobility limits their ultimate operating frequency to kilohertz or megahertz range [31, 32]. For flexible GHz active devices, semiconducting materials with high electron mobility and mechanical flexibility are required**.** The direct deposition of semiconductors on flexible substrate requires low temperature, resulting in amorphous or polycrystalline films with higher concentration of grain boundaries and defects. This degrades the transport properties of thin film transistors and ultimately its high frequency performance [30]. Non thermal approaches of achieving high mobility semiconductor on flex substrate has also been explored in the past; this includes micro/nanoscale semiconducting structures such as nanowires, ribbons, disks and platelets. These materials can be solution processed or dry transferred onto plastic substrates. Recently, both Si and GaAs have been transferred to create thin-film transistors (TFTs) on plastics [33-53]. III−V nanowires can reach the gigahertz range operation [36]. However, these 1D semiconducting nanostructures face challenge to achieve low resistance drain and source contacts without performing a high temperature annealing and also the challenge of achieving good quality gate dielectrics is there.

2D materials have attracted substantial interest for flexible electronics. Graphene in particular offers the offer excellent electronic properties needed for high frequency electronics and can be readily be integrated on flex substrates or host of other substrates. Another technology of interest is MIM, due to its high speed and frequency response and compatibility with flexible substrates. The properties, advantages, challenges and approach to counter those challenges for graphene based diodes and MIM tunneling diodes are discussed in the upcoming sections.

1.4.2 Graphene based Microwave circuits on flexible substrate.

Novel materials like carbon nanonotubes (CNTs) and graphene are good candidates for low power flexible GHz circuits. Both CNT and graphene have high current carrying capacity, and high thermal conductivity. The highest carrier mobility obtained from graphene ranges from 10000 $cm^2V^{-1}s^{-1}$ on SiO_2 substrate to 200000 $cm^2V^{-1}s^{-1}$ in suspended structures [17]. Meanwhile, CNT based transistors show hole mobility up to 790000 $cm^2V^{-1}s^{-1}$ at room temperature [16]. In addition, both materials show excellent mechanical properties such as high tensile strength and high young modulus as required for the fabrication of large area flexible circuits [37]. These properties suggest that carbon based nano-materials are excellent candidates for devices such as diodes and transistors. However, high impedance of a single CNT device makes it very difficult to impedance match it to a lower impedance (e.g., 50 Ω) external circuitry. High impedance is due to large contact resistance between a 1-D CNT and a 3-D metal electrode. Large contact resistance provides poor RF performance due to large impedance mismatch and large signal drop. In contrast, graphene has the potential to provide better impedance matching in comparison to CNT due to its larger scale and thus preferred for high frequency applications. Over the last decade, many researchers have demonstrated graphene based RF circuits/systems.

The initial work is based on transistors made using exfoliated graphene on SiO_2 /Si wafer using SiO_2 as a dielectric and the doped silicon substrate acting as the back-gate. Such devices suffer from unacceptably large parasitic capacitances from the substrate limiting the cut-off frequency (f_t). In addition, back gated transistors cannot be integrated with other components as practical graphene transistors need a top-gate. Recently, there is some work reported on top-gated graphene transistors with high-frequency characteristics for different gate lengths [38]. It was found that the cut-off frequency was inversely proportional to the square of the gate length. Different gate dielectric such as Al_2O_3 and HfO_2 has also been investigated for high frequency Field effect transistors (FETs) as the frequency response of initial graphene devices is limited by degradation in electronic properties due to its interaction with the top oxide layer [39]. The frequency characteristics of graphene also depends strongly on the material synthesis technique; for example, graphene FETs fabricated using graphene grown on insulating SiC show f_t of 100 GHz which exceeds Si MOSFETs with comparable gate length [40]. Besides f_t, the intrinsic voltage gain (A_v) is also very important for evaluating the RF performance of the devices. To obtain a high A_v, a drain current saturation is required. Although a drain current saturation has been reported in dual-gated bilayer graphene device due to an electrical field induced band gap opening [41], but the short-channel FETs (below 300 nm) lacks drain current saturation which leads to poor A_v.

Due to this limitation no significant progress on high frequency circuits, except few based on ambipolar nature of graphene, have been reported. An ambipolar electric field effect is when the charge carriers can be tuned between electrons and holes. Frequency doubling can be realized using this ambipolar property by dc biasing the gate of a graphene transistor to the minimum conduction point and superimposing a RF signal to the gate. The electrons and holes conduct for alternating half-cycles, to produce a drain signal with frequency twice that of the input. The first graphene based frequency doubler works at a fundamental frequency of 10 KHz [42]. Various other RF circuit based on graphene FETs (GFET) such as frequency multiplier [43, 44], RF signal mixer [45, 46] and a binary phase shift keying device have been demonstrated. RF detection has also been attempted using graphene nanoribbons (GNR) embedded inside coplanar waveguide structures as GNR is known to have semiconducting characteristics [47]. Majority of these circuits are fabricated on rigid substrates such as SiO_2/Si, quartz, sapphire and SiC. There is very limited work on characterization of practical RF flexible based on graphene based flexible circuits, as most of work done is focused on fabrication and DC characterization of GFET fabricated on flex substrates. The frequency performance of graphene based frequency doubler and RFID tags demonstrated on flex substrates have been limited to frequencies below 1 GHz [48-50]. To meet the need of low-cost flexible GHz applications, there is a need to investigate graphene based devices such as diodes or transistors operating in the microwave and millimeter wave frequency ranges.

Diodes are of great interest for applications such as rectification, switching, and frequency multiplication and mixing. While the high electrical conductivity of graphene and better impedance matching than CNT (due to its larger scale) makes it a promising material, it does not have a band gap in its natural state as in common semiconductors. Therefore, not much work has been carried out on high frequency diodes using graphene as an active material. In recent years, significant work has been done for band gap opening in graphene which involves substrate induced band gap opening in epitaxial graphene Quantum confinement in nano-ribbons and oxidation of graphene or graphite. Recently, graphene based diodes has been demonstrated by first opening its band gap through plasma oxidation and chemical modification [51, 52]. However, these diodes are fabricated on rigid substrate and more importantly there is no high frequency characterization of graphene diodes done so far.

This thesis presents Schottky diodes based on graphene. The diodes are realized by first opening the band gap by chemical modification (reduced graphene oxide or r-GO). To the best of our knowledge, high frequency applications of diodes based on semiconducting graphene has not been reported in literature. This thesis presents fabrication and high frequency characterization of r-GO on a flexible substrate. Details of DC characteristics, RF rectification, mixing and multiplication using r-GO diodes are presented in Chapter 2.

1.4.3. MIM Diodes for Microwave Circuits on Flexible Substrates

An ideal technology for flexible GHz circuits would be the one that is ultra-fast, compatible with any substrate, requires low-temperature processing, and low cost. A technology that can provide a non-semiconductor solution for flexible GHz electronics has the potential to be the ideal. MIM electronics seems to be a perfect fit for flexible circuits as these are comprised of only amorphous materials and thus avoiding any limitation of conventional semiconductors like grain boundaries, reduced mobility etc. MIM diodes are based on the principle of quantum tunneling through thin insulator layer. An MIM diode consists of two metal electrodes that are spaced apart by several nanometers of insulator or a stack of insulators. Conduction of charge carriers through the insulator occurs via the femtosecond-fast mechanism of quantum tunneling [20]. Tunneling leads to nonlinear current–voltage characteristics that depend on the shape of the barrier [53]. The conduction mechanism in dielectrics can be of two type: 1) Electrode-limited conduction mechanism, or 2) Bulk-limited conduction mechanism. In bulk-limited mechanism, the properties of the dielectric govern the conduction, however in case of electrode-limited conduction mechanism conduction depends on electrical properties at the electrode-dielectric interface i.e. the barrier height. Within electrode conduction mechanisms, there are different types: 1) Thermionic emission, 2) Tunneling. Thermionic emission is the conduction mechanism when electrons obtain enough energy to overcome the barrier at the metal-dielectric interface energy through thermal activation. This mechanism is the most common at relatively high temperature. The tunneling conduction mechanism refers to the quantum mechanical tunneling, where even the electrons not having enough energy, crosses the potential barrier. According to classical physics, when the energy of incident electrons is less than the potential barrier, the electrons should be reflected back; however, quantum mechanics predicts that potential barrier will not be enough to stop penetration of the electron wave function if the barrier is very thin (less than 10 nm).

In MIM diodes metals having work function higher than the electron affinity of the insulator produce a barrier at the metal/ insulator interface and the charge transport across the insulator occurs due to quantum-mechanical tunneling. Transmission probability of charge transport is the possibility of an electron tunneling through the classically forbidden region of the insulator. The probability of electron tunneling depends on the thickness of insulator and the barrier height, which changes shape with the voltage across the diode. Electron tunneling, which is the dominant in MIM diodes, occurs on a femtosecond timescale. Unlike semiconductor based diodes, MIM diodes are not limited by slow band conduction process. Also, all the electrodes are metal so very low parasitic is expected, and thus these can operate at high frequencies with high switching speed and faster response time. Due to their low voltage operation integration with CMOS circuitry is also possible. MIM diodes are also preferred due to their temperature insensitive characteristics. In addition, MIM diodes do not require any high temperature and high vacuum processes like epitaxy and chemical vapor deposition (CVD). The MIM diodes can also be easily integrated with other passive components like MIM capacitors, metal inductors, and thin film resistors. In addition, MIM devices can be fabricated on any substrate or even on top of existing CMOS circuitry by using the standard materials and fabrication facilities. As the MIM technology depends on thin vertical dimensions, devices fabricated on large area flexible substrate are expected to perform the same as any rigid counterpart. The high frequency response as well as the possibility to choose flexible substrate due to thin film fabrication makes MIM diodes a good choice for RF flex devices.

Various devices based on MIM structures including diodes [54], varactors [55], bipolar junction transistors [56], travelling wave diodes and plasmonic waveguides [57] are presented in the past. However, the focus has been on MIM tunneling diodes. Thin film MIM diodes are utilized more often in compare to point-contact MIM diodes or whisker diodes as they lack reproducibility and stability. The MIM diodes are simple to implement and a host of metal-dielectric combinations can be used to achieve desired diode characteristics. Generally, MIM diodes with dissimilar metals electrodes show significant non-linearity and asymmetry. In the literature, various combinations of dissimilar metals have been reported, including Ni-NiO-Au, Ni-NiO-Ni, Ti-TiO_2-Al, Ni-NiO-Cr/Au Al-AlO_x-Pt [54, 58-64]. In past, MIM diode has been investigated for infrared detection [61], solar rectennas [62] and switching memories [63], THz imaging and MMW detection. Most of the diodes presented in the past are fabricated on rigid substrates. This thesis demonstrates high frequency MIM diodes fabricated on flexible/polymer substrate.

As discussed earlier, for tunneling to occur the thickness of insulator should be few nanometers and thus the quality of thin insulating layer over entire contact area is very important. The thin film deposition technique utilized should provide a uniform layer with smooth surface. The dielectric is deposited using different techniques: in-situ oxidation for TiO_2 and plasma oxidation for NiO. This thesis presents the diodes based on two different dielectrics, i.e., TiO_2 and NiO with asymmetric contacts. This thesis presents the first experimental demonstration for Microwave rectification (up to 22 GHz), frequency multiplication (up to 2^{nd} order harmonic of 20 GHz) and frequency mixing for diodes fabricated on flexible substrate. In most of the work presented in literature the high frequency performance is predicted from the calculated sensitivity (ratio of second derivative and first derivative of the measured I-V characteristic) as opposed to measurements [59, 61].

1.5 Low Cost High Power Diodes for Microwave Applications

Low cost high power microwave devices are required for emerging applications in wireless communication as well as for continuous progress in defense applications. High power RF devices are an essential part of base station transceiver systems, high-speed communications, automotive collision avoidance and homeland security [64, 65]. Solid state devices are limited by transit time and thus require smaller sizes to perform at higher frequencies. However, compact devices suffer from increased temperature of operation as they cannot handle high power densities. For most of high power MMW applications such as frequency detection and multiplication, wide bandgap CS based devices are most widely used [66]. Compound semiconductors offer high band gap, high electron mobility, and the epitaxial growth allows for fabrication of complex layer structures. However, at MMW frequencies, the integrated circuits require on chip antennas/waveguide for signal coupling, which occupy a large surface area on the wafer as shown earlier in Figure 1.7. Thus, integration of these materials with Si is very important to enable mass production of low cost, high power devices for commercial MMW applications. It is also important to include CMOS backend circuitry along with high frequency circuits as required by many systems for data conditioning and signal processing. However, direct growth of these materials on silicon is still very challenging due to lattice mismatch and coefficient of thermal expansion (CTE) mismatch. The most commonly used integration techniques are hetero-epitaxy of different semiconductors and wafer/chip bonding (non-epitaxy) techniques. Different techniques and challenges associated with them are discussed in the following section.

1.5.1 Epitaxy Techniques

The biggest challenge for direct growth of compound semiconductors on silicon substrate is lattice mismatch and CTE mismatch. For example, common material system such as GaAS/Si, InP/Si and SiC/Si, the lattice mismatch is ~ 3 %, 8% and 20 %, respectively, and thus critical thickness is not very high, which results in degradation of electrical properties. The common techniques for epitaxy such as Molecular beam epitaxy (MBE) and CVD which uses temperature in range of 400-600 °C and 800-1000 °C, respectively. The different materials systems maintain their own lattice constant at growth temperatures; but, when the wafer is cooled down to room temperature strain is induced at interface leading to wafer bending and cracks in the epilayer. Number of growth techniques has been explored in the past to overcome this limitation, such as patterned substrate growth, use of buffer layers and use of complaint substrate, etc. Using very thin wafers helps to reduce the strain induced by lattice mismatch and allow growth of thick epilayer. However, handling of thin wafers becomes extremely difficult and to overcome this challenge compliant substrate is mounted on a mechanically rigid host substrate [67]. The most commonly used host substrate is silicon-on-insulator (SOI) substrate with a thin device layer as a compliant substrate [68].

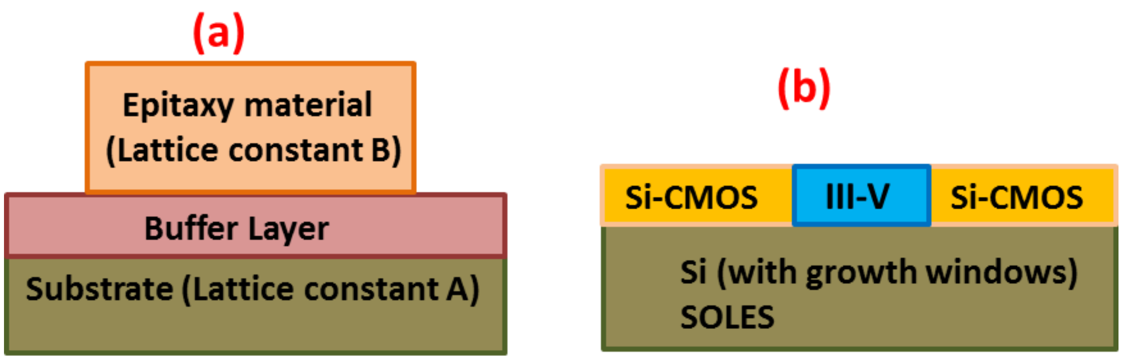

Figure 1.9 Use of Buffer layer for epitaxy (b) Patterned Si wafer (SLOES) for selective epitaxy

The other common technique to minimize dislocations is by introducing buffer layers (Figure.1.9 (a)). The key factor in this approach is to design and implement a buffer layer that provides a high quality “virtual substrate” on which growth can be done. The main advantage of this approach is that it provides large flexibility to the device layer designer by expanding the selection of the material systems and availability of lattice constants. The buffer layer should be carefully designed to minimize the increase on thermal resistance due to the extra added layer [69]. Various types of buffer layers have been explored in the literature depending on the epilayer material of interest. On Si, one of the most successful buffer layer is Ge (Germanium) for the growth of GaAs epitaxy. In general, $Si_{1-x}Ge_x$ is grown on Si substrate with graded Ge composition which enables dislocation free growth of GaAs [70].

A more attractive approach as compared to large area deposition of epitaxy layer on Si will be localized growth. This allows direct/selective integration of CMOS and III-V devices on a common silicon substrate. In this way systems performance can be optimized by the strategic placement of III-V devices adjacent to CMOS transistors and cells. As the growth area is limited to few $mm^{2,}$ the quality of heterogeneous grown III-Vs on silicon can be better optimized. The local epitaxy is achieved by patterning Si wafer and opening up growth windows (small area) where CS growth is carried out. The growth of high quality III-V epitaxial material is carried out directly on the lithography defined growth windows (Figure 1.9 (b)). The III-V growth windows are fabricated as a part of CMOS process, which allows selective growth. The epitaxy pattern or growth windows are usually created using SiO_2 or SiN trenches [71]. The most recent local epitaxy approaches using the SOLES (Silicon-on-Lattice Engineered Substrate) wafer [72]. But these techniques still require complex epi-layer engineering and use of special wafer for epitaxial growth, thus not very cost effective. In addition, the whole wafer has to be at high temperature thus the process is not post CMOS compatible.

1.5.2 Epitaxial Transfer Technique

A simpler approach to overcome stress and to reduce processing temperature is the direct transfer of epitaxial layer from a host substrate. The challenges with this approach include higher labor cost, difficulty of alignment and adhesion of epitaxial layers. Furthermore, the films can crack during the transfer process. Some of the existing non epitaxy techniques for heterogeneous integration involves involve chip to chip bonding, wafer to wafer or wafer to chip bonding (Figure 1.10). In contrast to epitaxial growth, wafer bonding is not limited by materials lattice mismatch. Depending on application and properties of materials to be combined different techniques are being used such as direct or indirect bonding. In the indirect bonding method, a thin layer of adhesive or metal is used as a bonding agent. In the adhesive approach both wafers are coated with a polymer before bringing into contact and depending on the adhesive being used it can be cured either by temperature or UV light. The techniques where temperature is needed for curing, CTE mismatch creates issues at the interface. If a thin metal layer is used for bonding (eutectic bonding), one of the wafer is usually covered with a thin layer of metal and heated above metal's eutectic point causing diffusion of silicon into the metal. The indirect wafer bonding technology has been successfully applied to silicon integrated Schottky diodes, transistors, solar cells [73, 74].

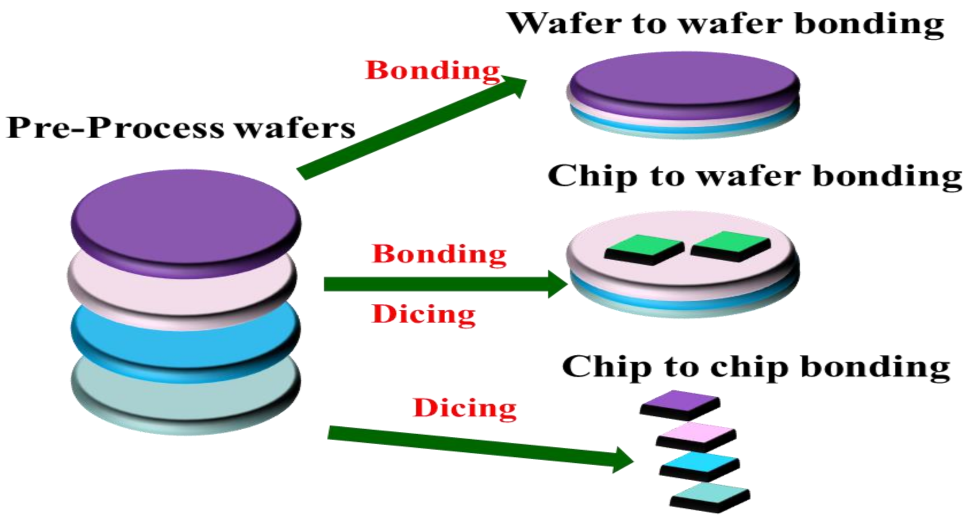

Figure 1.10 Wafer level bonding

In contrast to the indirect wafer bonding, the direct wafer bonding technique does not require an intermediate material between the joined wafers. Bonding is done by applying external force or by annealing the bonded pair at high temperatures. However, at high temperature CTE mismatch can change the material or structure properties. However, there are some low temperature (< 400 °C) direct bonding techniques, where wafers are treated with oxygen plasma before bonding in order to remove any contamination or hydrocarbon and water related species [75]. There is some recent work on direct wafer bonding for photonic and electronic integration based on Si but it is still very challenging. Most of the bonding techniques require temperature of several hundred degrees, so CTE mismatch can be a problem. For instance, if a GaAS patterned wafer is aligned on top of patterned Si wafer, the CTE mismatch will significantly deteriorates the alignment of patterns if the bonding is done at temperature higher than room temperature. Even if the bonding is done at room temperature, one still face the challenge of doing all subsequent processes at low temperatures. A way around this problem is to thin down one of the bonded wafers which will reduce the overall stress although not eliminates it.

1.5.3 Multichip Modules

Various techniques have been investigated to achieve integration of different chip technologies on a common substrate, see Figures. 1.11 (a) and 1.11(b). One of many approaches is monolithic integration of clusters of III-V devices next to Si CMOS on the same Si wafer/chip. The common substrate carries interconnects onto which these chips are flip chip or wire bonded. Traditionally, hybrid approaches such as wire bonded or flip chip multi-chip assemblies (Figure 1.11 (a)), were used, however the losses of the interconnects and the limitation in the placement of III-V devices relative to CMOS transistors limits the performance of these approaches. In wafer level packaging techniques, the fully fabricated wafers of individual technologies are integrated together (Figure.1.11 (b)). The successful integration of high speed materials with CMOS without compromising the yield and scalability of CMOS or the speed and breakdown of CS devices is still very challenging. It is desired that fabrication approaches allow seamless integration of different semiconductor technologies on a common substrate at low process temperatures, and have high compatibility with large-area manufacturing.

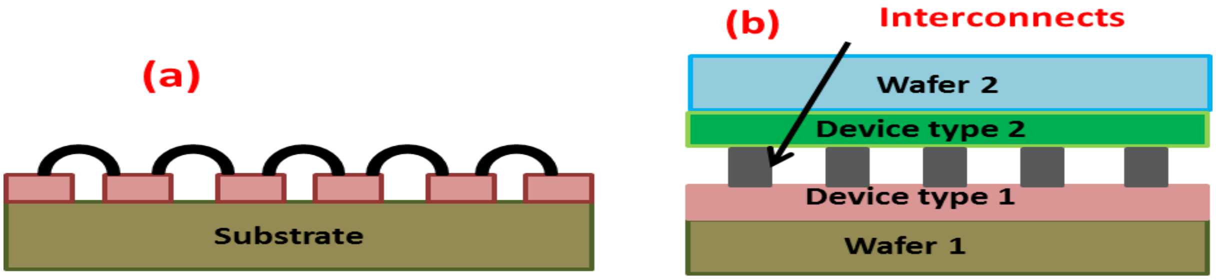

Figure 1.11 (a) Wire bonding technique (b) Wafer level packaging

1.6 SiC/Si Heterojunction Diodes: Challenges and trends of the growth

As discussed earlier, wide bandgap materials like GaN and SiC are of particular interest for high power high frequency diodes as they can handle high power densities unlike conventional semiconductors which are limited by saturated charge carrier velocity at high electric field [22, 23]. Although, different techniques have been used to grow these materials, there is still need for a novel fabrication process for direct/selective synthesis of wideband gap devices on Si substrate. Recently, SiC has regain interest for power applications. Comparing SiC to GaN, it has higher thermal conductivity and can theoretically operate at higher power densities. Although SiC has lower carrier mobility it is still adequate for high-power operation in the microwave frequency range. It also exhibits high saturation velocity at high electric fields [76, 77].

There are several SiC polytype films that can be grown. Out of the various existing polytypes, the most commonly researched are 6H SiC, 4H SiC, and 3C-SiC. The development of SiC devices have largely focused on 4H–SiC. In comparison to other polytypes, it has a wider band gap, higher breakdown voltage and higher mobility. Among the various existing polytypes, 3C-SiC can be grown directly on Si (hetero-epitaxy technique), which makes it a cheaper alternative in comparison to other polytypes. However, this material system experiences 20% lattice and 8% of thermal expansion coefficient mismatch, and the grown SiC contains a large number of extended defects. These defects result in high leakage currents in 3C-SiC/Si devices. Nevertheless, several research groups have been working on CVD growth of 3C-SiC [88, 89]. SiC/Si diodes have largely been investigated as a promising candidate for applications such as high-voltage converters, photovoltaics, optical diodes, high power, high frequency, and high temperature circuits. [77-79]. Low temperature processing is required for compatibility with post CMOS processing, which is essential when the circuits are need to be combined with data conditioning and signal processing circuits. The most commonly used method in the hetero-epitaxial growth of 3C-SiC is including low pressure CVD (LPCVD), Plasma enhanced CVD (PECVD), MBE and sputtering. During LPCVD and MBE processes, the deposition of SiC is carried out by maintaining the substrate under higher temperature (>1000 °C) and vacuum conditions, and processing time is long [80-82]. Long processing time coupled with high temperature can lead to significant diffusion of dopants from Si to SiC and accumulation of thermal mismatch at the junction of SiC/Si. Significant effort has been devoted to reduce the deposition temperature; however, it is generally reported that no single-crystalline SiC growth could be achieved below 1000 °C. Gas source molecular beam epitaxy (MBE), PECVD and sputtering are explored for low temperature 3C-SiC growth are low temperature techniques [83, 84]. However, low temperature MBE requires ultra-high vacuum range and thus not very cost effective for commercial applications. PECVD is low cost and enables low temperature processing. However, the grown films show compressive stress due to the hydrogen which can affect the stability of devices. The films made by sputtering always have the voids which affect the material properties. Thus, there is a need of novel fabrication process for direct/selective synthesis of such diodes. Alternate to conventional techniques, the growth of SiC on Si has also been demonstrated by diffusion of carbon into Si using thermal annealing of pre deposited carbon film [85]. In addition, the formation of SiC has been reported by using rapid thermal annealing of sputtered carbon layer on Si instead of traditional furnace annealing [86]. This approach shows that short pulse of temperature can be used to grow high quality SiC. However, it is still not compatible with CMOS post process as it requires heating of whole substrates. In order to overcome this challenge, a new process using laser annealing is proposed here.

Laser annealing has been used as an alternate to thermal annealing for doping of Si and SiC [87]. High power lasers, such as excimer lasers has been utilized to transform thin layers of amorphous Si (50 – 100nm) into high quality polycrystalline Si through melting and re-crystallization [88]. Laser based annealing offers the advantage of localized heating within the film while keeping the substrate at room temperature. Thus it is expected that laser irradiation with very high power is capable of dissociating solid carbon sources and melting silicon simultaneously which can give rise to a new mechanism of SiC growth. Recently, laser synthesis techniques have been used to transform solid carbon sources to graphene directly on Si and quartz substrates [89]. The goal of this work is to demonstrate the growth of SiC on Si by laser based local heating. The advantages of using laser for growth are localized heating, rapid heating and cooling due short laser pulse, limited damage to substrate or neighboring circuits, growth under ambient conditions and post CMOS compatibility. Thus, this process is attractive and is investigated in this thesis. This thesis presents process for the fabrication of SiC/Si heterojunction diodes by selective growth of 3C-SiC on Si substrate using a high power pulsed Krypton Fluoride (KrF) excimer laser.

1.7 Dissertation Overview and Key Contributions

This research builds upon the work that has been documented in the literature as discussed above. Realizing the importance of heterogeneous integration of different device technologies for MMW circuit applications; the goal of this dissertation is to demonstrate processes to overcome the challenges associated with it. As depicted in Figure 1.8, the thesis focuses on different approaches to integrate high frequency diodes on low cost large area substrates/wafers for low power as well as for high power GHz circuit applications. The dissertation research carried out several task as steps towards that ultimate goal while overcoming challenges of previously existing techniques. As a summary, the key contribution and outcomes of this thesis are highlighted (with respect to individual chapters) below:

Reduced Graphene Based Diodes: Chapter 2

- Fabrication of graphene based diodes on flexible substrates by first opening its band gap through chemical modification.
- First demonstration of GHz circuits applications (Microwave rectification, frequency multiplication, and mixing) using graphene (r-GO) based diodes on flexible substrates.
- Successfully demonstrated microwave rectification up to 22 GHz and frequency multiplication up to 10 GHz.
- Demonstrated low cost novel fabrication process for sub-micron r-GO devices using conventional optical lithography.

Metal Insulator Metal Diodes: Chapter 3

- First demonstration of fabrication and characterization of MIM diodes on flexible substrates.
- Successful demonstration of use of plasma grown metal oxide (Nickel oxide) as insulator layer for MIM diode. The diode shows good current-voltage and high frequency characteristics.

- Achieved microwave rectification up to 18 GHZ and frequency multiplication up to 10 GHz using NiO based diodes.
- Developed equivalent model for MIM diodes which an enable diode scaling for future applications requiring operation in THz range.

Laser Synthesized high power SiC/Si based Microwave diode: Chapters 4 and 5

- Proposed and demonstrated an alternative low cost technique for direct and selective growth of SiC on Si under ambient conditions which is very challenging to achieve using conventional methods.
- Achieved innovation by developing a new low-cost, fast and CMOS compatible process for the fabrication of SiC/Si heterojunction diodes using high power KrF excimer laser.
- Demonstrated diode with good rectification characteristics, low leakage current and high breakdown voltage of >200 V.
- Demonstrated microwave rectifiers with high sensitivity as well as wide band high frequency and high power doubler.

1.8 Dissertation Layout

The high level chapter layout of this thesis work is as follows:

Chapter 2 presents the presents the fabrication and characterization of reduced graphene oxide (r-GO), based diodes on flexible substrates for high frequency circuit applications. The background theory about properties and band gap opening of graphene, fabrication technique, and experimental validation results (DC and Microwave) are presented.

Chapter 3 demonstrated microwave circuit applications using MIM tunneling diodes fabricated on flexible substrates. The diode design, material selection, insulator deposition techniques, fabrication and experimental results (DC and Microwave) are presented.

Chapter 4 presents high power SiC/Si heterojunction diodes fabricated by the novel laser process. The background on alternate techniques for SiC synthesis, advantages of laser process, theory of laser process is discussed. The experimental details of fabrication process, material characterization (RAMAN, XPS, SEM) of the laser synthesized SiC materials is presented. In addition, experimental results for Current-Voltage characteristics, CV characteristics, and preliminary photovoltaic.

Chapter 5 presents the fabrication process to make small area SiC/Si diode (laser synthesized) and experimental results for microwave rectification and frequency multiplication.

Chapter 6 concludes the dissertation along with the presentation of possible future work based on this thesis work.

CHAPTER 2: REDUCED GRAPHENE OXIDE BASED DIODES FOR FLEXIBLE GHZ CIRCUITS

For development of flexible GHz electronics, materials with excellent electronic and mechanical properties are required. Novel materials like carbon nanonotubes (CNTs) and graphene are good candidates as they offer excellent electronic properties needed for high frequency electronics and can be easily integrated on flex substrates or a host of other substrates. However, there are some challenges that need to be addressed first. The high impedance of a single CNT devices makes it very difficult to impedance match it to a lower impedance (e.g., 50 Ω) external circuitry. In contrast, graphene has the potential to provide better impedance matching due to its 2D nature. Graphene Field-Effect transistor (GFET) has been explored in past for RF applications like mixing, switching and multiplication as discussed in Chapter 1. However not much work has been done on graphene based diodes due to missing bandgap. Recently, graphene based diodes has been demonstrated by first opening its band gap through plasma oxidation and chemical modification. To the best of our knowledge, high frequency applications of diodes based on semiconducting graphene has not been reported in literature. Therefore, the goal of this chapter is to demonstrate chemically modified-graphene based microwave and MMW diodes on flexible substrates. This chapter first discusses the electronic properties of graphene, different synthesis techniques and then techniques used for band gap opening. Details of fabrication process and experimental results for microwave rectification, frequency multiplication and mixing based on these diodes is also presented.

2.1 Electronic properties of Graphene

The monolayer of graphene consists of carbon atoms arranged in honeycomb crystal structure as shown in Figure 2.1 (a) which consists of the hexagonal Bravais lattice (Figure 2.1 (b)) with a basis of two atoms. The graphene hexagon lattice can be considered as one unit cell having 2 carbon atoms [90]. The two lattice vectors are given as:

$$a_1 = \frac{a}{2}(3, \sqrt{3}) \text{ , } a_2 = \frac{a}{2}(3, -\sqrt{3}) \tag{2.1}$$

The primitive lattice vectors b_1 and b_2 satisfying the condition $a_1b_1=a_2b_2=2*pi$, and $a_1b_2=a_2b_1=0$, are given as:

$$b_1 = \frac{2\pi}{3a}(1, \sqrt{3})\ b_2 = \frac{2\pi}{3a}(1, -\sqrt{3}) \tag{2.2}$$

Each carbon atom has six electrons with four valence electrons occupying 2s, $2p_x$, $2p_y$, and $2p_z$ orbitals. In graphene, the orbitals are sp^2 hybridized, meaning that two of the 2p orbitals ($2p_x$ and $2p_y$) that lie in the graphene plane, form three sp^2 hybrid with the 2s orbital [91]. Each atom is 1.42 °A from its three neighboring atoms, and shares one σ bond with them. The fourth bond is a π-bond, which is oriented in the z-direction (out of the plane). Electronic states close to the fermi level in graphene are described by taking into account only the π orbital, meaning that the tight-binding model can include only one electron per atomic site, i.e. in a $2p_z$ orbital.

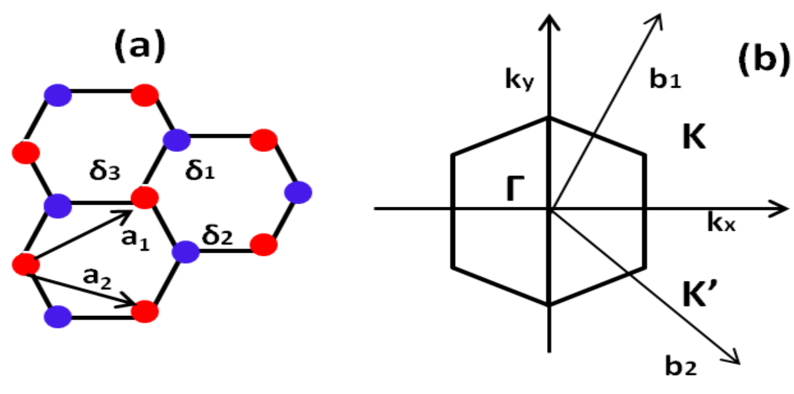

Figure 2.1 (a) Lattice structure of graphene with a1 and a2 as lattice unit vectors (b) corresponding Brillouin zone with Dirac cones located at K and K' points

In graphene the motion of electrons is limited to two dimensions, and thus the momentum space is also in two dimensions. A plot of the energy versus momentum dispersion relation for graphene can be found using the tight binding approximation. Graphene is a zero-gap semiconductor because the conduction and valence bands meet at the Dirac points. The K and K' points are the primary points of interest, and their positions are given as:

$$K = \left(\frac{2\pi}{3a}, \frac{2\pi}{3\sqrt{3}a}\right), \quad K' = \left(\frac{2\pi}{3a}, -\frac{2\pi}{3\sqrt{3}a}\right) \tag{2.3}$$

The three nearest-neighbors are given as:

$$\delta_1 = \frac{a}{2}(1, \sqrt{3}) \quad \delta_2 = \frac{a}{2}(1, -\sqrt{3}) \quad \delta_3 = -a(1, 0) \tag{2.4}$$

and six second nearest neighbors are $\delta_1' = \pm a_1$, $\delta_2' = \pm a_2$, $\delta_3' = \pm(a_2 - a_1)$, where a=1.42Å is the carbon-carbon distance. The energy band has the form [92]

$$E_\pm(k) = \pm t\sqrt{3 + f(k)} - t' f(k) \quad \text{, where} \tag{2.5}$$

$$f(k) = 2\cos(\sqrt{3}k_y a) + 4\cos\left(\frac{\sqrt{3}}{2}k_y a\right)\cos\left(\frac{3}{2}k_x a\right) \tag{2.6}$$

The plus sign corresponds to the upper π^* bands and the minus sign gives the lower π bands. These two Dirac points K and K' play important roles in electronic properties of graphene. By taking K as the zero point, a value of momentum q is measured relatively to K, and E-q relation can be obtained as:

$$E_\pm(q) \approx 3t' + \hbar v_F |q| - \left(\frac{9t'a^2}{4} \pm \frac{3ta^2}{8}\sin(3\theta_q)\right)|q|^2 \tag{2.7}$$

Where, υ_F is fermi velocity ($v_F = 3ta/2$) with value of ~1 x 10^6m/s and θ_q is angle in momentum space. Equation 2.5 shows that monolayer graphene is a zero bandgap semiconductor with linear, rather than quadratic energy dispersion. This behavior is of significant interest and is the main reason for which graphene has received significant research attention from many disciplines. Bilayer graphene allows band-gap opening by applying a perpendicular electric field to two layers or by doping. The tight-binding approach has been done for bilayer graphene with AB stacking. The distance between these bilayers is 0.3nm [91, 92]. With no external voltage (V=0), the effective Hamilton changes and resulting in energy dispersions is given as [93]:

$$E_{k,\pm} = \pm\hbar^2 v_F^2 k^2 / t_\perp = \pm\hbar^2 k^2 / 2m^* \tag{2.8}$$

This provides symmetric conduction and valence bands with parabolic curve shapes. The bilayer has a gap at $k^2 = 2V^2 / V_F^2$, and the gap depends on the applied bias which can be measured experimentally. The applied bias perpendicular to bilayer is able to open a gap, which makes bilayer valuable and significant in semiconducting applications.

2.2 Graphene Synthesis techniques

Within the past several years, various methods have been developed for synthesis of graphene such as mechanical exfoliation, epitaxial growth of graphene, CVD growth of graphene on transition metals, chemical exfoliation of graphite etc. The most commonly used method is mechanical exfoliation of graphite, although useful devices have been made using this method, the size of exfoliated graphene films is limited and not of practical use. This method produces graphene flakes by repeated peeling or exfoliation of highly oriented pyrolytic graphite (HOPG) using scotch tape and then releases flakes of single-layer graphene onto a SiO_2 substrate, stabilized by Vander Waals-mediated attraction between the graphene and the SiO_2 substrate [94,95]. However, finding a single layer flake is difficult as the flakes are not uniformly distributed on the substrate. The graphene flakes obtained are very small in size ranging from a few microns to a couple of millimeters. Thus this method is of use only for fundamental studies and is not scalable for commercial purposes.

The most commonly used techniques for deposition of wafer scale graphene is CVD onto transition metal substrates such Ni and Cu. The metal serves both as a catalyst and a substrate for growing graphene layers. The mechanism involves the diffusion of carbon into a thin metal film at a desired growth temperature. The growth occurs by the principle of diffusion, segregation and precipitation of carbon on the catalytic metal surface. But the graphene need to be transferred on other substrates to use it for electronic applications. Several techniques have been developed for transferring large-area graphene films [97]. The most common technique is to use polymethylmethacrylate (PMMA) as a supporting layer, i.e. graphene surface is coated with PMMA and then metal is etched using an etchant. The graphene layer is then transferred onto a desired substrate, and the PMMA is removed. Another method of transferring large scale graphene is using a roll-to-roll transfer method with a supporting layer of thermal release tape. This process enables the transfer of graphene films as big as 30-inch graphene [98]. The transfer of graphene can severely damage the thin graphene film and thus degrade its inherent properties. The CVD approach is attractive because it permits fabrication over large areas and allows the applicability of graphene for fabrication of devices on flexible substrates [99].

Epitaxial growth of graphene on wide band gap material like SiC enables direct electrical measurements on the substrate [96] without the need for transfer processes. High quality, large area epitaxial graphene’s are obtained using this method but it requires expensive SiC substrate and annealing of high temperature. However, due to direct growth of graphene on insulating substrate, direct fabrication of graphene high frequency devices can be realized. Recently a 100 GHz graphene transistor has been fabricated using this technique [40]. In addition, methods have been developed to transfer graphene films from SiC substrates to arbitrary substrates.

Another alternative method for producing scalable graphene films is through exfoliation of graphite by covalent and noncovalent interactions [100]. Several organic solvents N-methylpyrrolidone (NMP), N,Ndimethylacetamide (DMA), and dimethylformamide (DMF), with surface tensions matching that of graphene are used to exfoliate graphite and make single and few layer graphene sheets. The conductivity of resulting graphene is low in comparison to pristine graphene films due presence of residues from solvents and surfactants. Exfoliation can also be done by chemically modifying graphite to make graphite oxide (GO) using hummers methods. After oxidation, GO can be easily dispersed in water and can be exfoliated due to interactions between the water and functional group of oxygen, such as hydroxyl and epoxide present in GO sheet. The resulting GO suspension is mostly insulating in nature but it can be reduced to semiconducting or metallic graphene by, thermal or chemical reduction. Due to the low cost and scalability of these methods there is significant effort toward improving the film quality by repairing defects and chemical doping [101].

2.3 Semiconducting Graphene Structures

Despite its exceptional good electronic properties and huge potential for many applications, one of the greatest challenges in graphene as a future electronic material is the absence of bandgap. Graphene is a zero bandgap semiconductor, which limits its use in many applications such as diodes. The zero bandgap in graphene is a because of symmetrical environment for two carbon atoms in its unit cell. Therefore, in order to open the bandgap the lateral, in-plane symmetry should be broken which can be achieved by structural modifications (quantum confinement) or by chemical modification (doping/ attaching functional groups or stacking graphene layers). Some of the recent developments are discussed here.

2.3.1 Quantum confinement-induced bandgap in graphene

It has been demonstrated both theoretically and experimentally that the size and shape of graphene can affect its properties. By quantum confinement i.e. by patterning graphene in the form of graphene nanoribbons (GNR) or graphene nanomesh (GNM), a bandgap can be achieved in graphene. The bandgap of GNR is inversely proportional to the width of the GNRs [102, 103]. A bangap of 200 meV was achieved for a 15nm GNR, narrower widths may show even larger bandgap. But e-beam lithography has some resolution limits, also the small band gap achieved may be not enough for semiconductor application. Nananowires (NWs) lithography has been utilized to fabricate sub-10nm GNR by aligning the NWs on top of graphene and the exposing to oxygen plasma for etching graphene [104].

2.3.2 Plasma oxidation

Oxygen plasma has been used to functionalize the basal plane of graphene with oxygen group in order to open the bandgap. This approach can be very useful as it doesn't use any kind of harsh chemical treatments for oxidation and the oxidation rate can be easily controlled by power, exposure time and gas flow. Recently, Nourbakhsh et.al reports diodes based on plasma treated graphene using different exposure time [52]. Also, Schottky diodes have also been reported by using asymmetrical contacts with plasma modified graphene and metal. This is of great interest especially for applications like high frequency detectors.

2.3.3 Chemical modification, doping, or surface functionalization of graphene

Graphene properties can be modified by chemical treatment. Graphene is a highly inert and thermally stable material, and thus requires high-energy to re-hybridize. There are different strategies to functionalize graphene but the most commonly used is oxidation of graphite and its exfoliation in strong acids. The most commonly used strategy is to functionalize is to exfoliation of graphite in acid with functionalities such as carboxyl (-COOH), epoxy (=O), hydroxyl (-OH), carbonyl (-C=O) [105]. This converts graphene into an insulator called graphene oxide (GO). In GO, most of the carbon atoms are bonded with oxygen in sp^3 hybridization, and thus making it insulating it with large band gap. The most commonly used method is Hummer's method where graphite was oxidized using potassium permanganate and sulfuric acid [106]. The energy gap in GO can be controlled by controlling the oxidation and reduction rate. GO can be reduced chemically or thermally to obtain reduced graphene oxide (r-GO), which is semiconducting [107]. Energy bandgap tuning can be achieved by changing the O/C atom ratio. The higher the ratio of O/C, the larger the bandgap.

Reduced graphene oxide has been investigated for large area film deposition through simple processes [108]. The r-GO readily disperses in water as well as in various other solvents, and can be deposited on large area film through simple processes such as wet processing, dip coating [108], or selectively assembled using DEP. It can easily be integrated onto a variety of substrates (rigid and flex) which omits the need to transfer CVD graphene. In addition, low cost of synthesis and ease of material processing makes it an attractive alternative to exfoliated graphene. As an example, r-GO has already been used in the fabrication of large area organic solar cells [109], field effect transistors [110] and chemical sensors [111]. More recently, Schottky diodes based on r-GO have been demonstrated. The diodes were fabricated by (DEP) assembly of r-GO between two dissimilar metal contacts, i.e., Titanium (Ti) and palladium (Pd) on SiO_2/Si substrate [51]. Graphene oxide was reduced by both chemical and thermal approaches. Here, the measured current was very low due to high levels of disorder in r-GO sheets used. No significant work on high frequency applications of graphene based Schottky diodes has been reported. Schottky diode is one of the most important devices for high frequency circuit designs; so, it is worth investigating r-GO Schottky diodes for RF applications. This thesis will investigate the r-GO based diodes for high frequency applications such as detection, frequency multiplication and mixing.

2.4 Reduced Graphene oxide based diodes for high frequency circuits

There is significant growth in the area of high frequency devices on flexible substrates as this enables various applications in wireless communication; but, the realization of low cost large scale fabrication is still a challenge using conventional semiconductors due to low-temperature processing constraints. Graphene oxide is one of the potential candidates to meet this challenge. It can easily be deposited on flexible substrate which omits the need to transfer CVD graphene through complex processes. In addition, low cost of synthesis and ease of material processing makes it an attractive alternative not only epitaxial layers but also to exfoliated graphene. The level of oxidation affects significantly the electronic structure of GO. Fully oxidized graphene is insulating in its natural form having a direct band gap. This band gap can be tailored form insulating to semiconducting by controlling the oxygen to carbon ratio. In this thesis, graphene based diodes are realized by first opening the band gap by chemical modification (reduced graphene oxide or r-GO). Details of material synthesis and device fabrication are discussed below.

2.4.1 Background

Graphene oxide (GO), a chemically derived graphene and is of interest due to its solubility in a variety of solvents and promise of large area electronics. GO can be viewed as graphene with oxygen functional groups on the basal plane and edges. The electronic transport properties in

GO is very different from graphene due to the presence of substantial electronic disorder arising from variable sp^2 and sp^3 bonds. Oxidation process generates various types of defects in the graphene lattice, which limits transport. At a low oxidation levels, the band gap is small which gives GO the characteristics of a semiconductor. At high (saturated) oxidation levels the band gap extends closer to insulators. The possibility of band gap engineering in GO is of interest for its implementation in electronic and photonic devices. The transport in reduced GO (r-GO) occurs due to variable range hopping (VRH). In VRH model, the temperature dependence of the conductivity can be described by the form The carrier transport in lightly reduced GO was shown to occur via variable-range hopping whereas band-like transport begins to dominate in well-reduced GO [107]. Graphene oxide (GO) is a heavily oxygenated monolayer material consisting of a variety of oxygen bearing functional groups, such as hydroxyl, epoxy, carbonyl and carboxyl groups. The conventional reduction techniques include thermal reduction, chemical reduction or reduction by UV light. Based on the previous studies it is known that sp^2 domains form upon reduction which implies that the size of each sp^2 region in graphene decreases with reduction, but increases its overall presence in the samples, which increase the conductivity [112]. In this work chemical reduction technique is used to obtain r-GO. The details of material preparation, material characterization, and diode fabrication are presented in upcoming sections. The DC and high frequency characterization of fabricated devices is also presented.

2.4.2 Material Preparation

The single layer GO powder (oxygen content ~ 35%, purity ~ 99%) with flake size of 2 – 6 µm was purchased from Cheaptubes. As per the manufacturer datasheet, this material was synthesized using modified Hummers method. The received powder was first added to deionized (DI) water to make a solution with concentration of approximately 0.1 mg/ml. The GO is hydrophilic in nature because of the oxygenated graphene layers and it can be easily exfoliated in aqueous media. The solution was then pulsed ultrasonicated and centrifuged to obtain flakes with single or few layers of GO. The ultrasonic treatment helps in producing stable dispersion of thin graphene oxide sheets yielding an inhomogeneous yellow-brown dispersion as shown in Fig. 2.2 (c).

Figure 2.2 Preparation and dispersion of reduced graphene oxide

This dispersion was sonicated until it became clear with no visible particulate matter. As GO is insulating in nature, it has to be first reduced to make it semiconducting. Here, the reduction of GO is carried out by adding 2 µl of hydrazine hydrate and heat treating the solution at 95-100 °C. GO suspension in DI water changes color from light brown to black after hydrazine treatment as seen in Fig. 2.2 (c) and (d). The r-GO sheets were characterized by SEM, Raman spectroscopy, and by electrical I-V characteristics.

2.4.3 Substrate Selection and design

The devices were fabricated on a flexible polymer substrate. The key selection criterions for polymer substrates are high glass transition temperature, chemical compatibility and low dielectric loss. Commercially available thin polymer films like Polyetheretheretherketone (PEEK), polyethyleneterephthalate (PET) and Polyimide (PI) are compatible with chemicals used in the micro fabrication processes. These materials have already been tested by our lab for characterization of their dielectric constant over a wide frequency spectrum. All of these exhibits low dielectric loss and thus higher frequency devices can be utilized for making high frequency devices [112]. Devices in this paper are built on PEEK which has a glass transition temperature of 143 °C and thermal expansion co-efficient of 2.6 x 10^{-5} K^{-1}. The Schottky diodes based on graphene were implemented using asymmetrical metal contacts. The microelectrodes used to contact r-GO are coplanar waveguide (CPW) structures as needed for high frequency characterization of these diodes. The CPW structures were designed using Linecalc tool from Advance Design Systems (ADS) for a for PEEK substrate with dielectric constant of 3.3 thickness of 250 µm.

2.5 Microelectrodes Fabrication

Small size devices are required to realize RF circuits with working frequencies in GHz range as bigger devices are limited by transit time. Expensive high resolution lithography technique such as e-beam is required to attain device lengths that are less than 1 µm. Here, a low cost novel process is used that allows the fabrication of sub-micron r-GO devices on plastic substrates using conventional optical lithography by utilizing a novel undercut and self-alignment approach. This process is simple to implement, low cost and large area compatible. The microelectrodes were fabricated with the process as used shown in Figure. 2.3. The Schottky diodes based on graphene were implemented using asymmetrical metal contacts. Here Ti (Titanium) and Pd (Palladium) are selected as Schottky and Ohmic contacts with work function of 4.33 and 5.22 eV, respectively. The work function of pristine graphene is 4.4 - 4.5 eV, but the work function of chemically modified graphene and oxygen treated plasma increases to 4.5 - 4.7 eV and also shows a p-type behavior.

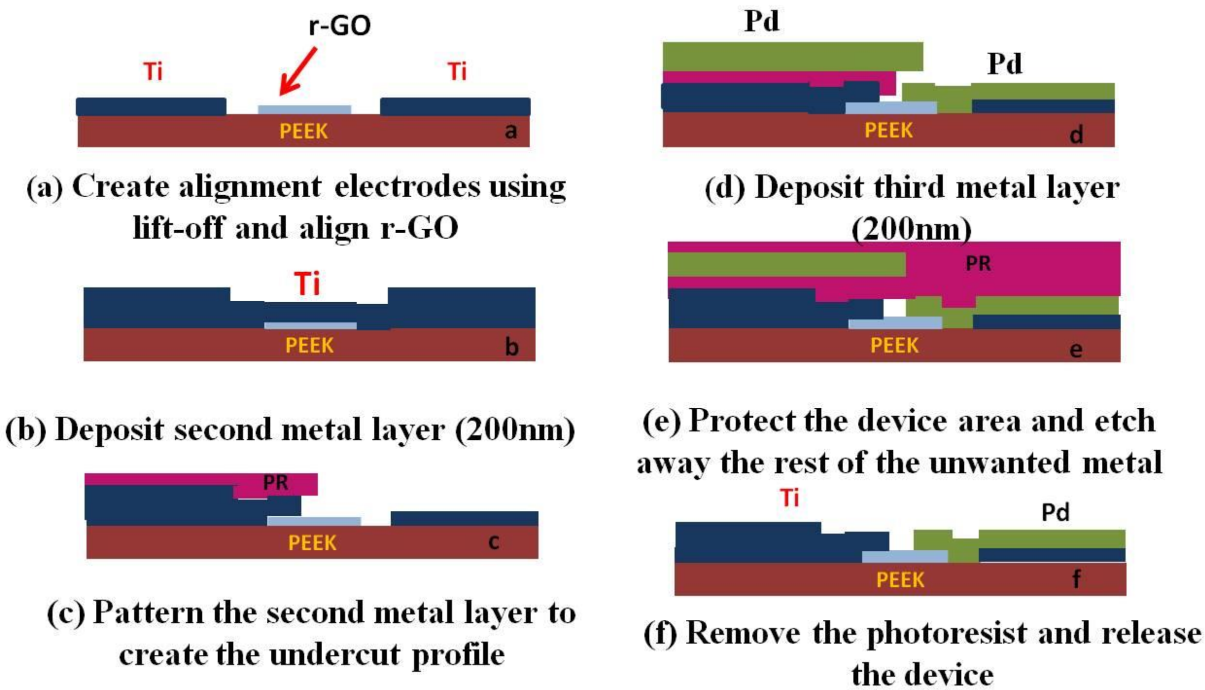

Figure 2.3 Fabrication of Microelectrodes for graphene based diodes

Metals with work function lower than graphene such as Titanium (4.3), Chromium (4.5) and Aluminum (4.06 - 4.26) can be used to make Schottky contact while metals with higher work function such as Pd(5.22-5.6) and Au(5.1-5.4 eV) can be used to form ohmic contacts. Both Ti and Cr were tested (Cr not shown here) to make a Schottky contact; but, Ti was found to show stronger non-linearity with r-GO. The fabrication process is mainly divided into three parts, deposition and patterning of first metal layer for alignment electrodes, aligning the dispersed r-GO between the electrodes, and depositing and pattering of Ohmic and Schottky contacts to r-

GO. In place of DEP, other methods of depositing r-GO can be used such as spin or dip coating.The PEEK substrate was first cleaned using acetone, methanol and DI water placed in ultrasonic bath. Figure 1 shows the fabrication steps. First, a thin metal layer of Ti with thickness ~100 nm is deposited using e-beam evaporation on patterned photoresist layer (positive resist S1813) on the PEEK substrate followed by lift-off, Figure.2.3 (a). The patterned gap between the patterned electrodes is approximately 6 μm. In the next step, r-GO sheets were aligned between the electrodes using a DEP process. DEP is commonly used to align or assemble solution dispersed nano-materials such as graphene, CNTs and other nanowires. Theoretical calculations about shaping the micro-electrodes to control the motion trajectories and positions of assembled nonmaterial using DEP can be found in [113]. A droplet of 1-2 μl of r-GO solution was drop casted between the electrodes while applying alternating voltage (8 Vpp, 1 MHz) between the electrodes.

In DEP, AC field generates a DEP force in gap between electrodes and thus forcing the polarizable object to confine between the electrodes (Fig 2.7(a)). The number of graphene layers between electrodes depends upon on the concentration of solution as well as the electric field drop across the electrode gap. In order to achieve good alignment, conditions such as r-GO concentration, sonication time, AC peak to peak (pp) voltage and frequency need to be optimized. In the third step, Schottky and Ohmic contacts for the diode are formed using a novel process. The second layer of 200 nm thick Ti is deposited by e- beam evaporation to form a Schottky contact. The Ti metal layer was patterned using optical lithography, and selectively etched (Figure 2.3 (c)). Etching of Ti (undercut) was carried out using HF:H_2O_2:H_2O=1:1:200 etchant, Figure 2.3(c). During this step, the undercut is controlled by the type of etchant used and by the thickness of the Ti layer. The depth of undercut determines the length of the

Schottky diode and can be tailored through precise control of etching rate, etchant concentration, and resist bake conditions. The Ohmic contact was then made by depositing 200 nm of Au using e-beam deposition (Fig. 2.3 (d)). The overhanging positive resist on the graphene from the previous step (patterning the Ti layer) acts as a shadow mask. This was followed by patterning and etching of Pd. It was patterned using $FeCl_3$ as the etching solution. The final step is to lift off Pd on one side of the electrodes, Figure 2.3(f), resulting in a final device with asymmetrical metal contacts with one acting as a Schottky while the other acting as an Ohmic contact.

The r-GO sheets can be assembled between the electrodes using two different ways giving two different type of r-GO-metal contact i.e. side metal contact and top metal contact (buried metal contact) as shown in Figure 2.4 (b) and (c), respectively. Side metal contact means graphene lies on top metal electrodes and DEP is done after fabricating the electrodes. Top-metal contact means graphene sheet is underneath the metal electrode or buried by the metal at contact (Figure 2.4(c).

For side-metal contact diodes the contact between r-GO sheet and metal is not good, which can make the contact resistance very high and thus degrades the high frequency performance. For top-metal (buried) contact the metal would be deposited on top of r-GO sheet and thus improving the contact resistance which is needed for better impedance matching. The previous related to Schottky diodes based on graphene is done using side metal contact process [19]. Here, top (buried) metal contacts devices are only presented as their performance is much better at high frequencies. The SEM and optical image of fabricated devices is shown in Figure 2.5 (b) and (c), respectively. The Raman spectra for prepared r-GO samples are shown in Figure 2.4(d), all measurements were carried out in backscattering geometry using a 532 nm laser. The Raman spectroscopy was used to identify the orderliness of the r-GO crystal structure.

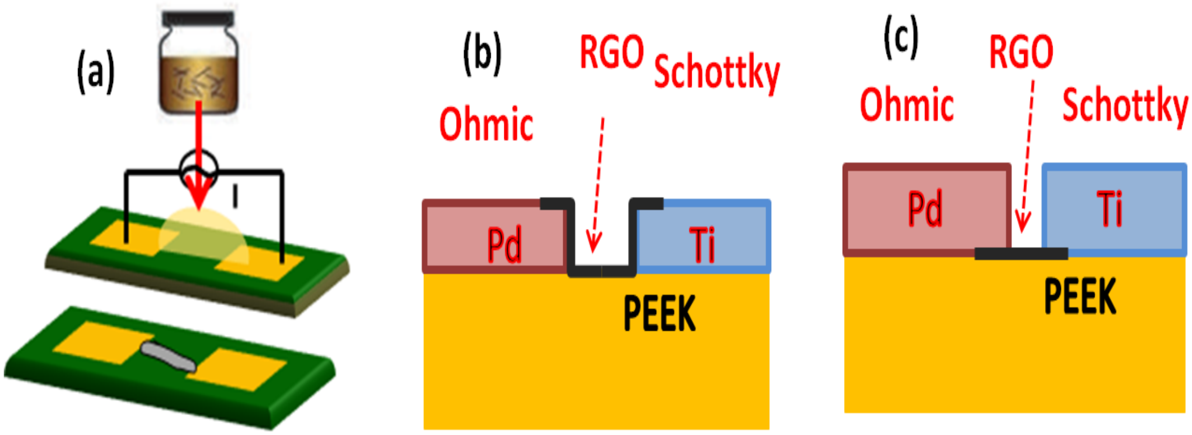

Figure 2.4 (a) Schematic of DEP (b) r-GO metal side contact (c) r-GO metal top contact.

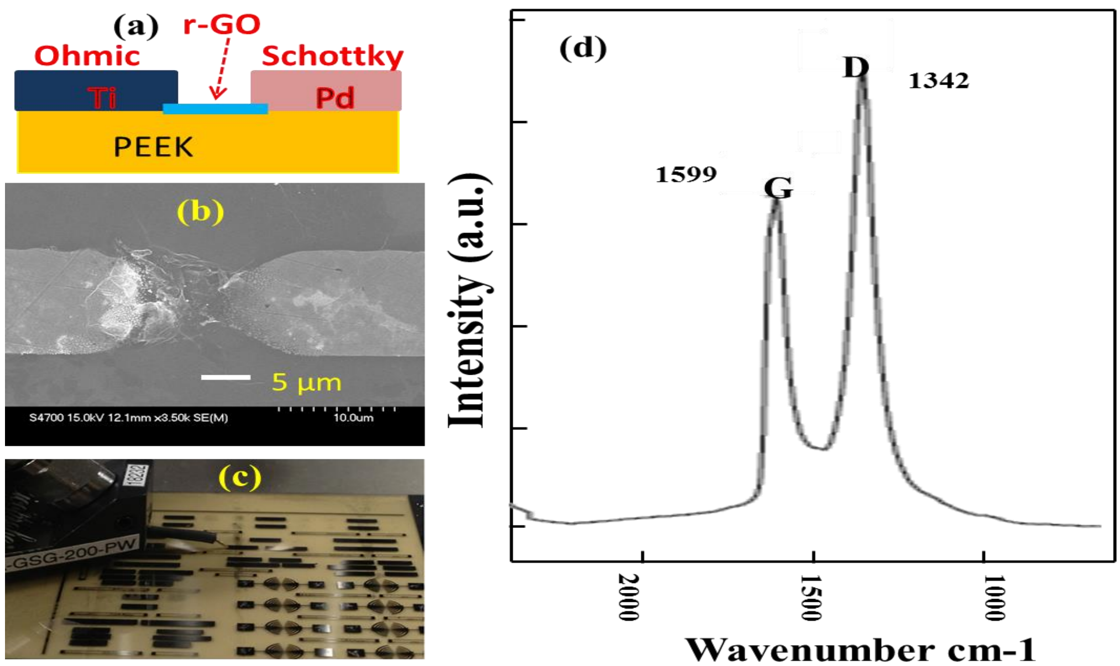

Figure 2.5 (a) Schematic of r-GO based diode with asymmetrical contact (b) SEM image of r-GO sheets aligned between electrodes (c) Optical image of fabricated diodes, and (d) Raman spectra of r-GO sheets.

The Raman spectrum of our r-GO sheets exhibits the D-band peak at 1342 cm^{-1} and the G-band peak at 1599 cm^{-1}. The intensity of the D band is higher than that of the G band (~1.5 times). The intensity of the D and G peak depends on the reduction level The Raman peaks of our r-GO sample matches well with many previously presented data [114, 115]. The high D band is related to the presence of sp^3 bonds as a result of functional groups in the GO sheet and decrease in the average size of the sp^2 domains upon reduction of the exfoliated GO [115]. This also indicates that in chemical reduction process of GO higher number of defects occur at higher reduction level. Thus a further study is needed to study and analyze the surface chemical composition and bonding of samples with different reduction times or levels. X-ray photoelectron spectroscopy (XPS) can be used to achieve this in future.

2.6 Current-Voltage (I-V) characteristics

The current-voltage (I-V) characteristics of the devices were measured at room temperature using a Semiconductor Parameter Analyzer (SPA). Figure 2.6 shows the measured I-V characteristics of a graphene based diode. The forward current achieved here is on the order of μA which is much higher than previously reported r-GO diodes and plasma oxidized graphene based diodes (nA) [51, 52]. The non-linear I-V characteristics also prove that the GO sheets were successfully reduced to r-GO. Several trial experiments were carried out in order to achieve optimum reduction. For example, too high of a concentration of hydrazine and long heat treatment can lead to full reduction to graphite like structure that showed linear I-V characteristics with low resistances. The r-GO layers aligned using optimized reduction process and DEP force shows good non-linearity. The recipe discussed in the previous section was chosen as the optimal one found in this work. In the previous work reported in [19], r-GO based Schottky diodes were fabricated by aligning graphene sheets on top of the fabricated electrodes.

To reduce contact resistance and improve the Schottky contact, here the metal contacts were deposited on top of graphene sheets. The quality of a diode can be assessed by its ideality factor (n), which can be calculated by fitting the measured I-V curve to the diode equation:

$$I = I_0[\exp\left(\frac{e(V-IRs)}{nkT}\right) - 1] \tag{2.8}$$

where, I is the measured current, e is the charge of an electron, Rs is the effective series resistance/contact resistance, T is the temperature, k is the Boltzmann constant, I_0 is the saturation current, n is the ideality factor and V is the applied bias voltage.

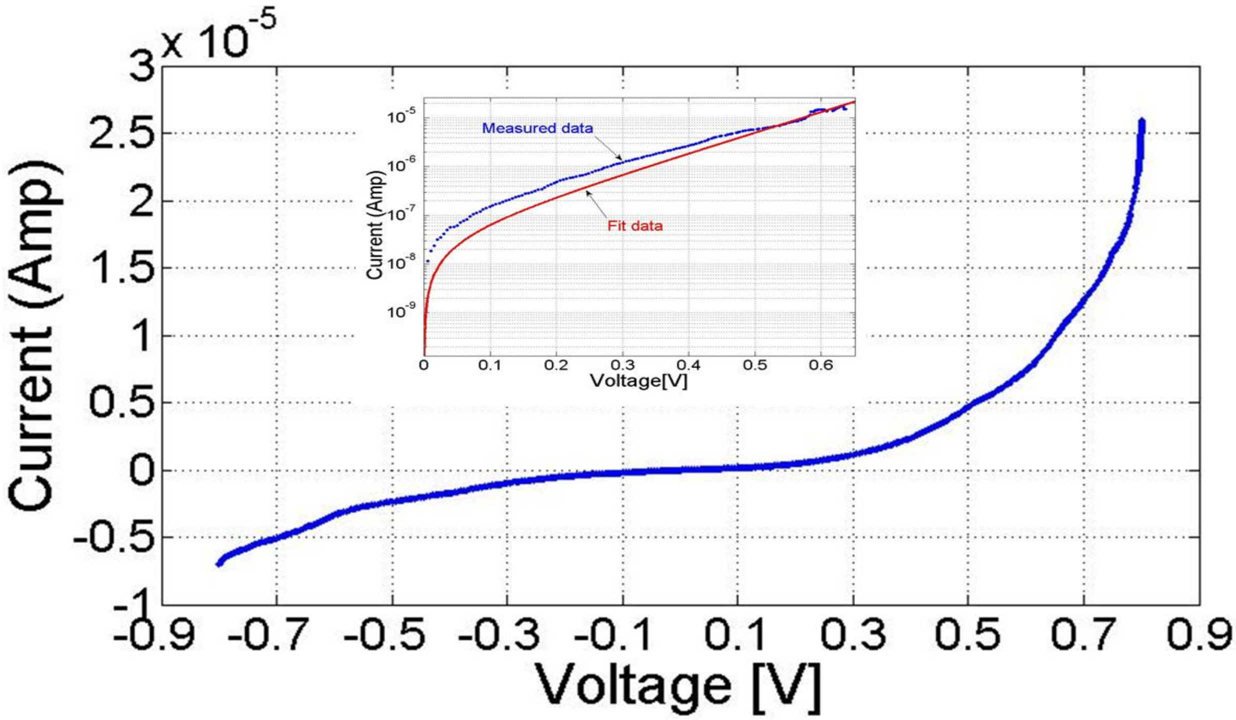

Figure 2.6 I-V characteristics of r-GO based diodes, and curve fit to the diode equation

The inset of Figure 2.6 shows curve fitting of the measured data to the diode equation (Eq. 2.8). The r-GO diodes show a series resistance of 8 KΩ and ideality factor of 2.9. The r-Go diodes shows lower series resistance is due to smaller contact resistance between r-GO and metal as expected from a 2D material like graphene. The contact resistance can be further reduced by annealing the graphene metal contact [116, 117]. This was not attempted here due to the limitations set by the T_g of the flex substrate.

2.7 Microwave Circuit Measurements

The experimental results microwave detection/rectification and multiplications are presented in the following section. All results are presented in this section are after performing system calibration. The high frequency losses were measured in order to estimate the actual power delivered to the device.

2.7.1 r-GO Based Microwave Detector (Rectifier Circuit)

A microwave rectifier produces a DC current/voltage in response to a microwave-frequency voltage. Microwave or millimeter wave rectifiers have applications in wireless power transmission, security, spectroscopy and medical imaging and energy recycling. Microwave rectification can be achieved using different technologies such as micro-bolometer and Schottky diodes. Each technique has different advantages and disadvantages for detection in terms of linearity, frequency cut-off, minimum detected power and the ability to detect fast signals. In this thesis, a r-GO diode based microwave rectifier is demonstrated.

The diodes (integrated in a CPW structures) were measured by directly probing using 50 Ω coplanar GSG wafer probes, and without the use of any matching networks. All the results presented in the thesis are after performing system calibration of the measurement set-up. Signals (RF +DC) are applied to the device through a CPW probe, T-Bias and via a directional coupler (HP87300B). The directional coupler is used to acquire incident/reflected signal from the device using a spectrum analyzer and rectified voltage is measured using a nano-voltmeter. The set-up was calibrated by measuring the incident/reflected signal without connecting the device under test (DUT) and the losses at higher frequency were measured for the input port network. The described setup allows estimating the actual RF power delivered to the device. All values presented are after correction for the reflected signal due to impedance mismatch between the probe and device in a CPW structure.

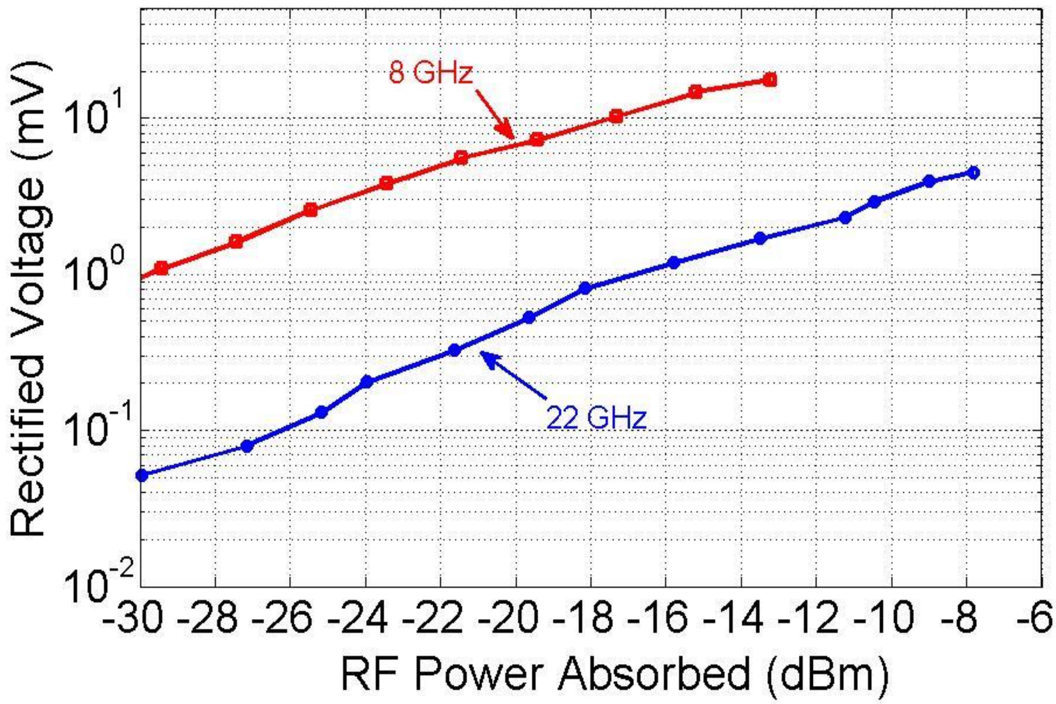

Figure 2.7 Measured rectified output voltage at zero bias versus input power for r-GO Schottky diode at 8 and 22 GHz.

Figure 2.7 shows the rectified voltage as a function of incident power at zero bias for 8 and 22 GHz. The measured result shows that the r-GO based diode has good sensitivity (detection), for instance, graphene diodes shows rectified voltage of 4.5 mV at input power of ~ - 7 dBm (22 GHz) and 11 mV at input power of approximately -13 dBm (8 GHz). From the slope of the curve it can be verified that the detected voltage response changes linearly with input power over a wide power range of - 30 to - 10 dBm for all the measured frequencies. The r-GO based diode shows higher rectification voltage (~ 33V/watt at 22 GHz) than previously reported using graphene nanoribbons based device (~ 8V/Watt at 20 GHz) [47]. Rectified voltage is also measured as a function of applied bias voltage and the results are shown in Figure 2.8. Here the microwave power and frequency were fixed at -15 dBm and 22 GHz, respectively. The low power levels are used for this measurement in order to avoid self-biasing of the diode. The highest rectified signal is at 0.6 V is near the strongest non-linearity part of the diode.

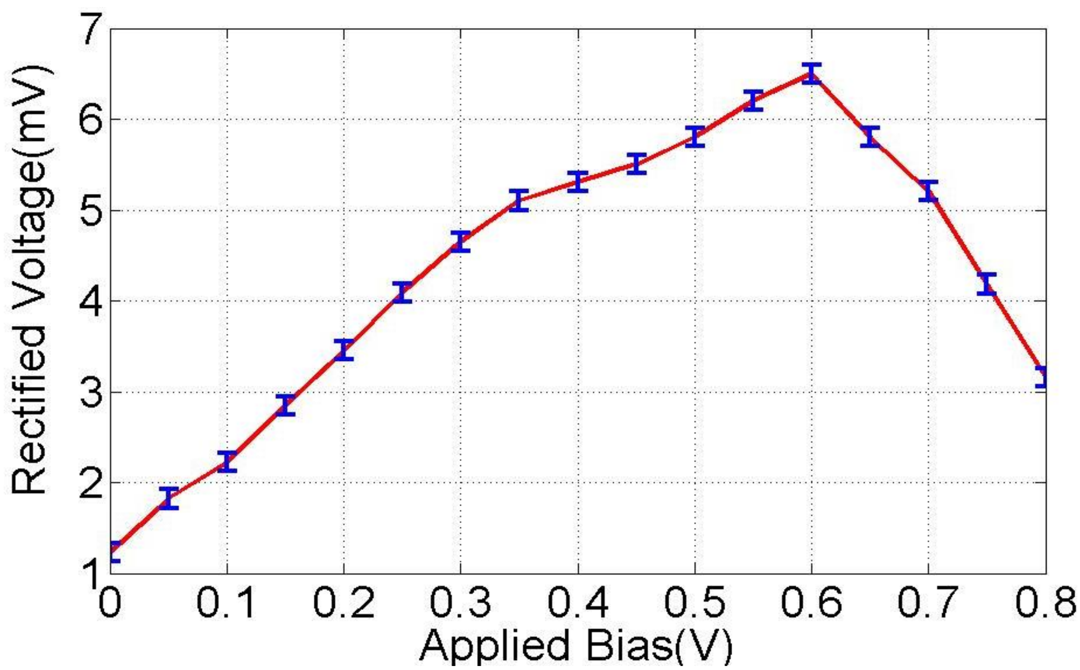

Figure 2.8 Rectified voltage vs applied bias for r-GO diodes at 22 GHz and input RF power of -15 dBm

2.7.2 r-GO Diode Based Frequency Multiplier

Frequency multiplier generates signal with a frequency that is a multiple of the input or fundamental frequency (f_{in}). Diode based frequency multipliers are actively used to generate high frequency signals in the RF to terahertz (THz) frequency range. Diodes with high current, lower series resistance and lower capacitance are required to achieve high frequency multiplication. Recently, graphene based field-effect-transistors have been explored for its application as frequency multiplier based on its ambipolar nature and the sublinear I–V characteristics near the minimum conduction point [42, 43]. Here, r-GO based Schottky diodes are tested for frequency multiplication. For experimental set-up, the RF signal from a signal generator was supplied to the diode through a directional coupler (HP87300B) and output power and frequency is measured using a spectrum analyzer. Frequency multiplication was measured for diodes fabricated in the CPW structures with no external impedance matching circuits. Frequency multiplication results are presented for the fundamental frequency (f_{in}) up to 6 GHz. In this work 3rd order frequency multiplication (3 x f_{in}) was observed, in comparison the output of the 2nd harmonic was lower by 20dB and not shown here. Figure 2.9 shows the output power of the third harmonic for fundamental frequencies in the range of 2 - 6 GHz. The r-GO diode shows an output power -50 dBm for 3 x f_{in} = 6 GHz, and the highest measured output power remains above -65 dBm for frequencies up to 3 x f_{in} = 18 GHz.

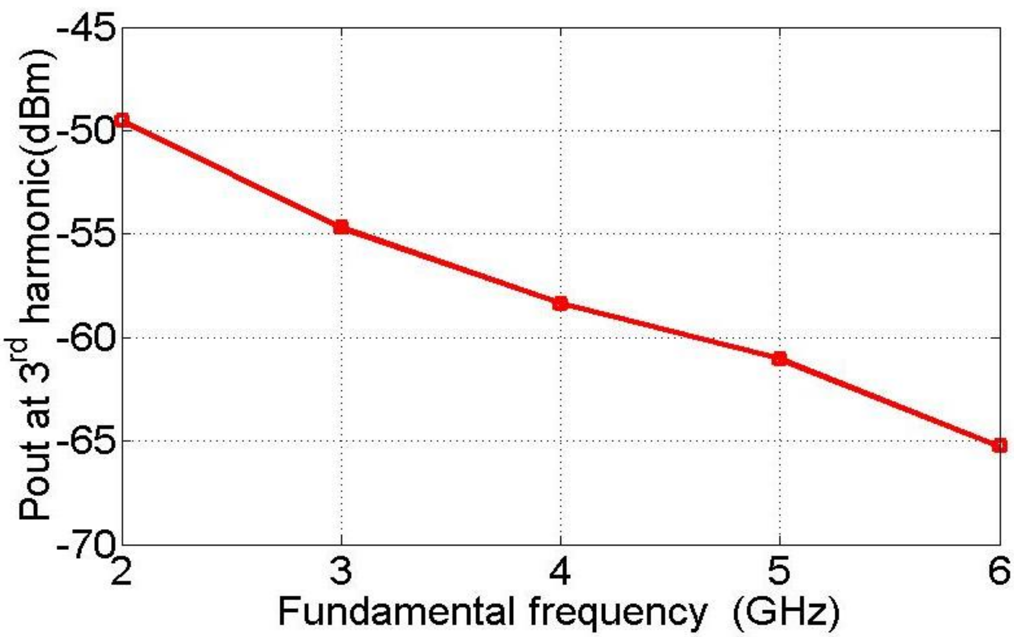

Figure 2.9 Measured output power of 3rd harmonic (3 x fin) versus fundamental frequency of a r-GO device at input power of approximately -3 dBm

The output or conversion efficiency of the diode decreases at higher frequencies due to impedance mismatch. The output power of the 3rd harmonic was also measured as a function of input power at fundamental frequencies of 2, 3 and 4 GHz. Figure 2.10 shows a linear increase in output power with increase in input power, the smooth behavior of the multiplied signal over the entire input power range shows a stable operation of the diode. The r-GO exhibited multiplication over a wide frequency range. Unlike GFET, only the odd harmonics are observed here. The presence of only odd harmonics can be described by nonlinear electromagnetic response in graphene as predicted in [118] which theoretically proves that radiating graphene with a frequency f_0 can generate only odd harmonics. To the best of our knowledge, this is the first report of frequency multiplication with output in the range of 6 – 12 GHz using flexible graphene based devices.

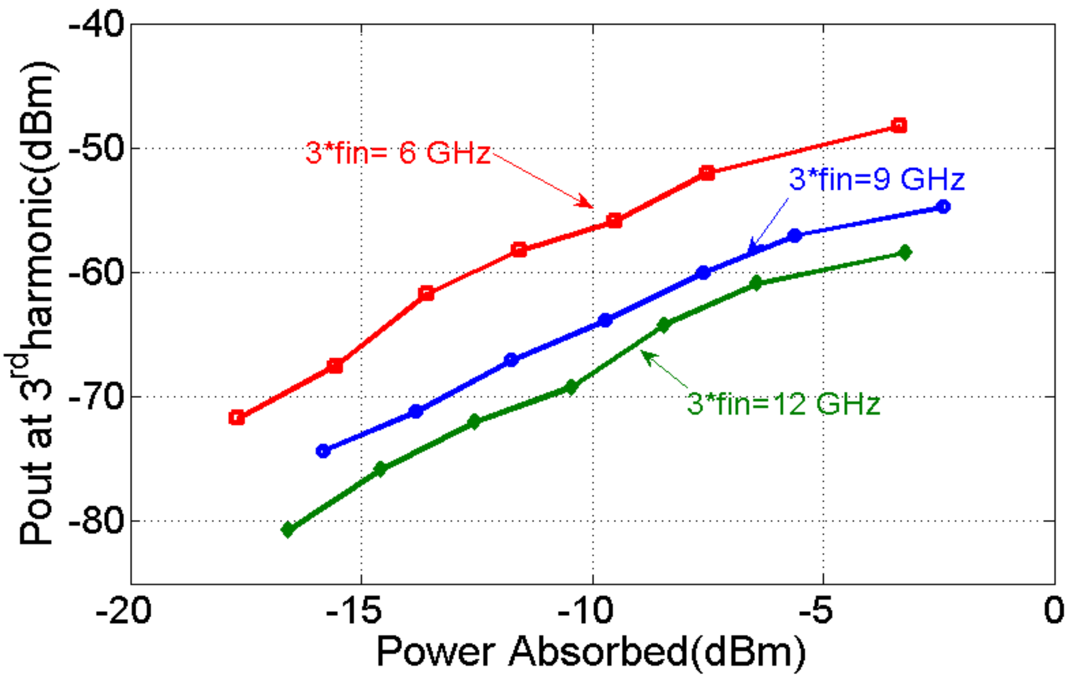

Figure 2.10 Measured output power of 3rd harmonic(3 x fin) for graphene device at fundamental frequencies of 2, 3 and 4 GHz

Previous reported frequency multiplication by flexible graphene circuits is in range of few MHz [49, 50]. In terms of highest frequency multiplied, results presented here are in comparison to recent graphene multiplier from state-of-the-art GFET fabricated on rigid substrate [44].These results are very important and encouraging for pushing the limits of high-frequency nanoelectronics on flexible substrates. All the measurements have been corrected for all the losses due to the cables, input and output port networks. These measurements were done at zero bias but biasing can be done in future to improve the device performance further. In the measured result, the conversion efficiency decreases at higher frequencies due to impedance mismatch. For even harmonics very weak signal was observed. Output signal, 3rd harmonic was also measured as a function of input power of the fundamental frequency.

2.7.3 r-GO Diode Based Frequency Mixer

The non-linearity of active devices can be utilized for RF frequency mixing as they can generate harmonics over a wide spectral range. Recently, a GFET based frequency mixer has been demonstrated using CVD synthesized graphene [45, 46]. Here we present down frequency mixing measurements using an r-GO based diode. Two signals, an RF input signal with frequency f_{RF} = 1.5 GHz and a local oscillator (LO) signal with frequency f_{LO} = 1.0 GHz, were applied to the diode and the intermediate frequency ($f_{IF} = f_{RF} - f_{LO}$) signal is measured. For the experimental set up, the LO signal and RF signals were fed using a broad band power splitter/combiner (11667B, DC - 26.5 GHz). Here, it is used as a power combiner while also providing isolation between the two input signals. The output of the power combiner was connected to the device through directional coupler (HP 873008) and a CPW RF wafer probe. The IF signal generated by the diode was measured using a spectrum analyzer. The measured IF signal vs RF power is shown in Figure 2.11, measured while holding the LO power fixed -14dBm.

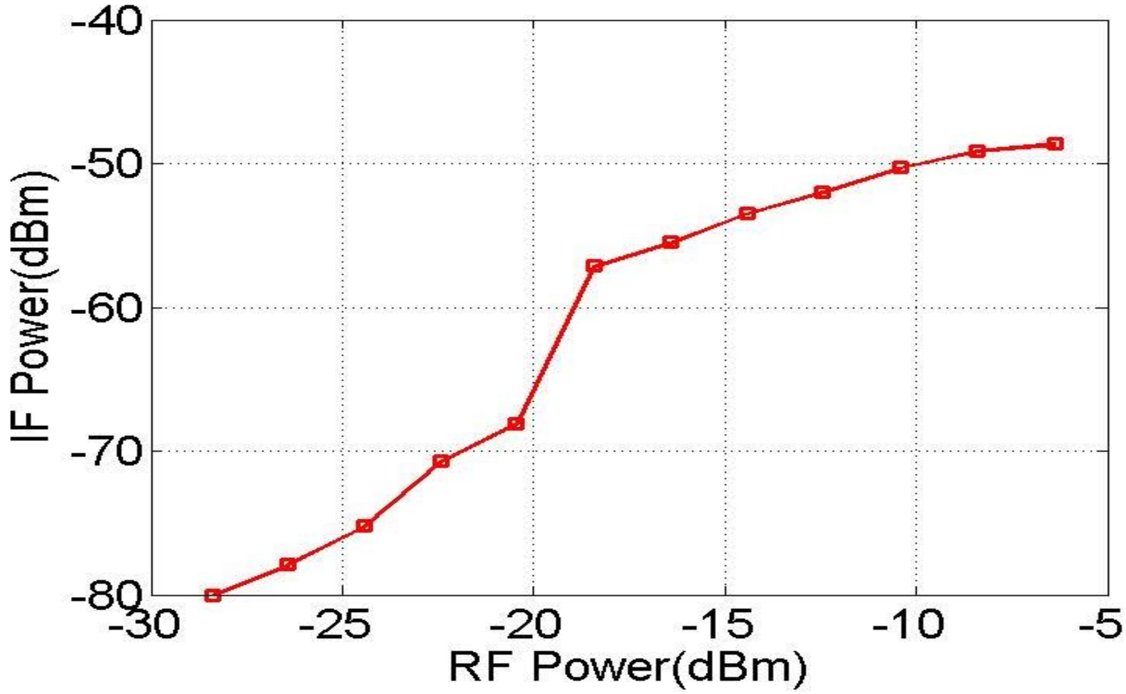

Figure 2.11 Measured IF signal power versus the input RF power with fRF = 1.5 GHz and fLO = 1.0 GHz. The LO signal power was fixed at -14 dBm

The measured results show close to a linear behavior as expected at low input power. A slight deviation from linearity around RF power of -17dBm can be attributed to self-biasing of diode at high input RF power. The frequency performance of this graphene based mixers is better than many previously presented frequency mixers which have operating frequencies in the MHz range [44, 45]. The results are also comparable to best reported graphene based mixer circuit where circuits are fabricated on a rigid SiC wafer [46]. The device was also tested for f_{RF} = 10.5 GHz and f_{LO}=10 GHZ; but the output power for IF (f_{IF} =500 GHz) signal was low approximately less than -80 dBm (Figure 2.12), this may be attributed to poor impedance matching at higher frequencies and lack of availability of high power LO source. In future better experimental set-up or circuit designing can be used to achieve mixing at even higher frequencies using r-GO based Schottky diodes.

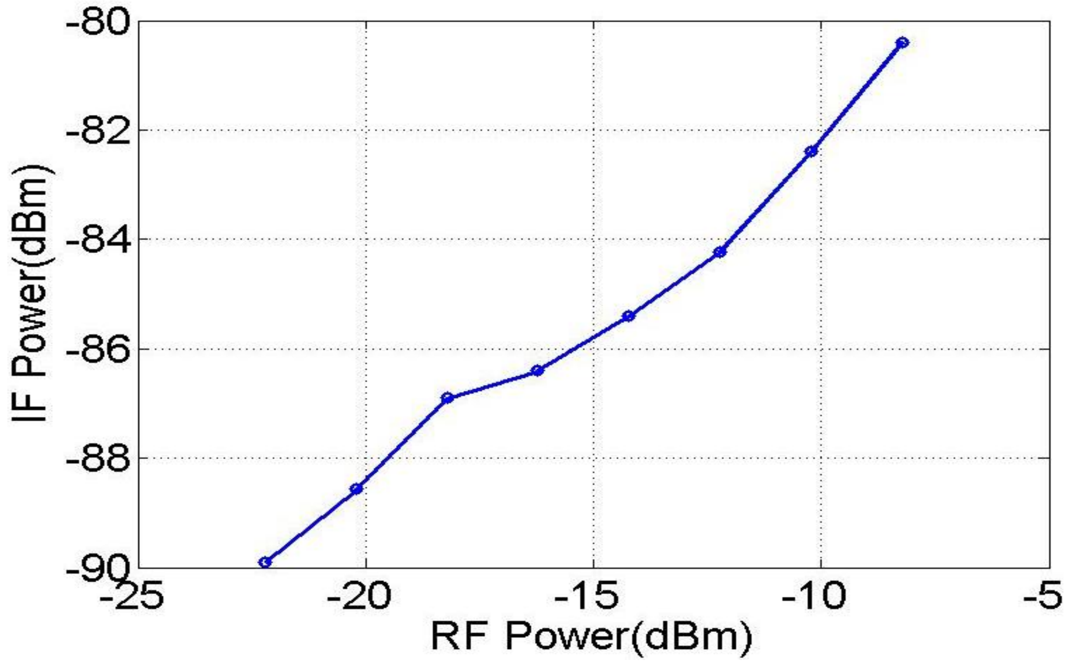

Figure 2.12 (a) Measured IF signal power versus the input RF power fRF = 10.5 GHz and fLO=10 GHz, (fIF =500 MHz)

Overall, r-GO based diodes have been implemented on high frequency compatible flexible substrate (PEEK). The undercut self-alignment process for fabrication of electrodes used allows the use of conventional optical-lithography to achieve small feature size. The diodes show strong non-linear I-V characteristics with forward current achieved on the order of µA and reasonably low series resistances. The r-GO based diodes show better impedance matching than CNT diodes and they show higher detection sensitivity of 33 V/Watt (at 22 GHz). In addition, r-GO based diodes show frequency multiplication in the frequency range of 6 – 18 GHz. The r-GO devices demonstrated here allows for separate control of device size and band gap opening through chemical reduction. This work will motivate further research on realization of high-performance flexible GHz circuits using r-GO.

CHAPTER 3: METAL INSULATOR METAL DIODES FOR FLEXIBLE GHZ CIRCUITS

3.1 Introduction

Metal-Insulator-Metal (MIM) diodes work on the mechanism of tunneling and have been used in a number of high-frequency applications. A MIM tunnel diode is made of two metal electrodes spaced apart by an extremely thin (few nanometers) insulator. Charge transport across the insulator occurs due to quantum-mechanical tunneling of electrons. The tunneling in MIM junctions occurs on a femtosecond timescale [20], which allows theses diodes to work up to THz. The most critical parameter for MIM diodes is thickness of insulator is the thickness of the insulating layer which should not be more than a few nanometers to ensure that tunneling, as opposed to bulk-limited conduction, is the dominant conduction mechanism [120].

3.1.1 Band Diagram

The operation of MIM can be understood from energy band diagram of an asymmetric MIM junction at equilibrium. Asymmetric MIM junction is diodes with two dissimilar electrodes with different work function as shown in Figure 3.1 (a). The band diagram of asymmetric MIM junction diode is shown in Figure 3.1 (b). Work function of the metal 1 and metal 2 are denoted as is Ψ_1 and Ψ_2. Work function is the minimum voltage required to displace an electron from fermi level to vacuum level. The barrier height of metal 1 and 2 is denoted by $Ø_1$ and $Ø_2$, respectively. The barrier height is the minimum energy required to move electron from metal to conduction band (CB). When metal comes into contact with the insulator layer, a continuous fermi level E_F has to be established at interface to bring thermodynamic equilibrium. For electrons in either metal, the potential barrier to overcome at interface is given by $Ø_0 = \Psi_m - \chi$, where χ is the activation energy of the insulator layer [121]. So for asymmetrical contact the barrier height would be different on both side and thus asymmetric I-V characteristics are expected. The barrier height and work function of the metal are related as $\varnothing_1 - \varnothing_2 = \Phi_1 - \Phi_2$

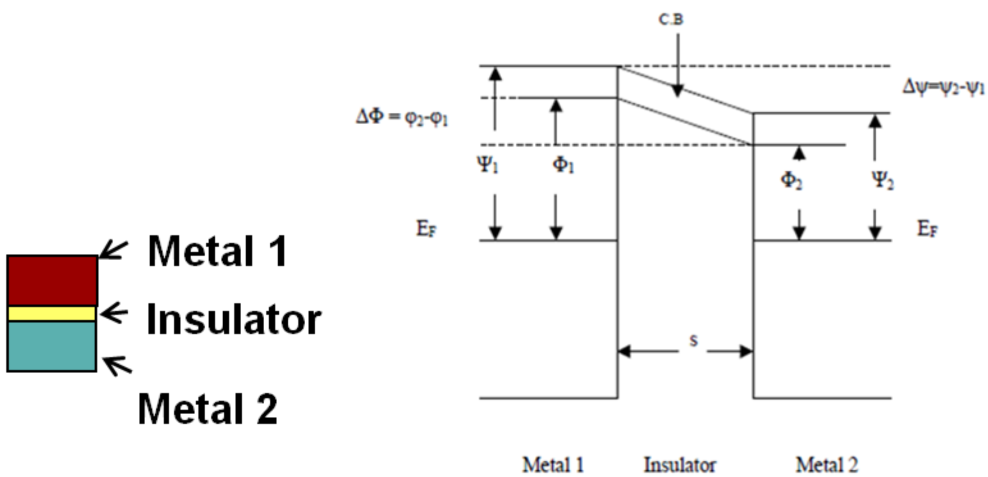

Figure 3.1 (a) and (b) Energy diagram of asymmetric MIM diode at zero bias

The interface of metal insulator does not have straight cut trapezoidal potential barrier in practical diodes/fabricated diodes because of barrier lowering due to image charges. As the electron approach the insulator layer it induces a positive charge at interface which act like image charge and reduce the barrier height by rounding off the corners and ultimately narrowing the barrier [121]. The MIM diodes non–linear behavior and the rectifying characteristics come from asymmetry in I-V characteristics. The height of potential barrier is modulated by applied bias, as when a bias of either polarity is applied; one of the two Fermi levels is elevated, thereby increasing the reference energy level. The barrier width is also affected by applying a bias voltage in similar fashion. When a bias voltage is applied, the Fermi level is moved above the reference energy level (barrier lowering) and thus helping the electrons to tunnel through an insulator with higher probability of finding itself on the other side. The work function of the two metal also affect the potential barrier in similar way as applied bias, and thus to achieve high asymmetry in I-V characteristics, metal with highly different work function should be used.

3.1.2 J-V characteristics

The current obtained from the MIM structure was modeled by Simmons [122] using the Somerfield and Beth Model and WKB approximation. An approximate expression for the tunneling current in the MIM system can be written as

$$J = \frac{J_0}{\Delta S^2}\ [\ \Phi\exp\left(-A\Delta s\sqrt{\Phi}\right) - (\Phi + eV)\exp(-A\Delta s\left(\sqrt{\Phi} + eV\right)]\ ] \qquad 3.1$$

Where J(Amp/cm^2) is the current density at applied voltage V, J0 and A are constants, Δs is the effective barrier thickness in A^o units and Φ is barrier height in V. From this equation it can be observed that the MIM diodes characteristics is highly dependent on dielectric thickness and therefore depends largely on the fabrication methodologies.

3.1.3 Cut-off frequency

The MIM diodes can be considered as a parallel plate capacitor with a thin insulating layer sandwiched between the two electrodes. The performance of a tunneling diode depends on various factors such as dielectric constant of insulating layer, thickness of insulating layer, barrier height (difference in work function between the two metals), device area, etc. Selection of insulator layer is very important for high frequency application as it controls the cut-off frequency. The metals electrodes with the insulator layer(s) between them form a junction capacitance C_d in parallel with nonlinear voltage dependent resistance R_d [123]. The shunt resistance and capacitance are key factors that affect its cutoff frequency, which depends primarily on the oxide thickness and junction area [124]. The cut-off frequency is given as

$$f_c = \frac{1}{2\pi R_d C_d} \qquad (3.2)$$

The estimated frequency of operation of MIM diode can be determined by capacitance which is given by the relation as:

$$C_d = \frac{\varepsilon_0 \varepsilon_r A}{d} \tag{3.3}$$

here ε_0 is the dielectric constant of dielectric, ε_r is the permittivity of free space, d is the thickness of the insulator layer and A is the area of the diode. In order to reduce the capacitance, the contact area or the dielectric constant has to be reduced or the insulator thickness has to be increased. However, from the current vs. voltage relation (Eq. 3.1) it can be seen that the current density of the tunnel junction is exponentially dependent on the insulator thickness. Hence reducing the area of diode and choosing lower dielectric constant is preferred to reduce the capacitance. Also smaller the size of the diode the more uniform is the dielectric deposition. For tunneling to occur the thickness of insulator cannot be more than few nanometers and thus the development of thin insulating layer over entire contact are is very important.

3.2 Heterogeneous Integration of MIM Diodes On Flexible Substrates

The goal of this work is to develop a high speed, high frequency thin film diodes based on MIM technology, which does not require crystalline semiconductor materials, and can be fabricated using standard IC lithographic techniques. This work demonstrates fabrication and characterization thin film Metal-Insulator-Metal (MIM) diodes with carefully selected designed junction area, insulator and metal materials to strengthen nonlinearity and asymmetry of the I-V response. Perform DC and RF Characterization at high frequencies. Characterize the newly developed thin-film MIM diodes using on-wafer. RF probing measurements up to 20 GHz and extract equivalent circuit models. The fabrication process is CMOS-compatible and because the materials are amorphous, may be realized upon on a variety of substrates, thermally grown or deposited SiO_2, chemically mechanically polished SiO_2 on top of existing CMOS circuitry, fused quartz wafers, and polyimide. MIM diodes can work up to THz regime [58]. The use of low loss flex substrate can potentially reduce the cost and improve the performance for high speed communication applications. Two different types of insulators TiO_2 and NiO are used here. Different processes were used to obtain the insulators i.e. in-situ oxidation for TiO_2 and plasma oxidation for NiO. The MIM diodes are fabricated with asymmetric metal contacts i.e. Ti-TiO_2-Pd and Ni-NiO-Ti/Pd to obtain good I-V characteristics. The details of fabrication process, insulator layer deposition, DC and RF characteristics of the diodes are presented.

3.2.1 Design of MIM diode

As discussed earlier to attain a high cut-off frequency low C_d is required which can be achieved with small contact area and smaller dielectric constant of insulator layer. Some of the most commonly used dielectric for MIM diodes are listed in Table. 3. 1 [125].

Table 3.1 Properties of commonly used dielectric for MIM diodes

Material	**Dielectric Constant ε_r**	**Bandgap E_g**	**Electron Affinity EA**
Al_2O_3	9	8.7	1.35
TiO_2	80	3.5	2.95
NiO	11.9	4.0	3.05
HfO_2	25	5.7	2.65
Ta_2O_5	26	4.5	3.75

This work demonstrates the fabrication of MIM diodes on flex substrate using two different dielectric systems are studied i.e. TiO_2 and NiO with different dielectric constant of 80 and 11.9 respectively. As discussed earlier diodes with asymmetric electrodes (work function difference) exhibits non-linear current-voltage characteristics [59-61]. Here, Titanium (Ti)-Palladium (Pd) and Nickel (Ni) -Molybdenum (Mo) are used as asymmetrical metal contacts to TiO_2 and NiO respectively. Pd (5.22 eV) and Mo (4.36) is used as the top layer because it is nonreactive and its work function is different from Ti (4.33) and Ni (5.04) respectively. In the rest of the paper, the diodes are referred as Diode type A for Ti-TiO_2-Pd based diodes and Diode type B for Ni-NiO-Mo [21]. The performance of two different dielectrics is compared using their DC and RF measurements. The NiO based diodes works at higher frequency in comparison to TiO_2 based devices. This can be contributed due to lower permittivity of NiO which can lead to smaller capacitance and thus higher cut-off frequency. For tunneling to occur the thickness of insulator cannot be more than few nanometers, thus thickness cannot be decreased below that. As, the quality of insulating layer is very important for DC and high frequency performances, various techniques has been investigated in past such as atomic layer deposition, sputtering, and electron beam deposition [59-62]. Here, the dielectric layer was obtained using two different approaches i.e. in-situ oxidation for TiO_2 (Type A) and plasma oxidation for NiO (Type B). In addition, diodes with different area were fabricated listed as Diode A1 (48 μm^2), Diode A2 (9 μm^2), Diode B1 (36 μm^2) and Diode B2 (48 μm^2) and their DC and RF performances are compared.

Here, coplanar waveguide (CPW) feed network is used for on-wafer probing and characterization. The MIM diodes are coupled into CPW structures for measurements like rectification, and multiplication. CPW's consists of a center (signal) conductor and a pair of ground planes on each side of the center conductor (GSG). The CPW structures were designed using Linecalc tool form ADS (Advance Design System). The CPW's are designed for 50Ω characteristics impedance for substrate with a dielectric constant of 3.3 and thickness of 250 µm. Along with CPW structures for embedding diodes, calibration circuits are also designed for de-embedding the characteristics of MIM diodes using S-parameters measurements. The electrodes for MIM diodes are fabricated using standard optical lithography to achieve different contact areas. Two lithographic mask layers were utilized to realize the structure, the first mask layer was used to define structure on bottom metal layer (Figure 3.2 (a)) and second mask is used to define the top metal layer (Figure 3.2(b)). The small overlapping area between two mask layers defines the diode area as shown in Figure. 3.2(c). The selected dimensions for GSG are shown in Figure 3.2 (a). The diode was designed to fit within the CPW design as shown in Figure 3.2 (c).

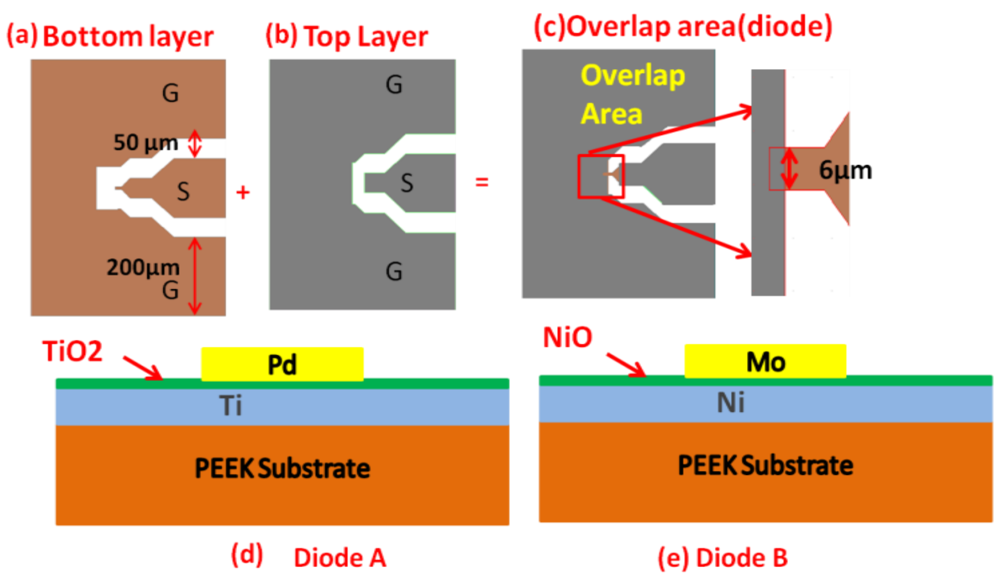

Figure 3.2 Top view of CPW structures (a) Bottom layer of metal/dielectric. (b) Top layer of metal. (c) Small overlap area of two layers defining the diode. (d, e) Schematic of the diodes Ti-TiO2-Pd (Type A) and Ni-NiO-Mo (Type B)

3.2.2 Diode Fabrication

The diodes were fabricated on commercially available flexible high frequency compatible PEEK substrate [113]. The detailed discussion about key selection criteria and properties of various high frequency compatible flexible substrates were discussed earlier in Chapter 2.

Figure 3.3 shows the steps for fabricating type A and type B devices. The PEEK substrate is first cleaned by ultra-sonicating in Acetone and Iso-propanol. For Type A diode (Ti/TiO_2/Pd), the first lithography step is done and the Ti (150 nm) is deposited (Figure 3.3 (A-ii)) using standard e-beam evaporation. A thin layer TiO_2 is then formed using in-situ oxidation technique (Figure 3.3 (A-iii)), by flowing high purity oxygen in the chamber and depositing Ti at slower deposition rates. In-situ oxidation has been done in past to achieve thin TiO_2 films for MIM structures [127, 128].For in-situ oxidation it is desirable to control pressure of oxygen to get thinner oxide layer. Then the lift off of Ti/TiO_2 layer is done (Figure 3.3 (A-iv)) to define the bottom layer of CPW structures (Figure 1(a)). In the next step a thin layer of Pd (150 nm) is deposited using e-beam evaporation and patterned (Figure 3.3 (A-v)). The Pd is selectively etched using $FeCl_3$ releasing the CPW coupled diode.

The small overlapping area between the top (Ti/TiO_2) and bottom (Pd) defines the diode as shown in Figure 1(c). Different area diodes 48 μm^2 (Diode A1) and 9 μm^2 (Diode A2) are fabricated and their RF performances are compared which depends on transit times as discussed earlier. For Type B diode (Ni/NiO/Mo), the first lithography step is done on clean PEEK substrate and the bottom electrode of Ni (150 nm) is deposited (Figure 3.3 (B-ii)) using e-beam evaporation. A thin insulating layer of NiO is then formed through plasma oxidation process (Figure 3.3 (B-iii)). Here, different sets of flow rate of the oxygen, power and plasma time are tried in order to determine a recipe for the continuous film of NiO. Experiments show that an oxygen flow of 60 sccm, power of 200 w and plasma time of 480s generated sufficient barrier layer and also confirmed by nonlinear electrical characteristics of the device in next section. To avoid the etching of PEEK polymer during plasma, the lifting off the metal layer is done after plasma oxidation process (Figure 3.3 (B-iv)). The top metal layer of Mo (150 nm) is deposited using sputtering and patterned using a lift off process (Figure 3.3 (B-v)).

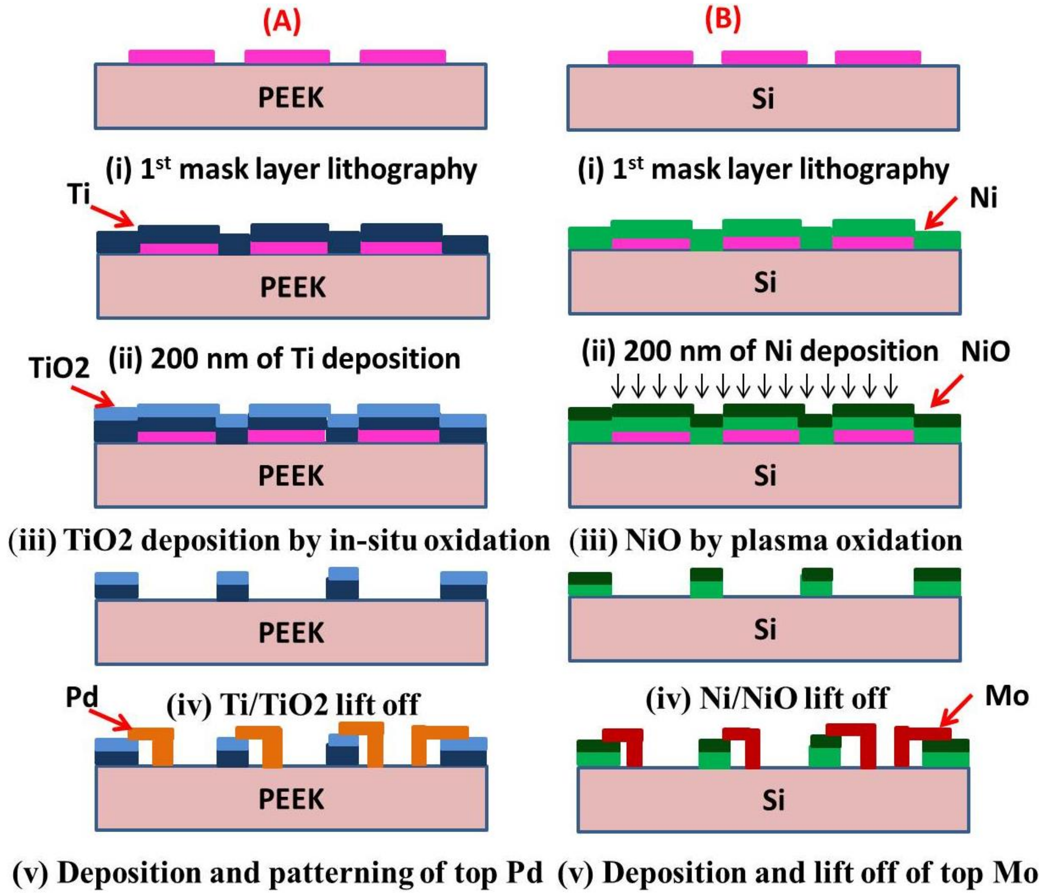

Figure 3.3 Fabrication process for type A (Ti/TiO2/Pd) and type B (Ni/NiO/Mo) MIM diodes

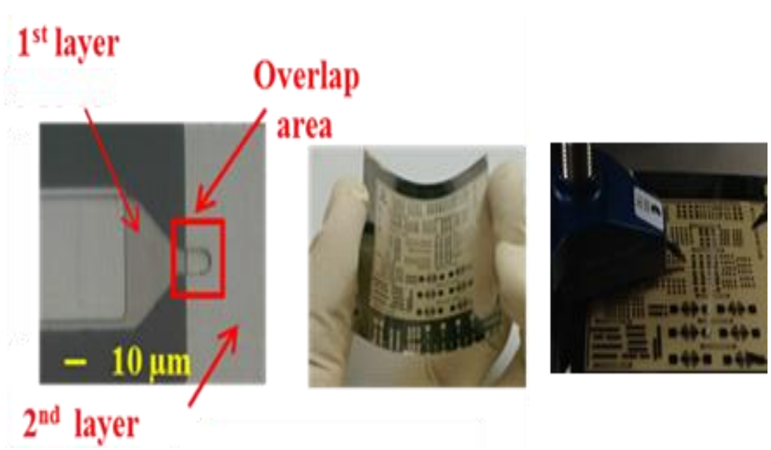

Figure 3.4 Fabricated structures on flexible PEEK substrate

3.3 Current Density- Voltage (J-V) Measurements

The Current Density-Voltage (J-V) characteristics of the MIM diodes are carried out at room temperature. The J-V characteristics of type A diode and type B diode are shown in Figure 3.5 and 3.6 respectively. The type A diodes show the current density much higher than previously reported MIM diodes using native oxide TiO_2 as the insulator layer [127, 128]. The type B (NiO) diode shows current density of 450 mAmp/cm^2 (+ 0.2 V) which better than previously reported diodes (Ni-NiO-Cr/Au) using plasma grown and sputtered NiO and as insulating layer [59, 61, 129]. This can be contributed to barrier height and thickness of insulator layer [53, 54]. The magnitude of J depends on oxide thickness and also on the type of metal used as different type of J-V characteristics can be realized by using different type of diode structures Comparing type A and Type B diode, the former have lower turn on voltage, stronger non-linearity, higher asymmetry and higher current density.

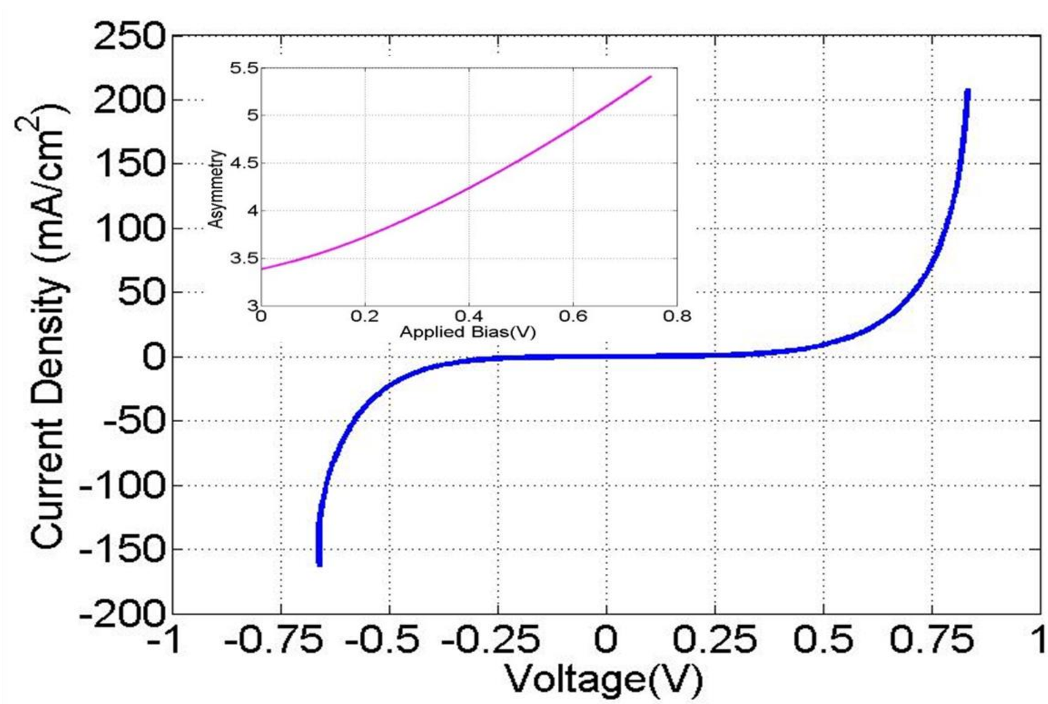

Figure 3.5 Current density characteristics of Ti-TiO2-Pd (Type A) MIM diodes

This can be contributed to thinner and better quality of insulator layer achieved by plasma oxidation. The diodes are fairly asymmetric as required for microwave rectification, however Type B show higher asymmetry (ratio of forward to reverse bias current) in comparison to NiO based diodes (inset Figure 3.5 and 3.7). The Type B diodes shows higher asymmetry than previously reported NiO based diodes [59,61]. Overall,both the diodes show significant non-linearity and asymmetry and thus confirming that the current is due to tunneling of the electrons through thin barrier layer. Overall both diodes show significant non-linearity and asymmetry and thus confirming that the current is due to tunneling of the electrons through thin barrier layer.

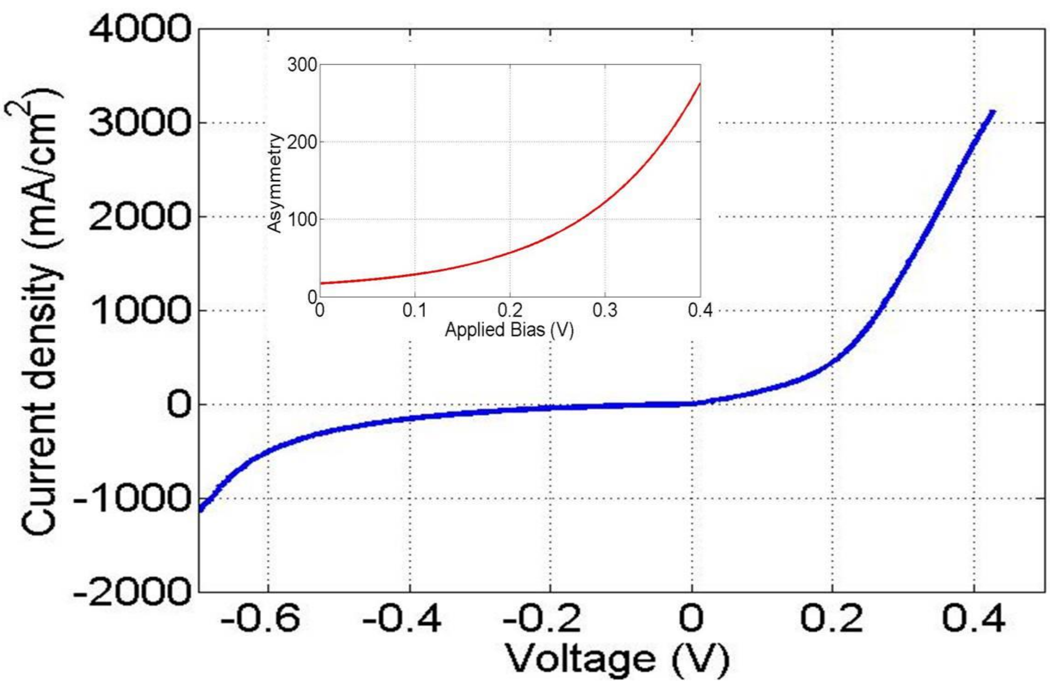

Figure 3.6 Current density characteristics of Ni-NiO-Mo type (B) MIM diodes

In past, MIM diodes has been explored for rectenna applications which requires lower zero bias differential resistance (R=dV/dI) in order to integrate the diodes and antenna with minimum impedance mismatch loss. The diodes presented here show lower zero bias resistance in comparison to previously reported diodes. Bias resistance of 0.2MΩ and 6KΩ are achieved for type A and Type B diodes, respectively. The NiO based diodes have lower differential resistance than TiO_2 based diodes which can be contributed to thinner tunneling barrier. The differential resistance obtains here is much smaller than many of the previously presented NiO based diode [61]. The lower zero bias resistance of Type B diodes further verifies that good quality oxide can be obtained used plasma oxidation process. The diodes reported here exhibits a significant degree of non-linearity and asymmetry as required for microwave circuits of interest microwave rectification and frequency multiplication.

Typically, the I-V characteristic of a MIM diode is measured under forward biased conditions. When the diode is forward biased, the average height of the barrier lowers thereby increasing the tunneling probability and hence the current flow. The tunneling probability is increased when the barrier width of the insulator is also extremely thin. An approximate value of the dielectric thickness and the barrier height between the metal-oxide interfaces can be determined theoretically by using the relationship formulated by Simmons [121]. For a MIM tunnel junction with dissimilar electrodes separated by a thin insulator, the electron tunnel effect was defined by Simmons [121] and given by as:

$$\mathrm{J} = \frac{6.2*10^{10}}{s^2}\ [\ \Phi \exp\left(-1.025\mathrm{s}\sqrt{\Phi}\right) - (\Phi + \mathrm{eV})\exp(-1.025\mathrm{s}\left(\sqrt{\Phi} + \mathrm{eV}\right)]\ ] \qquad (3.4)$$

where J is the current density in A/cm^2, s is the effective barrier thickness in Å units and Φ is the mean barrier height in eV. The barrier height value at each interface plays the key role regarding the tunneling efficiency, asymmetry and non-linearity in MIM diodes. The barrier height value is defined as the difference between the work function of the metal and the electron affinity χ of the insulator at metal-insulator interfaces. There will be two different potential barriers that are between metal one and the insulator $\Phi1$, and between the metal two and the insulator Φ1. These two interfaces determine the turn on and breakdown voltages depending on the work-functions of the metals.

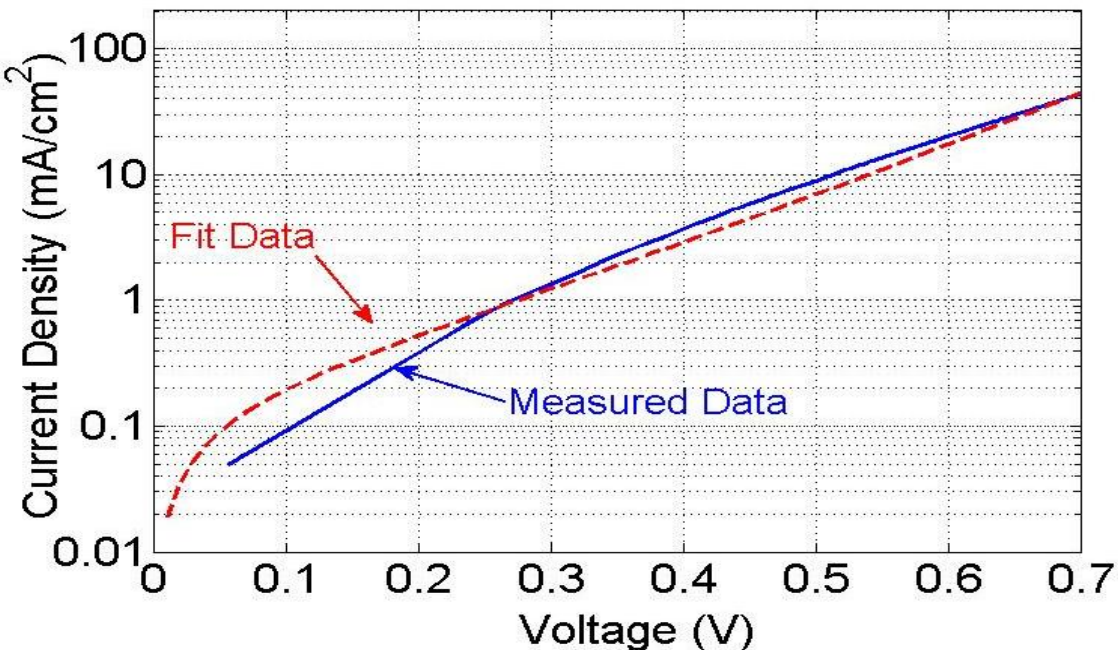

Figure 3.7 J-V characteristics of TiO_2 based diode showing measured data and theoretical fit.

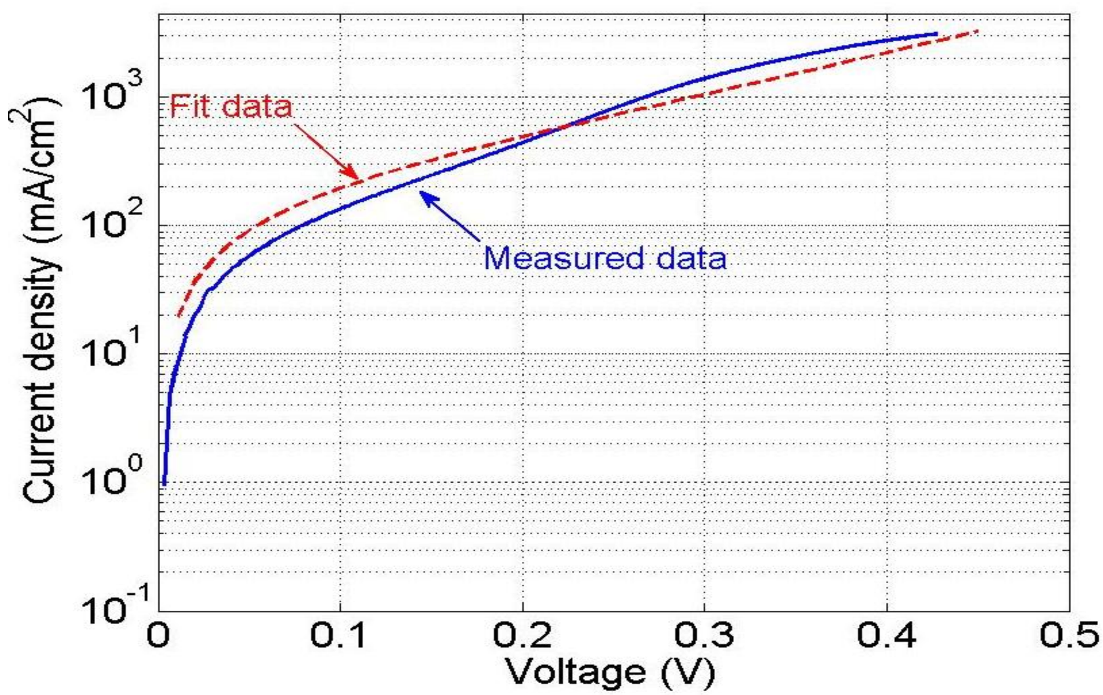

Figure 3.8 J-V characteristics of NiO based diode showing measured data and theoretical fit

For a forward bias, the tunnel current density was obtained by substituting S as physical thickness of the insulator and $\Phi=(\Phi1+\Phi2-V)/2$ in Eq. (3.4). To determine the theoretical current density–voltage (J–V) fit, it is necessary to determine the parameters s, Φ. Typical barrier heights reported were much lower, usually 1 eV or less. Hence the barrier height was determined by curve-fitting to measured data points. Fig. 6(A) and (B) shows the theoretical fit to TiO_2 and NiO based diode. The parameter obtained by curve fitting for TiO_2 based diode are as Φ1=0.45 eV, Φ2=1.32 eV and s=30 Å. For a NiO based diode parameters obtained are as: Φ1=0.45 eV, Φ2=0.95 eV and s=24 Å.

3.4 Microwave Measurements

All results are presented in this section are after performing system calibration. The high frequency losses were measured in order to estimate the actual power delivered to the device. All power values presented in this letter are corrected for this effect unless otherwise noted. The experimental results for S-parameter measurement, microwave detection/rectification and multiplications are presented in following section.

3.4.1 S-Parameter Measurements and Equivalent Modeling

The S-parameters are measured using Network Analyzer (Agilent N5227A) in the frequency range of 1-20 GHz, with input power (P_{in}) of -10 dBm and at a fixed DC bias of 0.25 V and 0.2 V for Type A and Type B diode respectively. The measured S-parameter data is then fitted to the equivalent RLC circuit model of the diode using Agilent ADS. The equivalent RLC circuit model includes voltage dependent diode resistance (R_d), series resistance (R_s), series inductance (L_s) and diode shunt capacitance (C_d) as shown in Figure.3.9. The extracted values from the fitted model for all the devices are shown in Table 3.2. Devices with high cut-off frequency requires smaller RC constant.

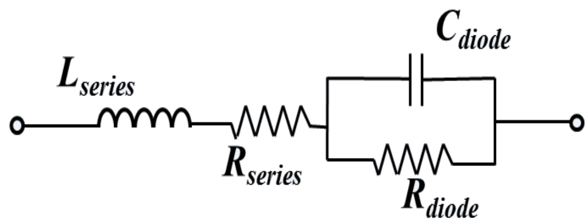

Figure 3.9 Equivalent circuit models for MIM diode

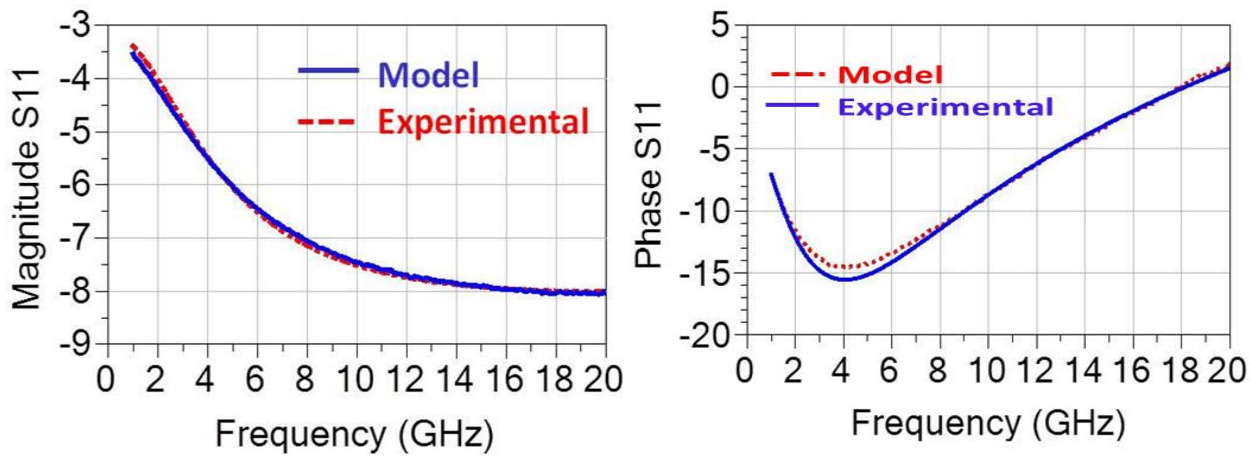

Figure 3.10 Measured S-parameters and fit using extracted equivalent circuit for Ti-TiO2-Pd diode (Type A1)

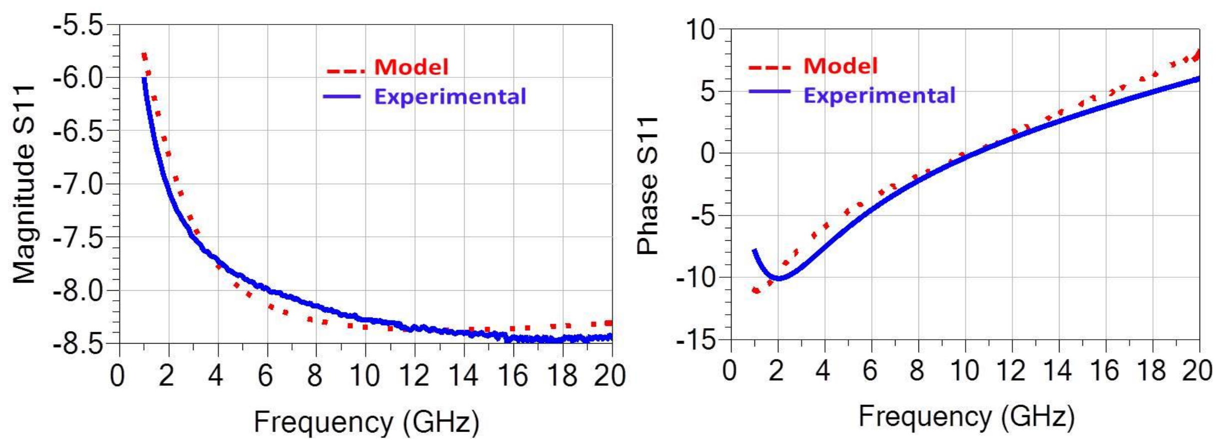

Figure 3.11 Measured S-parameters and fit using extracted equivalent circuit for Ti-TiO2-Pd diode (Type A2)

The measured S-parameters (magnitude and phase) and fit to the s-parameters from equivalent circuit for Type A1 and Type A2 diodes is shown in Figure 3.8 and 3.9, respectively. Figure

3.12 shows measured and fit data (S-parameters- Magnitude and Phase) for diode B2, diode B1 is not shown here as the s-parameter is almost similar to diode B1 due almost similar area. Type A diodes also show higher series resistance which can be contributed to thicker oxide and lower conductivity of the Ti metal itself and can be improved by increasing the thickness of the metal. The diode resistance depends on voltage while capacitance of diode is mainly related to contact area, dielectric constant and thickness and the cut off cutoff frequency of the diode was determined from its RC constant. Comparing the same type of diodes with different area, i.e. Diode A1 vs A2 and Diode B1 vs. B2, the capacitance scales with area.

Table 3.2 Equivalent model values derived from measured S-parameters

Device	**Area (μm^2)**	**C_d (fF)**	**Rd (Ω)**	**L_s(pH)**	**R_s (Ω)**
$Ti/TiO_2/Pd$	A1($9\mu m^2$)	165	68	225	102
	A2($48\mu m^2$)	802	40.9	225	102
Ni/NiO/Mo	B1($36\mu m^2$)	310	50	165	15
	B2($48\mu m^2$)	400	40.91	165	15

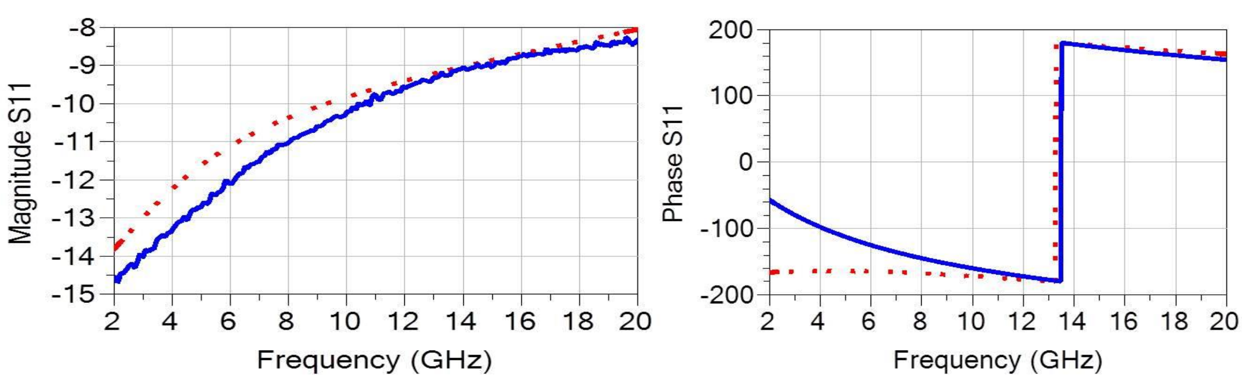

Figure 3.12 Measured S-parameters and fit using extracted equivalent circuit for Ni-NiO-Mo diode (Type A2)

Thus from the equivalent model, area required for devices with cut off frequencies in MMW or THz range can be estimated/calculated. Diode B2 shows lower value of Capacitance than diode A2 although the area is same, this clearly shows that the dielectric constant of NiO used here is much smaller that TiO2 and hence more suitable for circuits with higher cut off frequency. Type A diodes also show higher series resistance which can be contributed to thicker oxide and lower conductivity of the Ti metal itself. Metal loss can be reduced by increasing the thickness of the metal. The area required for higher cut off frequencies can be estimated from these results.

3.4.2 MIM Diodes Based Microwave Detector/Rectification

Microwave rectifiers convert a high frequency signal into a low frequency electrical output. Microwave rectification has applications in wireless power transmission, concealed weapon detection, spectroscopy and medical imaging and energy recycling. Diode detectors are especially desirable since no cooling or vacuum packaging is required as needed in thermal detectors. High frequency MIM diodes coupled with antennas/waveguides are increasingly explored for application in microwave circuits as they provide good device scalability for Microwave/MMW detectors [53, 54]. However, in most of the previous work, rectification sensitivity is calculated from I-V characteristics (ratio of second derivative and first derivative of the I-V characteristic of the diode). There are only few papers presenting direct measured results of rectification for MIM diodes fabricated on rigid substrates [130]. In this work, we presented experimental results for rectification by MIM diodes fabricated on flexible substrate. The diodes (embedded in CPW structures) were measured by directly probing using 50 Ω coplanar GSG probes and without the use of any matching networks. For the measurement, the signal (RF +DC) is applied to the device through a CPW probe, T-Bias, directional coupler, spectrum analyzer and nano-voltmeter. All results presented in this section are after performing system calibration and after measuring the losses at higher frequency. The power values presented are actual power delivered to the device. Figure. 3.13 and 3.14 shows the measured rectified voltage signal as a function of input power for Diode type A and B with fixed bias of 0.25 V and 0.2 V, respectively. All measurements were performed at room temperature and power levels between 0 dBm and -25 dBm are used. The rectified voltage is measured at different frequencies.

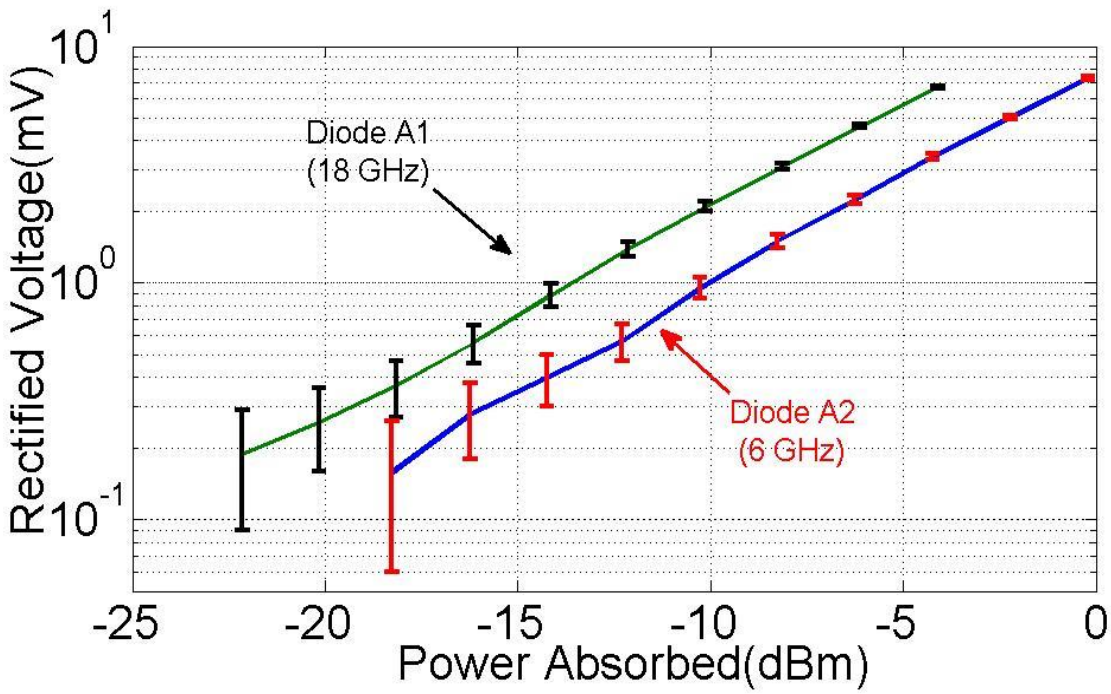

Figure 3.13 Measured rectified voltage versus input power for Type A(Ti/TiO2/Pd) devices at 6, and 18 GHz

The rectified voltage decreases as frequency increases due to the parasitic associated with the diode. The measured result shows reasonably high rectified voltage for both type A and type B diode. Type A diodes shows rectified voltage 4.6 mV (18 GHz) and 2.25 mV (6 GHz) for Diode A1 and A2 respectively, at input power levels of -6 dBm. Type B diode shows rectified voltage 12.56 mV (18 GHz) and 4.6 mV (16 GHz) for Diode B1 and B2 respectively, at input power levels of -6 dBm. In general, smaller area diodes show good rectification even at higher frequencies, whereas the bigger devices are limited by transit time. The performance of the device at higher frequencies can be improved by lowering the junction capacitance (smaller area diode).From the slope of Figure 3.13 and 3.14, it can be verified that the rectified voltage response is linear (log scale) over a wide power range and follows the square law detection with slight deviation. Comparing the rectification performance of best performing TiO_2 and NiO based diodes at 18 GHz, diode A1 shows of 18 V/Watt while diode B1 shows and 70 V/Watt. This clearly shows even larger diodes (B1 ~ 36 μm^2) can be used to get better performance than smaller area diode (A1~ 9 μm^2) depending on the dielectric chosen. Overall diodes type B is performing better than type A devices. This can be contributed to smaller turn-on voltage and smaller work function difference between two electrodes and most importantly due to lower dielectric constant of NiO

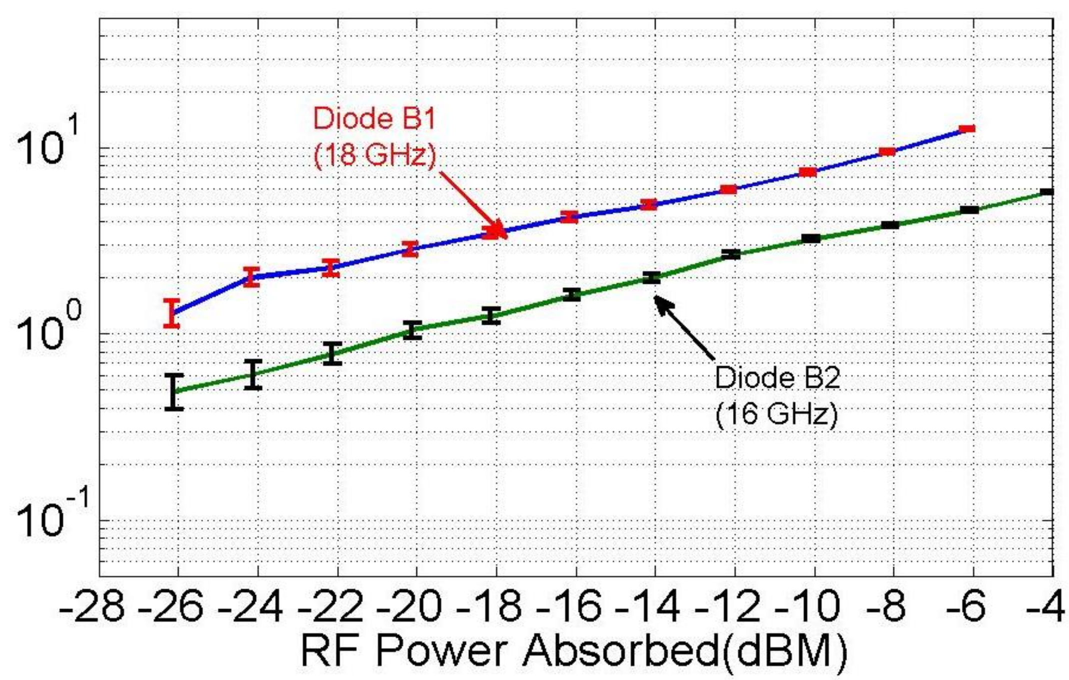

Figure 3.14 Measured rectified voltage versus input power for Type B (Ni/NiO/Mo) devices at 16, and 18 GHz..

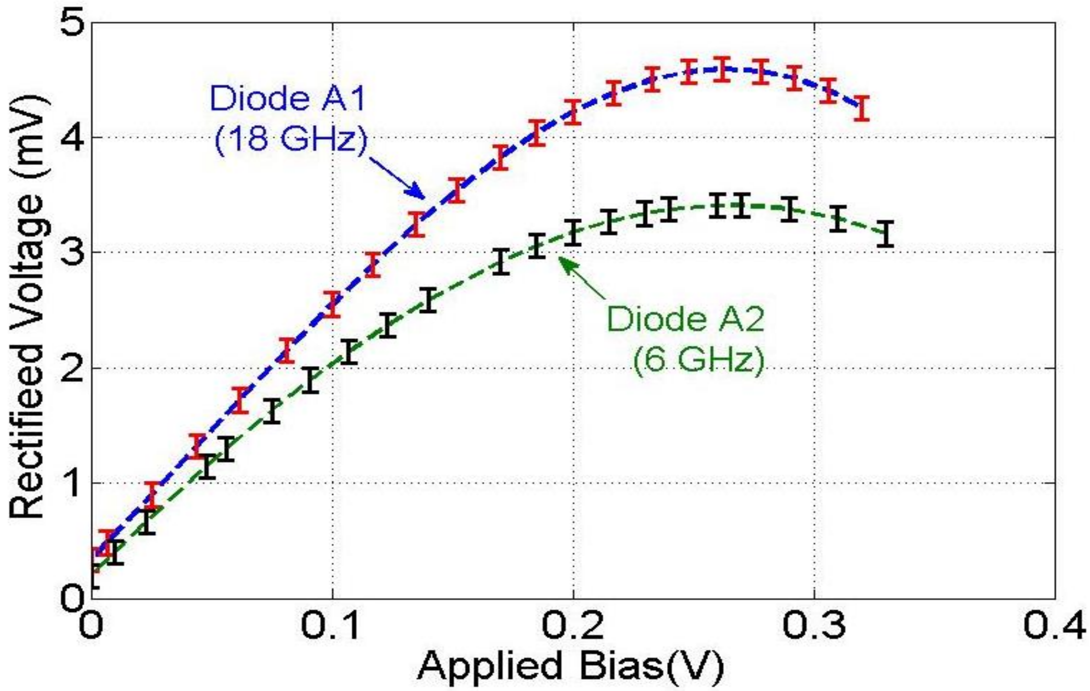

Figure 3.15 Rectified voltage vs Input Bias for Diode type A(Ti-TiO2-Pd) with different area A1(9 µm2) and A2(48 µm2)

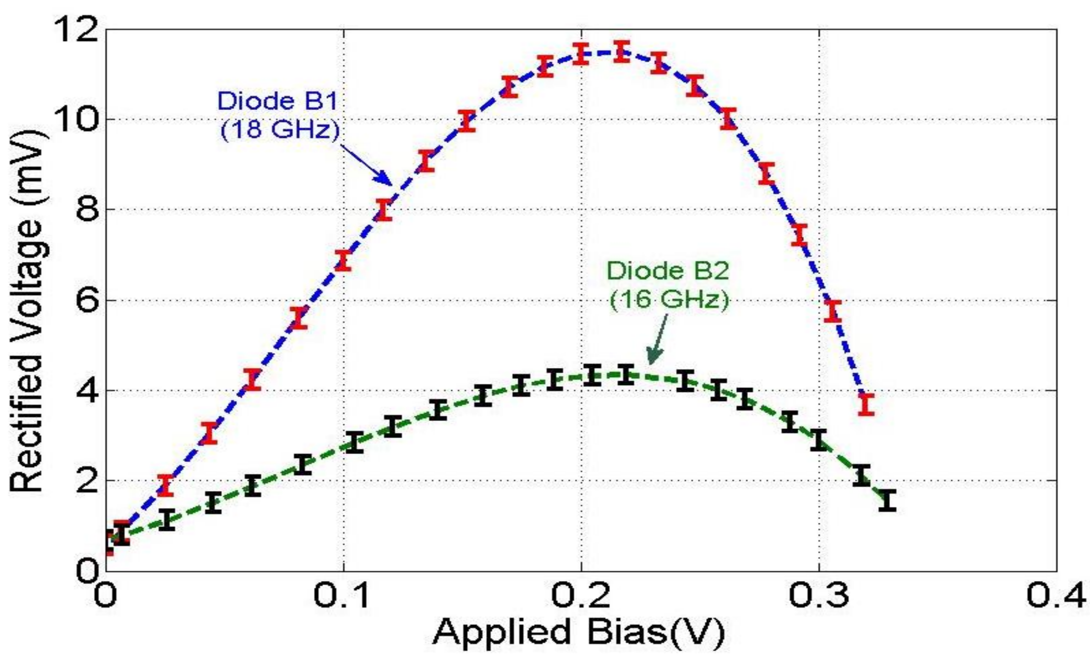

Figure 3.16 Rectified voltage vs Input Bias for Diode type A(Ni-NiO-Mo) with different area B1(36 µm2) and B2(48 µm2)

Rectified voltage was also measured as a function of bias with fixed frequency and input power. Figure 3.15 and 3.16 shows the measured rectified voltage as a function of applied DC bias for a fixed incident power ~ -6 dBm. The highest measured rectified voltage is near the applied bias of 0.25V (Type A) and 0.2 V (Type B) which is slightly lower than the strongest non-linearity point of the diode based on I-V measurements. This can be attributed to self-biasing of the diode due the high input RF power. These preliminary results clearly show device that devices have good sensitivity and it can significantly be improved by reducing the series resistance of the diodes and through good impedance matching.

3.4.3 MIM Diodes Based Frequency Multiplier

Frequency multipliers have been used as signal generators to generate high frequency signals and can be achieved using non-linearity of the device. Frequency multiplication is an important part of RF communication and can be realized using non-linear devices like diodes and FETs. Diodes based multipliers have higher bandwidth than transistor based amplifiers although the conversion efficiency decreases at the higher harmonics. Diodes based frequency multiplier coupled with antennas are often used for wireless sensor and wireless power transmission application. Diode with high current density, lower series resistance and lower capacitance is required to achieve frequency multiplication. To the best of our knowledge, this is the first report of frequency multiplication using flexible MIM diodes. For experimental set-up, the RF signal from a signal generator was supplied to the diode through a directional coupler (HP87300B) and T-Bias and output power and frequency is measured using a spectrum analyzer. Second (2 x f_{in}) and third (3 x f_{in}) order frequency multiplication was observed for both TiO_2 and NiO based diodes, but the output of 3rd harmonic is smaller in comparison to 2nd harmonic as expected. Figure 3.17 and 3.18 shows the output power of the 2nd and 3rd harmonic for Type A and Type B diode as a function of frequency with fixed input power level. Comparing the performance of TiO_2 and NiO based diodes with same area (48 μm^2) i.e. Diode A2 vs. Diode B2, the later shows 2nd order frequency multiplication for higher fundamental frequencies i.e. up to 10 GHz while Diode A2 shows multiplication up to 4GHz only. In addition, Diode B2 shows much higher output power at 2nd harmonic of -52 dBm ($2*f_{in}$=20 GHz) in comparison to diode A2 which shows an output -66 dBm ($2*f_{in}$=8 GHz) at same input power of -4.0 dBm. Comparing Diode A1 and Diodes B1, the later performs better at higher frequencies although its area is 4 times larger than Diode A1.

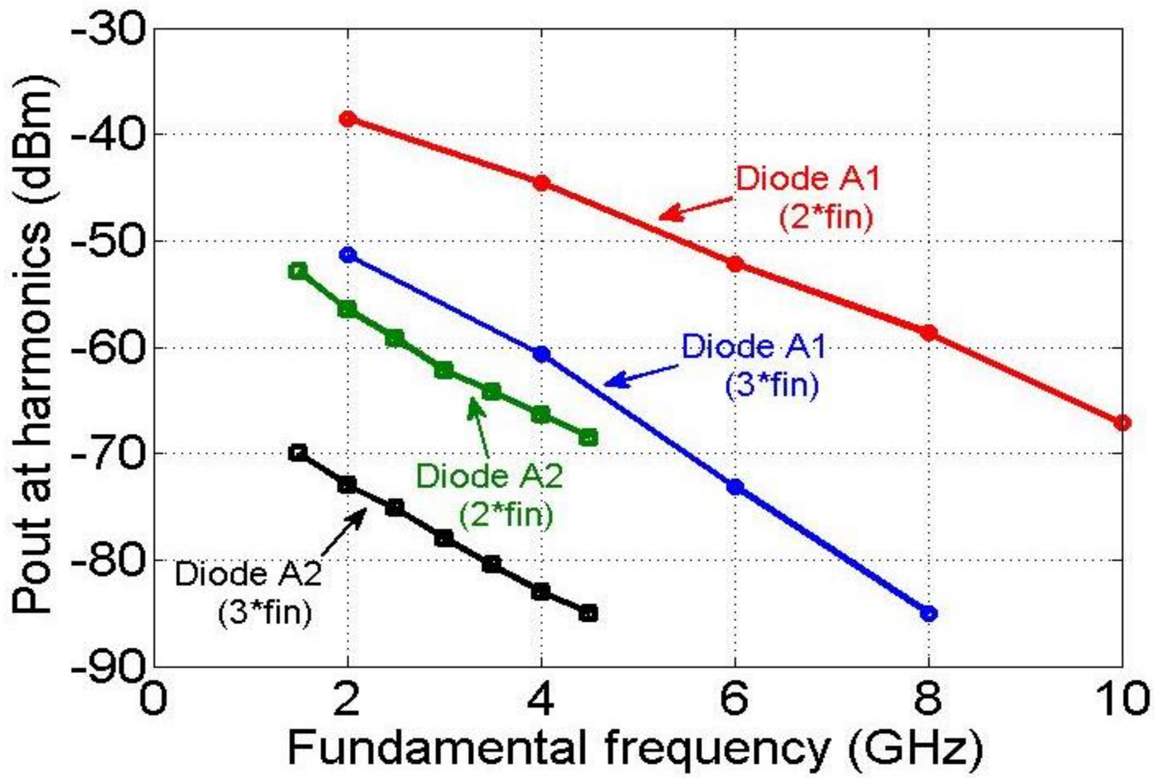

Figure 3.17 Measured output power of 1st and 2nd harmonic versus fundamental frequency forTi-TiO2-Pd based devices with different area, at input power of ~ -4 dBm

Overall, NiO based diode has better performance. It can be contributed to smaller series resistance due to thinner oxide and lower capacitance due to lower dielectric constant of NiO based devices. The MIM diodes also shows third harmonic. The best performing TiO_2 (Diode A1) based diodes shows 3rd harmonic for f_{in} of 2- 6 GHz, while NiO based diodes shows 3rd harmonic up to much higher input frequencies. In the measured result, the conversion efficiency decreases as the fundamental frequency increase which is expected due to transit time loss and impedance mismatch. . To achieve frequency multiplication at even higher frequencies smaller area diodes can be fabricated in future.

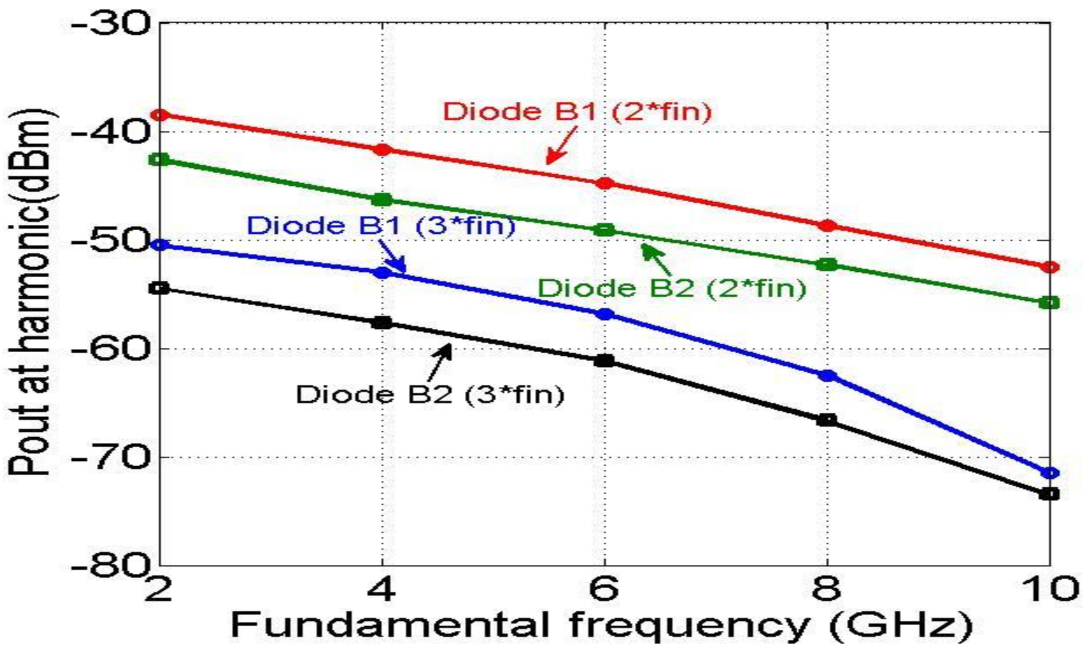

Figure 3.18 Measured output power of 1st and 2nd harmonic versus fundamental frequency for Ni-NiO-Mo based devices with different area at input power ~ -5dBm

The output power of 2nd harmonic was also measured as a function of input power. Figure 3.19 and 3.20 shows the output power of the 2nd harmonic as a function of input power for Type A and Type B diodes at different fundamental frequencies. The output power increases linearly with input power over the entire input power range, and a smooth behavior shows a stable operation.

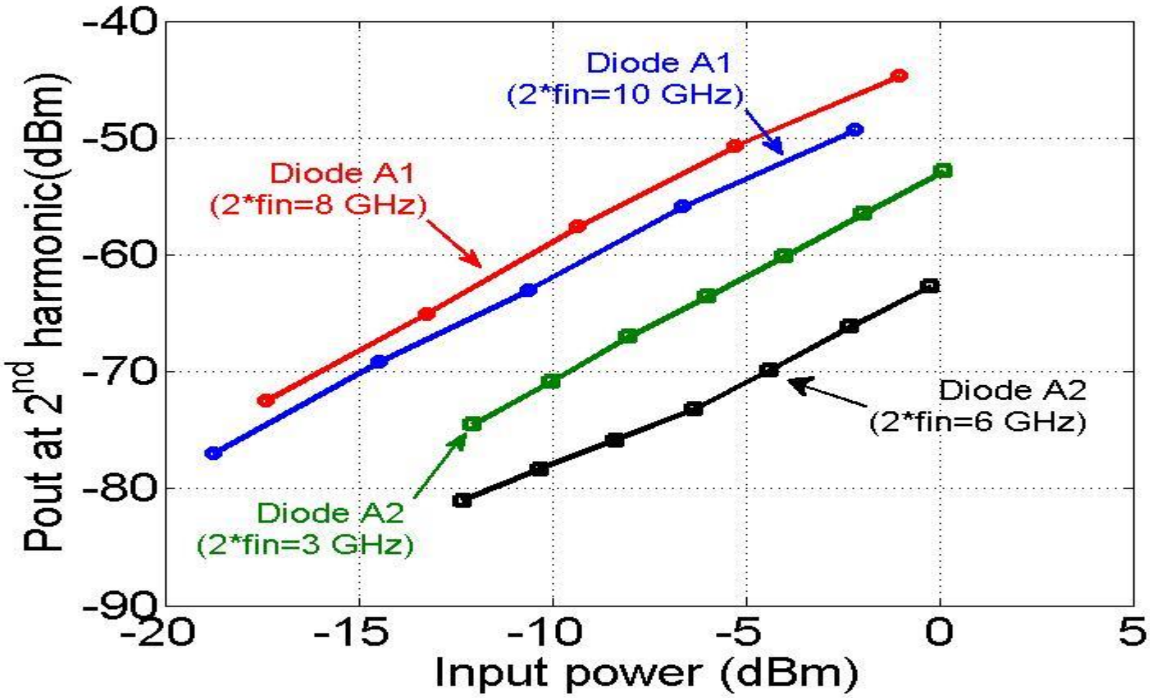

Figure 3.19 Measured output power of 2nd harmonic for Ti-TiO2-Pd based devices with different area

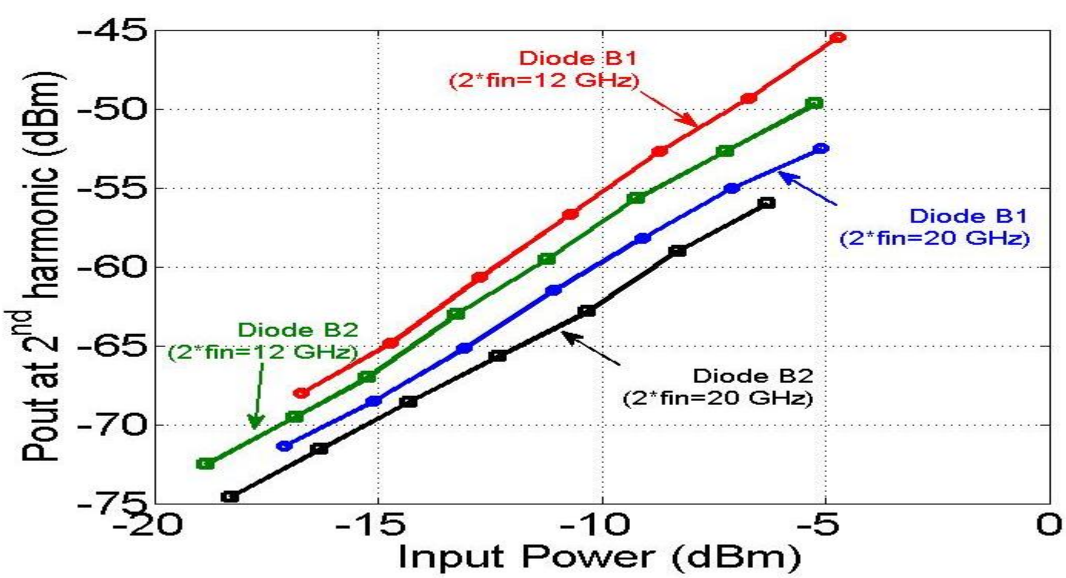

Figure 3.20 Measured output power of 2nd harmonic for Ni-NiO-Mo based devices with different area.

This linear change further proves that the diodes were driven effectively and the nonlinearity was good enough to trigger harmonic signal. The P_{out} for A2 is much smaller than A1 due to bigger area. The result for frequency multiplication shows the same trend as for detection, i.e. NiO device performing better than TiO_2 devices. In future the results can be further improved by employing an impedance technique and bandpass filter to filter the desired harmonic and suppress unwanted frequencies.

3.4.4 MIM Diodes based frequency mixer

The non-linearity of MIM diodes can also be utilized for RF frequency mixing to generate the frequency difference. Here, we demonstrate the use of these diodes for mixing applications. For the experimental set up, the Local oscillator(LO) signal and RF input signal(RF) were fed using a power splitter (11667B, DC-26.5 GHz) which was used here as a power combiner and also to provide isolation between LO and RF signal. The output of the power combiner was connected to a directional coupler (HP 873008) which in turn was connected to CPW probe through T-Bias. The output of coupler is connected to the spectrum analyzer to measure the output intermediate frequency (IF) signal. Figure 3.21 shows the output power for IF signal vs. Input RF power for Diode A1and Diode A2 for f_{RF}=4 GHz and f_{LO}=3 GHz. These measurements are done at fixed bias of 0.25 V and at room temperature. The IF signal is also measured at three different LO powers, and the results show close to a linear behavior as expected. The performance of Diode A1 at f_{RF}=4 GHz and f_{LO}=3 GHz is much better than Diode A2 for approximately same RF and LO input power. The Diode A2 due to its large contact area and thus smaller cut off frequency doesn't show down conversion at frequencies above 4 GHz. Diode A1 performs well even at f_{RF}=16 GHz and f_{LO}=15 GHz with a strong down-conversion of ~ -63 dBm at a LO power of -14.67 dBm as shown in Figure 3.22. Down conversion efficiency can further be improved by increasing the LO power.

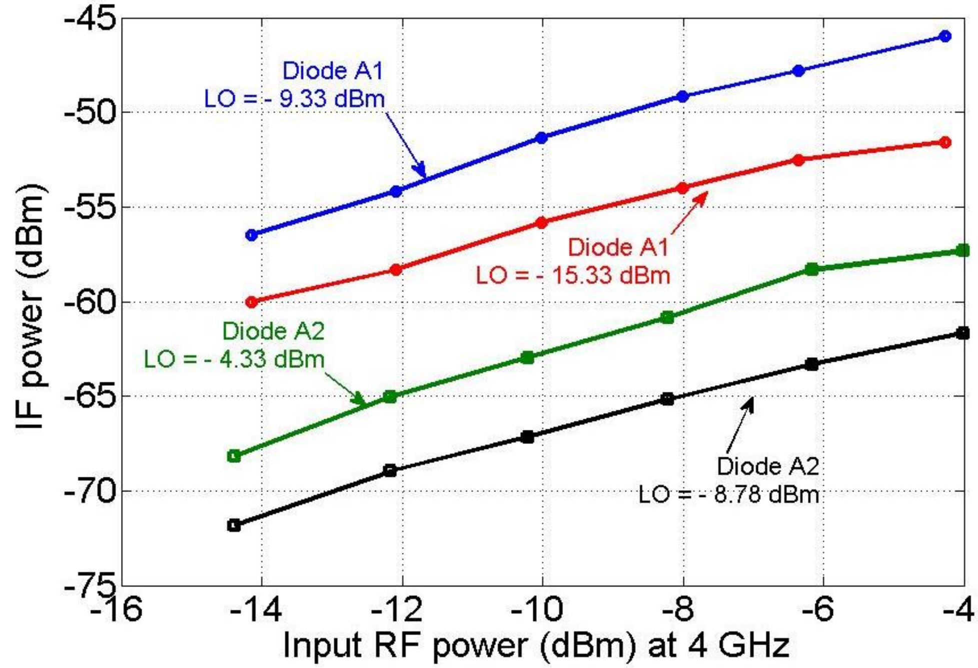

Figure 3.21 Measured output power of 2nd harmonic for Ni-NiO-Mo diodes with different area

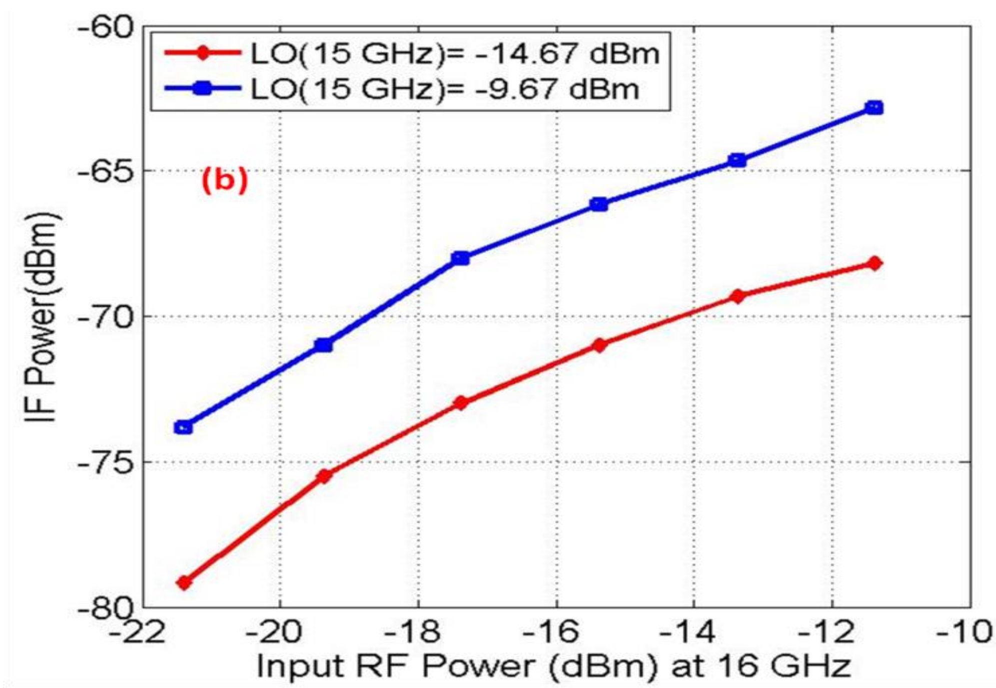

Figure 3.22 Measured IF signal power versus the input RF power for Diode A1 and A2 for fRF = 4 GHz and fLO = 3GHz

3.4 Conclusion

In conclusion, thin film MIM diodes with asymmetrical electrodes (Ti-TiO_2-Pd and Ni-Ni-NiO-Mo) fabricated on flexible substrate are characterized for microwave circuit applications. Both types of diodes show strong non-linearity with fairly asymmetric I-V characteristics. The NiO based diodes shows higher current densities and higher ideality factor in comparison to TiO_2 based diode, which can be contributed to growth of thin and high quality NiO using plasma oxidation. Both diodes work as efficient microwave rectifier, frequency multiplier, and mixer. This work will motivate further research on realization of high-performance flexible GHz circuits using MIM diodes. Additionally, the most promising aspects of this technology is the process integration. Here the diodes are made on polymer substrate but the diodes can be easily integrated onto standard CMOS platforms.

CHAPTER 4: SELECTIVE FABRICATION OF SILICON CARBIDE/SILICON HETEROJUNCTION DIODES USING EXCIMER LASER

4.1 Background

The wide band gap semiconductors such as SiC and GaN are of great interest due to their ability to operate at high temperature, high voltage, high power densities and higher frequencies. These materials perform much better than their Si counterparts for high power switching and RF applications because of their large bandgap, and high breakdown field strength, high thermal conductivity. In comparison to other wide gap semiconductors SiC is of interest due to its very high breakdown field strength, high thermal conductivity, ability to dope both p and n type, SiO_2 as the native oxide, indirect bandgap as needed for bipolar power devices, and most importantly the possibility of growth on low cost Si substrate using hetero-epitaxy. Out of the various existing polytypes of SiC the most commonly researched are 6H SiC, 4H SiC, and 3C-SiC. 3C-SiC is the only polytype that can be grown hetero- epitaxially on large area inexpensive Si substrates for the development of Si/SiC electronic devices.

3C-SiC exhibits the lowest bandgap and excellent electronic properties such as high electron mobility. However, this material system experiences 20% lattice and 8% of thermal expansion coefficient mismatch, and the grown SiC contains a large number of extended defects. These defects result in high leakage currents in 3C-SiC/Si devices. There have been several techniques to grow silicon carbide including low pressure CVD (LPCVD), PECVD, MBE and sputtering. Typical epitaxial temperature is 600 °C and above and can be as high as 1200 °C depending on the process being used such as MBE and CVD. The epitaxial layers are under severe stress and for any layers with thickness more than hundreds of nanometers there will be defects and cracks [78-80]. Unless the epitaxial is grown near very low temperature (which is generally not), the epitaxial layer will be under stress and will have stress induced defects. In past effort had been made to reduce the deposition temperature, however, it is reported that no single-crystalline SiC growth could be achieved below 1000 °C. SiC film grown by low temperature processes like PECVD shows compressive stress, due to the trapped hydrogen inside, which might affect the stability of devices. Films made by sputtering which is also a low temperature process results in issues like hollow voids which affect the material properties [129, 130]. Thus there is a need of novel fabrication process for direct/selective synthesis of SiC on Si.

4.2 Alternative Techniques for SiC Synthesis

Alternate to direct deposition of SiC on Si, growth of SiC has also been demonstrated by diffusion of carbon into Si using thermal annealing of pre deposited carbon precursors on Si [131-135]. The most commonly used precursor is C60, because it does not contain or introduce any unwanted contamination into the growing film. The samples were usually prepared by depositing very thin layer of fullerene (C60) using while keeping the substrate at high temperature. The formation of silicon-carbide films on Si substrates is a carbonization process. It was also found that silicon carbide formation process initiates upon annealing at T >870°C and the interaction between C60 molecule and Si surface is a function of annealing temperature [133]. During the annealing process the C60 cage is deformed and finally broken, with more and more carbon atoms from C60 molecule are bonded with Si atoms. Since the diffusion rate of Si in SiC is very small, the diffusion occurs preferentially via structural defects or grain boundaries of Silicon - Carbide domains. The structure is crystalline, relaxed but the growth is more of island like due to high lattice mismatch between two materials [134, 135]. Formation of nanoparticle SiC (np-SiC) has also reported by thermal annealing of C/Si multilayers on Si wafers. The size of nanoparticle and particle density depends on temperature, the higher the annealing temperature was, the higher the density and the larger the size of particle was [136]. Rapid thermal annealing (RTA) and laser based annealing are also used as an alternative to furnace annealing.

RTA based annealing has been used to grow SiC on Si substrates [86]. It was found that the same crystalline quality of SiC can be obtained at much lower temperature (750 °C) using RTA in comparison to conventional furnace anneal (FA) which requires T > 900 °C. The lower reaction temperature of SiC in RTA was attributed to high heating rate effect on the crystallization behavior and the variation of activation energy and surface energy during reaction of Si and C. In addition, RTA is much faster in comparison to FA, for example np-SiC can be formed by RTA at 750 °C for 1 min while FA requires 900 °C for 1 hr [86, 137]. Thermal energy is the driving force for the crystalline SiC formation through inter-diffusion between C and Si. In brief, the RTA offers many faster diffusion paths for C atoms to diffuse into Si and form SiC formation. Thus C and Si can intermix and rearranged their positions at temperature below 750 °C to form nanocrystalline SiC. The density is much higher than conventional nanoparticles synthesis using CVD or PVD. The reaction temperature of SiC is also lower than the conventional CVD or FA because of RTA enhanced SiC crystallization at high heating rate. Formation of SiC has also been demonstrated by implantation of carbon ions into single-crystalline silicon and subsequent rapid thermal annealing. It was found that rapid thermal annealing leads to a carbon redistribution resulting in the formation of a SiC. Although RTA annealing has advantages over FA, but it still requires heating of whole substrate and thus not post CMOS compatible.

Another promising annealing technique is laser based annealing process; it has been used as an alternative to classical thermal annealing or RTA for various applications such as doping of crystalline Si and SiC, recrystallization of amorphous Si wafer for Thin film transistors. The biggest advantage of laser based annealing is localized heating within keeping the rest of the substrate at room temperature [138, 139]. High power lasers, such as excimer lasers have been used to transform thin layers of amorphous Si (50 – 100nm) into high quality polycrystalline Si through melting and recrystallization. Laser annealing has been demonstrated as an alternate to thermal annealing for doping of Si and SiC [87, 88]. Laser process has also been used for recrystallization of amorphous silicon deposited on plastic substrates with no evidence of damage to the plastic [88]. Successful demonstration of excimer lasers for these applications gave us the confidence that growth of SiC on Si substrate can be carried out using selective laser annealing of Si wafer coated with carbon source.

4.3 Laser Processing: Advantages over Conventional Techniques

4.3.1 Laser Material Interactions

Excimers lasers have the ability to deliver large amounts of energy into confined regions of material in order to achieve a desired response. For materials with high absorptions, the energy is absorbed near the surface region modifying surface chemistry, crystal structure without altering the bulk. Confinement of energy to selected regions can be achieved by controlling the laser spatial profile which can be done by focusing of beam through optics, and beam shaping through homogenizers, apertures and refractive elements [140].

When the laser hits the surface of a material, some of the light is transmitted into the material and rest reflected due to the discontinuity in the refractive index. The reflectivity of a given material will depend upon the wavelength of the laser. For instance, values for reflectivity of metals in the near UV and visible range are typically between 0.4 and 0.95. Once the light is inside the material, the intensity decays with the depth at a rate depending on material’s absorption coefficient. The intensity decay exponentially with depth according to Beer–Lambert law given as:

$$I(z) = I_0 e^{-\alpha z} \tag{4.1}$$

Where, I_0 is the intensity just inside the surface after considering reflection loss, z is the depth and α is the absorption coefficient. The absorption depth ($\delta=1/\alpha$) is the depth at which the intensity of the light drops to 1/e of its initial value. For UV lasers the absorption depths of most of metals and semiconductors (Silicon, Aluminum, and Gold etc.) are short relative to bulk material thickness. Therefore, choosing laser with smaller wavelength allow local modification of surface properties without altering the bulk of the material. When dealing with nanosecond (ns) duration laser pulses, it is typically assumed that most of the absorption is due to single photon interactions. However, for picosecond (ps) and femtosecond (fs) lasers, the instantaneous intensity enables phenomena such as multi-photon absorption and optical breakdown and which can significantly decrease absorption depths [141].

4.3.2 Laser Energy Mechanism

The mechanism by which the absorption of light occurs depends on the type of material and photon energy. Photons will couple into the available electronic or vibrational states in the material depending on the photon energy. Photons with energy lower than material's band gap will not be absorbed. The time it takes for the excited electronic states to transfer energy to phonons and thermalize depends on the specific material. When the laser-induced excitation rate is lower than the thermalization rate, the absorbed laser energy is directly transformed into heat. Such processes are called photothermal (pyrolytic) and the material response is purely thermal. Laser processing of metals or semiconductors with laser pulse times of nanoseconds or higher is typically characterized by photothermal mechanisms. For photothermal processing, the material modification is due to the elevated temperatures, thus the temperature field inside a material is governed by the heat equation. The heat equation is derived from the conservation of energy and Fourier's law of heat conduction, which states that the local heat flux is proportional to the negative of the gradient of the temperature. However, when the laser induced excitation rate is higher than the thermalization rate, excitations can build up in the intermediary states. These excitation energies can be sufficient to directly break bonds (photo-decomposition) and is a non-thermal change as is referred as photochemical (photolytic) processing. During purely photochemical processing, the temperature of the system remains relatively unchanged. For polymers irradiated with shortwavelength laser light, where the photon energy is on the order of the chemical bond energy, photochemical processing occurs [141, 142].

4.3.3 Material Response

In the case of photo thermal mechanism, the material response to a particular laser is a function of local heating and cooling rates and the maximum temperatures reached. As with high power excimer lasers, heating rates can be extremely high and thus significant changes can occur to the material. Even with the laser fluences below threshold, various temperature related processes can occur. For instance, the high temperatures can enhance diffusion rates for impurity doping [87, 88], sintering of porous materials [141] and the reorganization of the crystal structure.

Fluences above the threshold of melting can lead to the formation of molten material on the surface. The molten material will support much higher solubilities than in the solid phase, resulting in rapid material homogenization. In addition high solidification rates and self-quenching rates and can be achieved due to rapid dissipation of heat into the cooler surrounding bulk material [141].The surface tension for most of the materials (liquid) decreases with increasing temperature and thus the liquid is pulled from the hotter to the cooler regions [142].

Laser based annealing can be of two type i.e. non-melt laser annealing (NLA) and excimer laser annealing (ELA). NLA utilizes rapid surface heating to enhance atomic mobilities and reorganize the crystal structure and is commonly used to activate the diffusion of ion implanted dopants in silicon and SiC wafers to create shallow junction and repair lattice damage created during the implantation process The short thermal penetration and lack of melting allow processing of shallow junctions. On the other hand, ELA utilizes melting a thin layer of material at the surface, which then rapidly recrystallizes to relieve internal stresses, remove defects, and enhance crystallinity. The ELA process is used in production of high performance, large-area polycrystalline silicon (poly-Si) thin-film transistor (TFT) devices for flat panel displays. It is also used to recrystallize poorly conducting amorphous silicon to produce larger grain sizes and reduce defects [143].

4.4 Selective Fabrication of SiC/Si Diodes by Excimer Laser

As discussed, laser processing offers new and unique processing capabilities that are not possible with current available technologies. As laser annealing has been also used an alternative to thermal annealing for doping of Si and SiC, we believe that a high power laser can also be used for growth of SiC growth by locally melting the Si and dissociating solid carbon sources which leads to formation of SiC bond and weakening of C-C bond. Recently G. Račiukaitis etal. showed formation of SiC type bond formation during the laser ablation process carried out in air, and carbon source was coming from air environment [143]. Recently, laser synthesis techniques have been used to transform solid carbon sources to graphene directly on Si and quartz substrates [89]. The goal of this chapter is to demonstrate the growth of SiC on Si by laser based local heating while holding the substrate under ambient conditions (in air at atmospheric pressure and at room temperature).

This thesis present a novel method to synthesize SiC using pulsed laser KrF laser radiation (λ=248 nm, pulse duration~25 ns). The technique used here is based on using a focused laser beam through a carbon (C) film layer onto an absorbing substrate (Si) and creating a local hot-spot where the Si surface melts and a reaction between Si and C takes place to form SiC. Here, a thin layer of PMMA provides a carbon source through pyrolysis. The efficiency of laser depends on wavelength and the absorption of substrate (Si). The laser intensity is also very important parameter to control as the energy below the melting points of the silicon is not expected to grow SiC. Due to the high absorption of UV light for most of the solid materials high spatial resolution can be easily achieved which makes this process more localized/selective. Laser surface melting can also be used to incorporate new material into an existing surface. In laser cladding and hardfacing, new material complete mixing of the new material into the molten surface can form a homogenously alloyed layer and rapid re-solidification ensures minimal segregation, allowing many materials to be alloyed regardless of their mutual solubility. Although the laser can melt surface of thin films of semiconductors and metals, temperatures at few microns into the substrate rise by no more than a few hundred degrees.

High power excimer laser can deposit high energy and raise the temperature within a short amount of time (nanoseconds) in near surface (localized region) while maintaining the substrate at room temperature. As the UV laser pulses have short duration, it is relatively a cold process with little or no effect to the surrounding region. Successful demonstrations of excimer laser induced doping of silicon deposited on plastic substrates in past [88] further justifies advantage of local heating. The use of laser based technique offer several advantages 1) limited damage of substrate 2) high quality film due to heating of small area 3) spatial resolution- simultaneous synthesis and patterning 4) low-cost 5) rapid heating and cooling 6) atmospheric pressure processing 7) integration with existing CMOS electronics and 8)Surface texturing- for photovoltaic application. The laser based synthesis technique for SiC is presented for first time as per our best knowledge.

4.5 Fabrication of SiC/Si Diodes

The SiC/Si diodes were fabricated by growing SiC on Si wafer using laser synthesis technique. Most of the common excimer lasers operate at a wavelengths of 193nm (ArF gas, 6.4eV), 248nm (KrF gas, 5.0eV) and 308nm (XeCl gas, 4.0eV). Excimer lasers are commonly used in eye surgery, photolithography and micromachining. In semiconductor industry, lasers have been used to transform thin layers of amorphous Si (50 – 100nm) into high quality polycrystalline Si, with greatly enhanced electron mobility. The output power, reliability, duty cycle of pulses and wavelength purity have been greatly enhanced over the last two decades and thus have found great reception in the manufacturing industry [88, 138, 140]. Not only used for fine resolution processing, excimer lasers have been utilized in large-area fabrication and annealing of thin films by expanding the beam through optics [87]. Here, high power KrF excimer laser generates UV light at 248 nm with pulse duration of 25 ns. The lasers parameters such as number of pulses, repetition rates and voltages can be controlled. In this experiment, the laser voltage is kept constant at 16 kV with repetition rate of 1Hz and the gas pressure is set at Torr. The excimer laser experimental set-up is shown in Figure 4.1. The frequency of the function generator and the excimer laser system is fixed at 1 Hz and the number of pulses of laser beam exposed on the thin film target is, controlled by the external trigger unit In this works, the number of pulse is varied from 1 to 8 pulses. The wafer was then placed on a XYZ manipulator of the laser system. The wafer was at room temperature and under atmospheric pressure with air background during the whole growth process. The excimer laser beam was directed onto the substrate through an optical path which homogenizes and shapes the intensity profile of the beam to achieve uniform illumination across the desired focal area. Maximum laser performance can be achieved by aligning the laser mirrors and focusing the beam. The mirrors are aligned via the guidance of a visible of red laser which is aligned to co-axis with excimer laser beam.

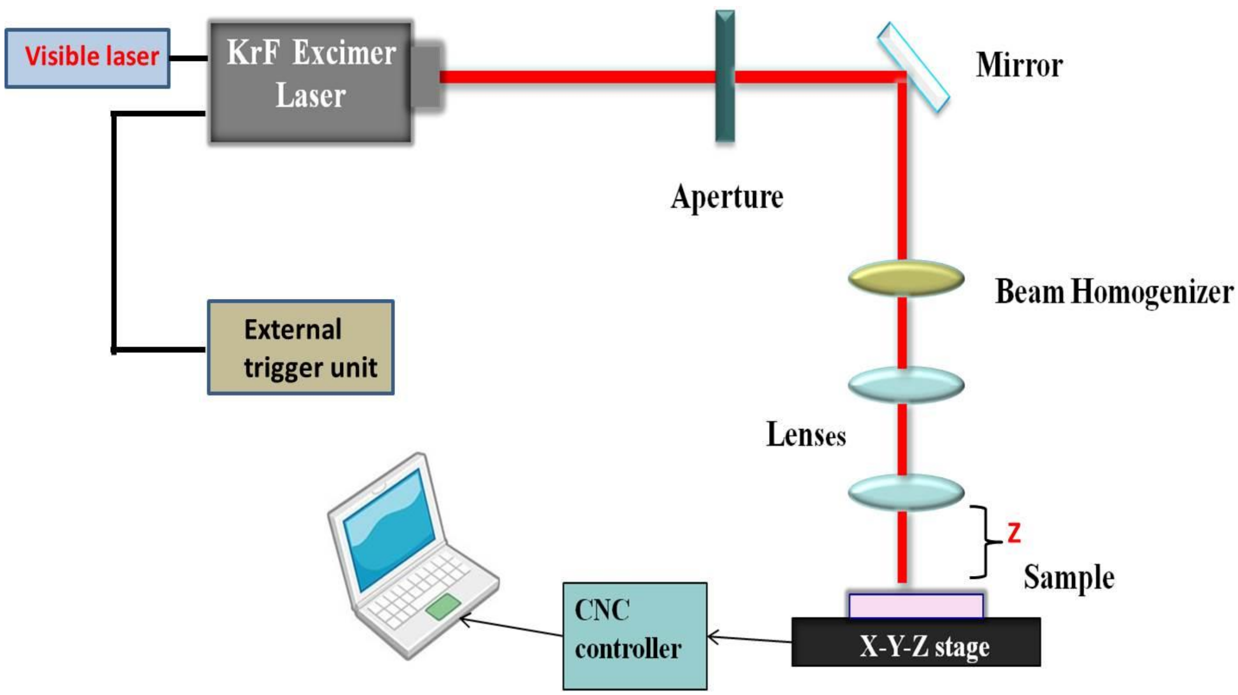

Figure 4.1 The schematic diagram of KrF excimer laser based growth process

The devices are fabricated on wafer with doping of 4.3×10^{14} cm^{-3} and thickness of 250µm. The silicon wafer was prepared by first removing the native oxide using 1:10 hydrofluoric acid (HF) : H_2O solution. Then a thin layer of PMMA (~400 nm) is spin coated at 1000 rpm for 45 sec, followed by bake at 145 ºC for 1 min. The focused excimer laser beam was then directed onto the substrate place on XYZ stage. The focal spot on the beam is also adjusted by moving the stage up and down (z direction). Various experiments were done by varying z It is very important to find out the perfect spot size/focal spot in order to get maximum laser performance and initiate growth/melt process. In addition to focused beam, optimum number of pulses is also required to form high quality SiC film.i.e. distance between the substrate and the lens (last one in the optical path) as shown in Figure 4.1.

The optimum distance z and number of pulses needed to form SiC film was determined by measuring electrical/photovoltaic characteristics (presented in upcoming section). The laser irradiated area of Si undergoes melting and re-crystallization during the pulses (1 Hz repetition rate). The laser beam simultaneously decomposes PMMA while melting the surface of Si. The PMMA provides a solid carbon source through pyrolysis for SiC synthesis. As the pulse width is narrow (~ 25 ns), cooling takes place immediately following the pulse. Electrical and optical characteristics were measured for devices made with different number of pulses and for different focal points. The average area of the as it is grown device is approximately 350 x 520 μm^2 which is dictated by the focusing of the laser beam impinging onto the Si wafer. Large area devices can be formed by rastering the laser beam across the substrate. A thin film of nickel (Ni ~50 nm) was deposited to form an Ohmic contact to SiC and aluminum (Al) was used as a back contact to p-Si wafer. No annealing was carried out after the deposition of these metal films and prior to any measurements.

4.6 Material Characterization

The Raman spectra for samples are shown in Figure. 4.2, all measurements were carried out in backscattering geometry using a 532 nm laser, before depositing the top Ohmic contact. The large peak at 521 cm^{-1} originates from the silicon substrate and the spectral peaks between 930cm^{-1} and 990cm^{-1} are due to acoustical and optical phonon modes of cubic polytypes SiC (here β-SiC is dominant). The peak broadening is related to the damping of phonon modes due to the short range ordering of SiC crystallites and the effects of surroundings i.e. having Si, as well as C-clusters [144]. The change in the number of SiC bonds due to the irradiation with multiple pulses could be inferred from a change in the intensity of Raman signal, see inset of Figure 4.3 (b).

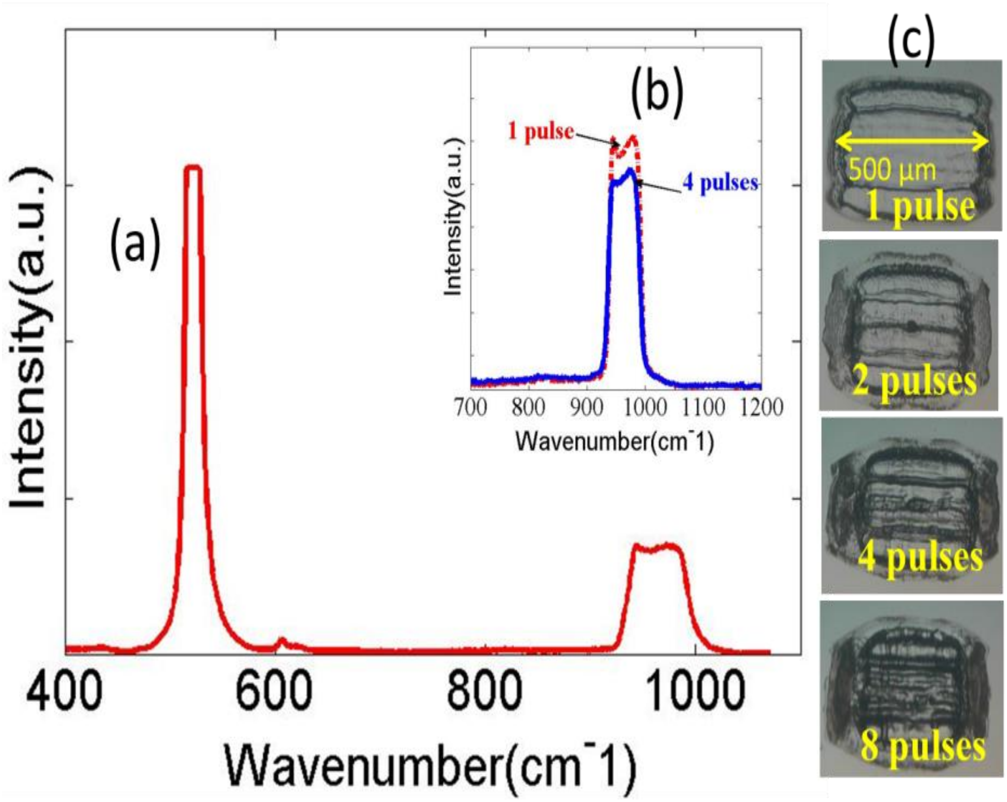

Figure 4.2 Measured Raman spectra of SiC/Si over a wide range of wavelength, (b) Raman spectra for devices fabricated using different number of pulses (c) Optical micrograph of selectively grown SiC film using different number of laser pulses

For normal incidence of Raman signal on β-SiC/Si or 3C-SiC/Si the i.e. the backscattering configuration the TO mode is forbidden [145, 146]. The absence of forbidden TO mode also confirm the absence of stacking faults, stress and dislocations at the interface [147]. The Raman signal can be further enhanced by opening a window from back side of the wafer after etching Si. But by removing the Si substrate the 3C-SiC LO phonon is enhanced in intensity and the forbidden TO phonon became active as both the LO and TO phonons become unpolarized. Due to the zinc blende structure of β-SiC, the polarization behavior produces a long-range Coulomb force and splits the LO and TO phonons.

The TO phonons are forbidden and the LO phonon is allowed. But on removal of Si these selection rules can be broken which leads to different Raman spectra. For a free film (Si removed) the β-SiC phonon appears near 796 cm $^{-1.}$ This is contributed to multiple reflection from the rear end leading to forward scattering and allowing the forbidden TO mode. The appearance of forbidden TO mode for β-SiC can also be contributed due to stacking faults, stress and dislocations between the crystal orientation of SiC and Si. The Raman studies of β-SiC/Si have been well documented in literature and agree well with our results. Wasyluk et al shows that there is a large enhancement in the peak intensity of the forbidden transverse optical (TO) mode (770-790 cm^{-2}) for the Raman signal measured at the void area i.e. Si is removed from the backside of 3C-SiC as stated by the authors of the paper [146].

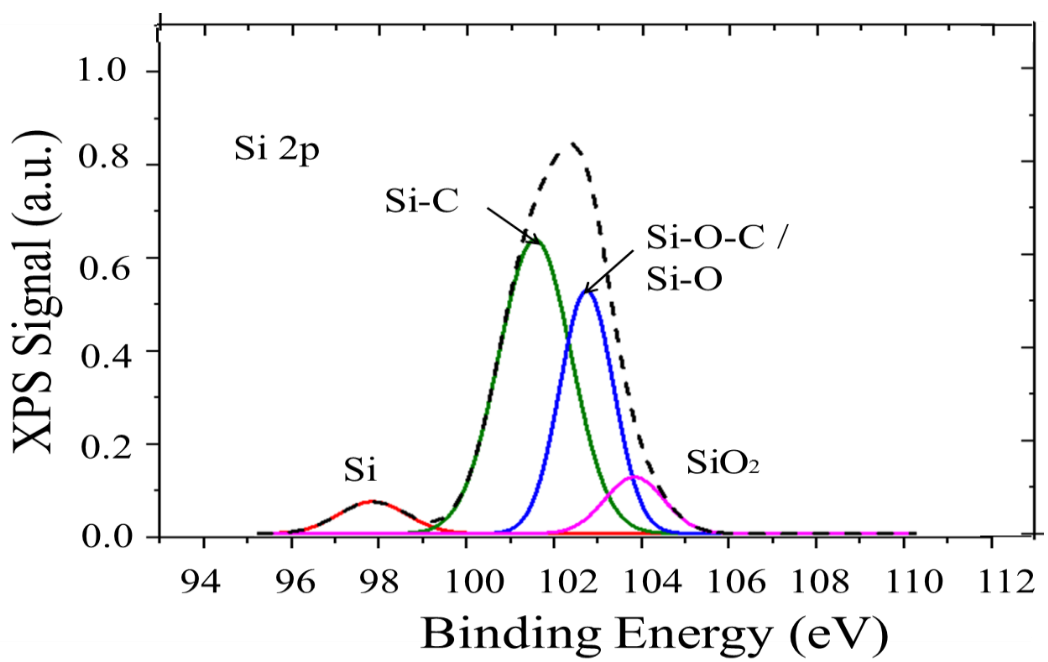

Figure 4.3 Normalized XPS spectra of Si 2p line, spectrally resolves components 98 ev (Si0); 101.2 eV Si-C; 102.7 eV Si-O-C; 103.7 eV SiO_2

X-Ray photoelectron spectroscopy (XPS) was also used to characterize the surface layer. The normalized XPS spectra of Si 2p line in sample are shown in Figure. 4.3. Deconvolution of Si 2p spectra shows two main components corresponding respectively to a Si-C bond in SiC at 101.2 eV and Si-O/Si-O-C bond in Silicon oxide/Silicon oxycarbide at 102.7. The oxy carbide phases might have formed on the surface of film was exposed to atmosphere [148, 149].

4.7 Focusing of Laser: Electrical Characteristics

As discussed earlier it is very important to find out the out the best focus of the laser beam to initiate growth/melt process. Various experiments were done by varying z and the electrical characteristics of those devices are presented in this section. Here, z is the distance between the substrate and the lens as shown in Figure 4.1. The value of z was varied between 10 to 20 mm, however best devices found was using z=13.

4.7.1 Current -Voltage Characteristic

Here current-voltage characteristics of devices with z=13 (In focus) and z=12 and 14 mm (Out of focus) are presented. These devices are formed using 2 laser pulses. All the measurements presented in this section were carried under dark conditions and at room temperature. The measurements show that good Si-SiC diodes can be formed with laser beam focused. The diodes formed with in focus (z=13) show higher current density of 24 mA/cm^2 at a fixed bias voltage 0.75 V in comparison to out of focus devices z=12 &14 show current density of 17 and 14 mA/cm^2 respectively. Figure 4.5 shows the measured current density-voltage (J-V) characteristic of the SiC/Si devices with different focus over a large voltage range using a Keithley 2400 source meter. The measurements show that high quality Si-SiC diodes can be formed with optimum value of z (optimum power transfer).

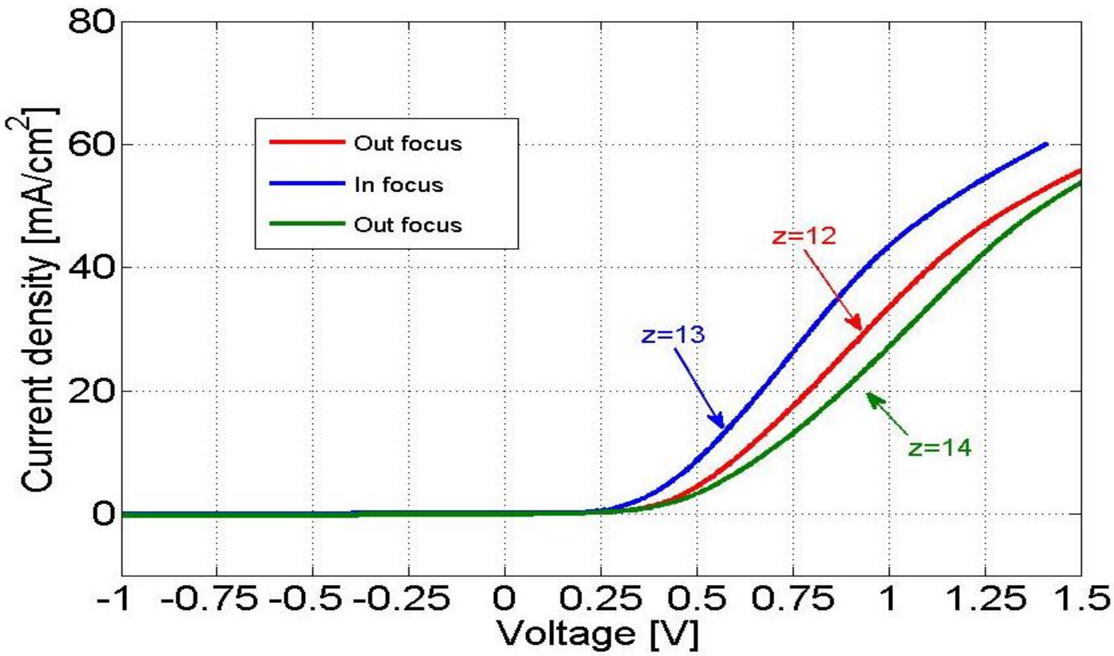

Figure 4.4 Current density-Voltage characteristics of SiC/Si diodes fabricated at different focal point i.e. z=12, 13 &14. All three devices are made with 2 laser pulse

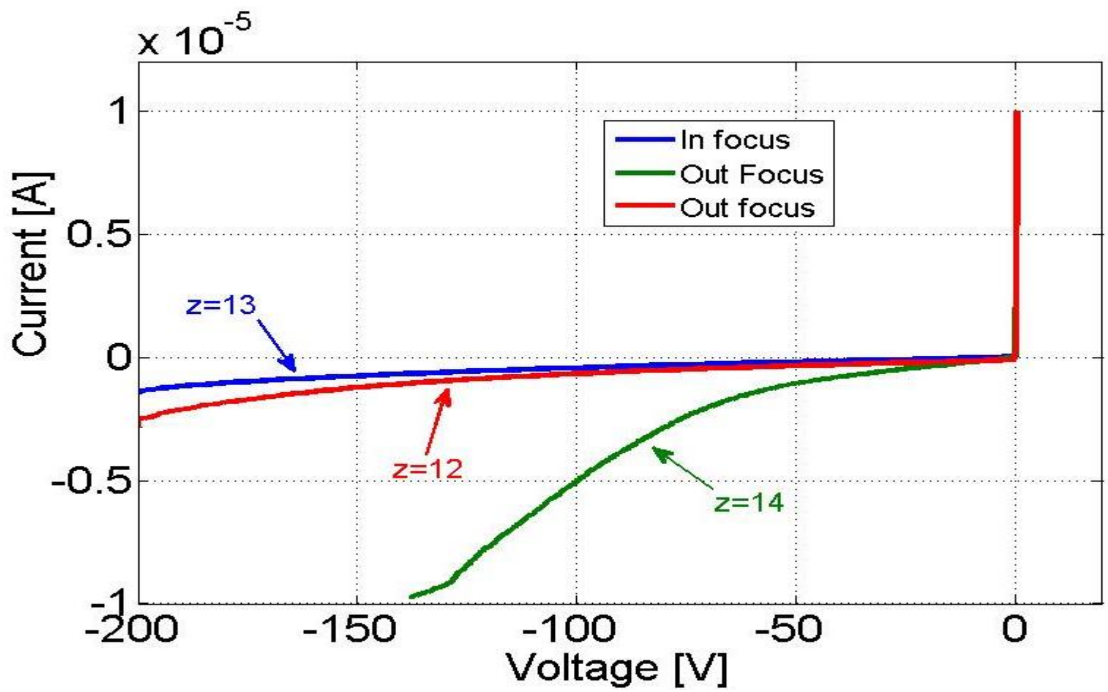

Figure 4.5 Measured I-V characteristics Diodes fabricated using different focal point i.e. z=12, 13 &14 (2 laser pulse) over a wide voltage range showing high breakdown.

Devices with z=13(in focus) shows a high reverse breakdown voltage >200V (bias source limited) with leakage current of 8.7 nA and 35 nA at reverse bias of 10 V and 50 V, respectively. In comparison, devices made with laser out of focus i.e. z=12 and z=14 shows higher leakage current of 0.05 µA and 0.8 µA. Here the resultant low leakage current indicates fewer defects at the interface. This can be due to higher can be contributed to the edge effects of carbon rich sharper edges i.e. z=12, 13 &14. All three devices are made with 2 laser pulse.

4.7.2 Photovoltaic Characteristic

The photovoltaic characteristics of diodes were also measured. The J -V characteristics of a device made with different focal point is shown in Figure 4.6. Devices with z=13(in focus) shows short circuit current density (J_{sc}) of 12 mA/cm^2 and open circuit voltage (V_{oc}) of 0.36 V. In comparison, devices made with laser out of focus i.e. z=12 and z=14 shows much lower J_{sc} of 3.3, 2.59 and V_{oc} of 0.33, and 0.32 respectively.

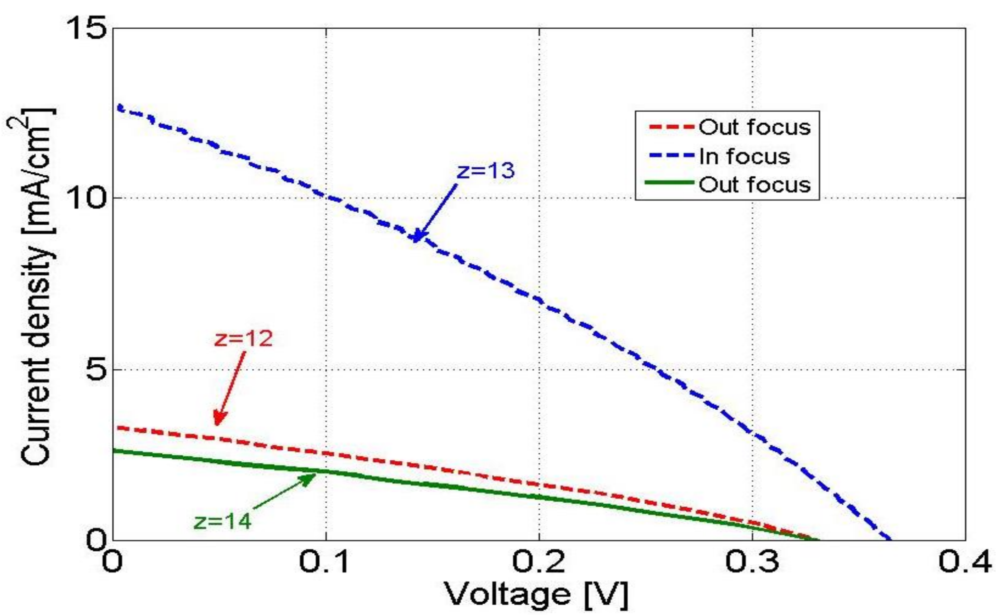

Figure 4.6 Measured J-V characteristics of a SiC/Si photovoltaic cell fabricated using different focal point i.e. z=12, 13 &14. All three devices are made with 2 laser pulse

4.8 Experimental results: Number of laser pulses

It is clear from the results presented in section 4.7 that in focus laser beam is required to fabricate diodes with good rectification characteristics with low leakage current. It is also interesting to know how the number of laser pulses or irraradition required for forming good quality SiC. Several devices were formed by irradiating polished Si with different number of pulses (1, 2, 4 and 8). The optimum number of pulses needed to form high quality SiC film was determined by measuring electrical and optical characteristics of the devices.

4.8.1 Current density-voltage (J-V) characteristic

All the measurements presented in this section were carried under dark conditions at room temperature. The measured current density-voltage (J-V) characteristic of the SiC/Si devices is shown in Figure 4.7.

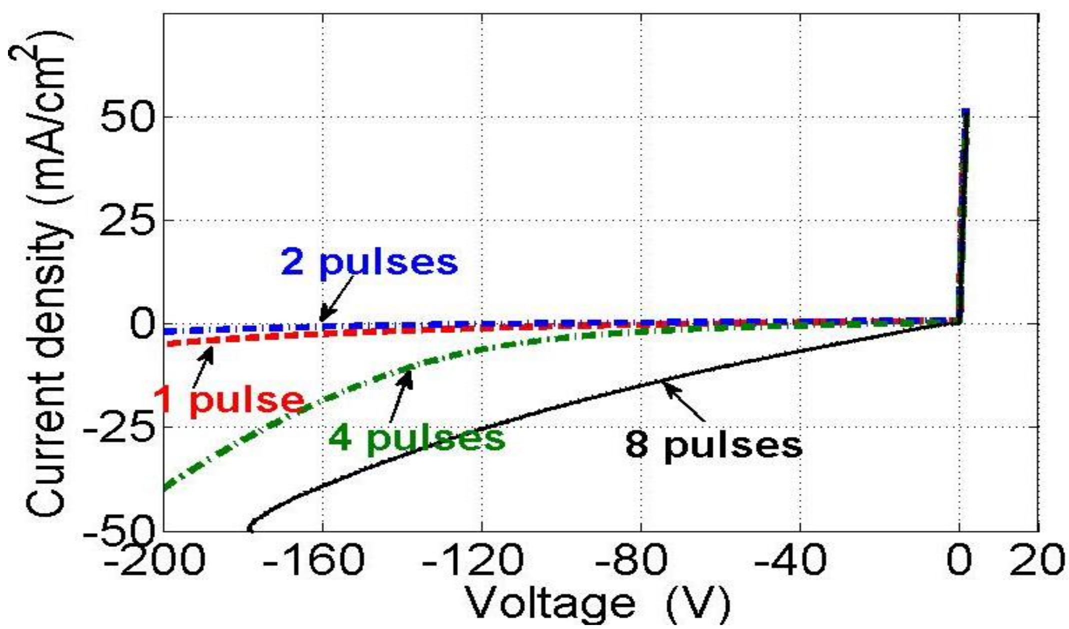

Figure 4.7 J-V characteristics of SiC/Si diodes fabricated using different number of laser pulses with breakdown voltage > 200 V

The devices are measured over a large voltage range using a Keithley 2400 source meter. The measurements show that high quality Si-SiC diodes can be formed with optimum number of pulses (optimum power transfer). For the best performing diode, i.e. diode with 2 laser pulse a rectification ratio of 3x 10^4 (at ± 1V) was obtained. It also shows a high reverse breakdown voltage of > 200V (source limited) with leakage current of 1 $\mu A/cm^2$ and $44 \mu A/cm^2$ at reverse bias of 1 V and 50 V, respectively. This leakage current is smaller than previously reported for SiC/Si diodes [78, 150-152]. The breakdown voltage for the best devices is much higher than 200V but results shown here are limited by the measurement setup. Figure 4.8 shows a simplified band diagram of the heterojuction formed during this process. Figure 4.9 shows the forward voltage characteristic, i.e log (J) vs V. It shows the barrier height of ~ 0.4 eV and ideality factor of 3.2. Typically, the SiC/Si material system experiences ~20% lattice and 8% of thermal mismatch and thus the CVD grown SiC contains a large number of extended defects which results in high leakage currents in 3C-SiC/Si devices. Here the resultant low leakage current indicates fewer defects at the interface. The devices fabricated using 1 and 2 pulses show the highest reverse breakdown voltage with very small leakage current densities. The The diodes will break down at this region first due to higher field strength. These preliminary J-V measurements show that high quality Si-SiC diode can be formed by selecting an optimum number of pulses (optimum power transfer).

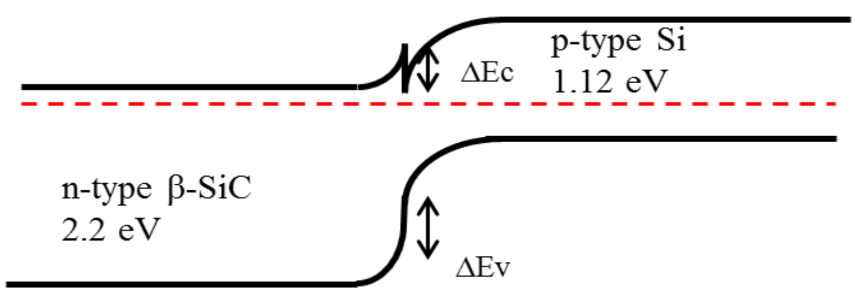

Figure 4.8 Band diagram of SiC/Si heterojunction diodes

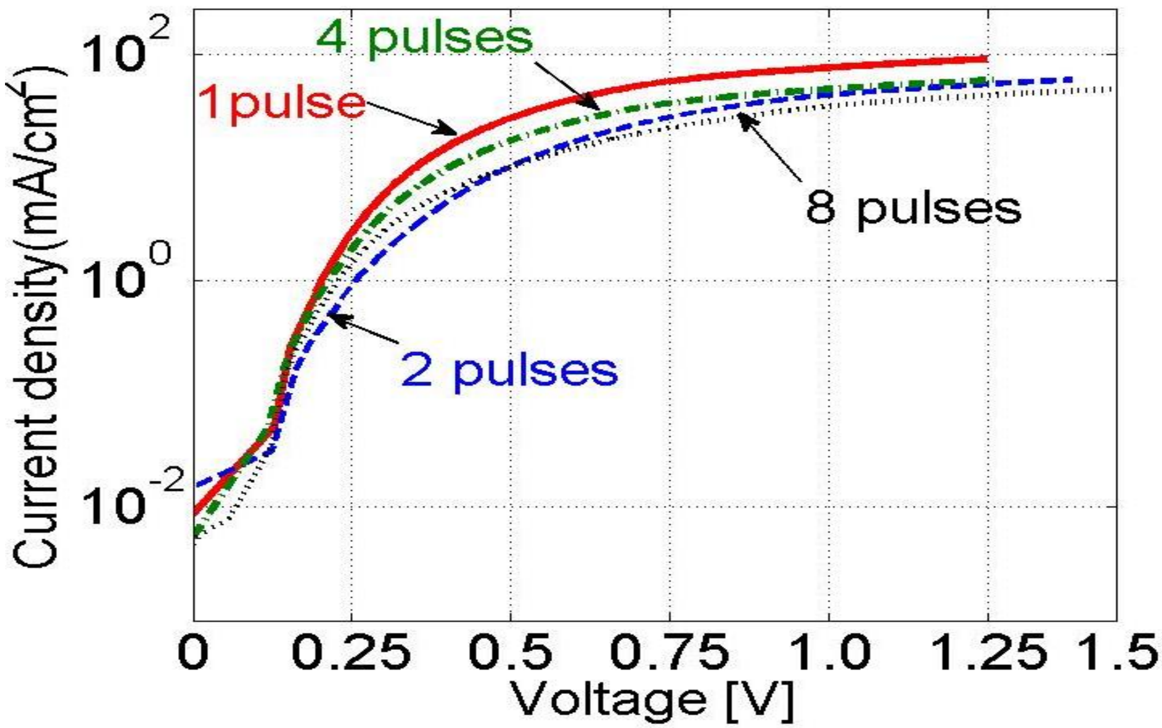

Figure 4.9 Forward log (J)-V characteristics of SiC/Si for different devices number of devices.

From J-V measurements it can also be concluded that the conductivity of the SiC layer is n-type which is due to unintentional doping of SiC with shallow donor nitrogen. The origin of the n-type doping is due to shallow donor Nitrogen with a binding energy of 15–20 meV. The donors can be present in as deposited SiC film in concentrations less than 10^{18} cm-3 [153]. The SiC film grown using chemical vapor deposition process are mostly unintentionally n-type doped due to presence of nitrogen source during growth from gas precursors such as methylsilane (99%), or due to other contaminates [154]. Nitrogen is also the most commonly used n-type dopant for SiC. The nitrogen doped film can be grown by addition of Nitrogen gas to the source gas during CVD process. The carrier concentration can be controlled by changing the mole ratio of N_2 gas to other gases (used for SiC synthesis). In situ doping of sputtered SiC has been achieved in past by introducing nitrogen into the electric discharge during the growth process [155]. Doping of SiC is complicated by two facts: (i) the dopant can occupy either the Si or the

C site (ii) the diffusion rate in tight bond and dense structure of SiC is slow. In the fabrication of SiC layer using laser, nitrogen from the ambient is incorporated in the film during diffusion of carbon into Si melt. Thus, n-type doping can readily be achieved. The most common methods of doping are thermal diffusion, ion implantation and spin on doping. Thermal diffusion of dopants requires higher processing temperature and can cause impurity contamination and deterioration of crystallization of SiC. Ion implantation can also severely damage the lattice structure. Laser-induced doping of SiC films has been used in past to dope SiC without going to very high temperature [87]. Laser can be used to assist doping of SiC with nitrogen, aluminum, chromium, phosphorous and boron. Laser process offers the advantage of locally increasing the temperature without heating the whole substrate. Moreover, both doping and activation of dopant can be achieved in a single process.

The high power pulsed laser (excimer laser) with nanosecond durations enables large energy in short duration. Under controlled conditions the surface melting of SiC does not exceed a depth of few hundred nanometers for the rapid solidification from the bulk, allowing the dopant to be incorporated by liquid phase diffusion. This is same as principle of laser induced dopant incorporation for Si which is also a melt/growth process. In future, p-type doping of SiC can be achieved by boron spin-on dopant solution and irradiation with high power excimer laser pulse. The thickness of the doped layer depends on the absorption of laser energy by SiC. SiC has higher absorption at 248 nm and thus results in thinner doped layers. This also causes concentrated localized temperature rise which also help in diffusion of boron. Due to localized heating, the temperature drops down quickly and thus the dopant gets trapped in the film. The doping profile may be controlled by energy density of pulse which needs further study.

4.8.2 Capacitance –Voltage (C-V) characteristic

In anisotype heterojunction like β-SiC/p-Si, the capacitance as a function of applied bias voltage is given by the relation in Equation (4.2), where N_d is the effective density of state of n-type β-SiC (donor), N_a is the density of acceptor impurities of p-Si, ϵ_d, and ϵ_a are the dielectric constant of β-SiC and Si respectively, ϵ_0 is the permittivity of free space, V_{bi} is the built in potential, V is the applied voltage, C is the capacitance and A is the area of HJ.

$$\frac{C}{A} = \sqrt{\frac{q\epsilon_0\epsilon_a\epsilon_d N_a N_d}{2(N_a\epsilon_a+\epsilon_{d_a}N_d\ )(V_{bi}-V)}} \tag{4.2}$$

The C-V characteristics of the SiC/Si diodes were measured at 100 kHz and room temperature. The small area of diodes makes the capacitance measurement more sensitive to edge effects and other parasitics [151].

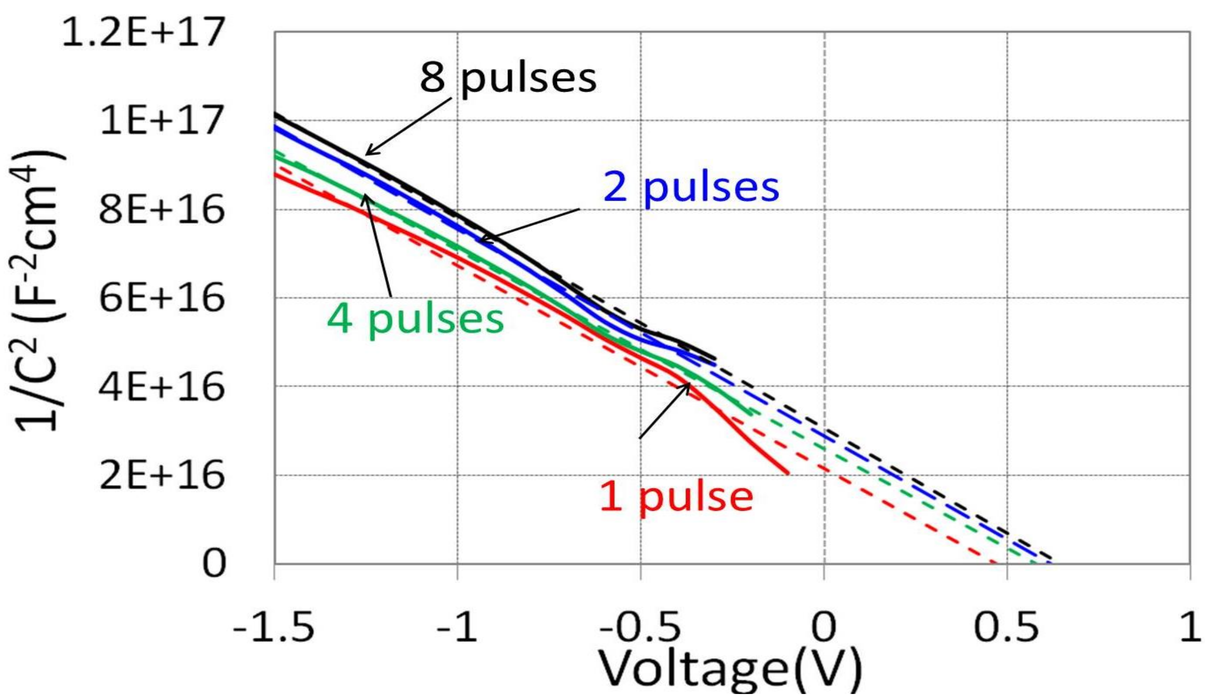

Figure 4.10 The $1/C^2$ vs V for SiC/Si diodes fabricated using different number of laser pulses

The $1/C^2$ per unit area square ($F^{-2}cm^4$) vs V data shows a linear relationship indicating that the junction is abrupt with a built in voltage of ~ 0.5V as shown in Figure 4.10. In anisotype heterojunctions like n-SiC/p-Si, the capacitance as a function of applied bias voltage is given by the relation found in [152]. Given the density of acceptor impurities (p-Si) ~ 4.3 $x10^{14}$ cm^{-3} and assuming the dielectric constant of SiC to be 9.8, the doping level in SiC is found to be ~ $5x10^{15}$ cm^{-3}.

4.8.3 Photovoltaic Characteristics: Polished Wafers

Fig. 4.11 shows the illuminated J-V characteristics of diodes with different number of pulses. It is clear that device with single pulse is perfoming much better than devices made with higher number of pulses. For example device made with single pulse J_{sc} of 17 mA/cm^2, V_{oc} of 0.33 V , while device with 4 pulses shows much lower J_{sc} of 17 mA/cm^2, V_{oc} of 0.33 V . The J -V characteristics of a device with a single pulse under dark and illuminated conditions is shown in Fig. 4.12 (left). The devices clearly shows a fill-factor (FF) of 62 % and good optical conversion efficiency (~8%). In the past, similar results have been obtained using CVD grown and sputter deposited SiC/Si diodes [79, 156].

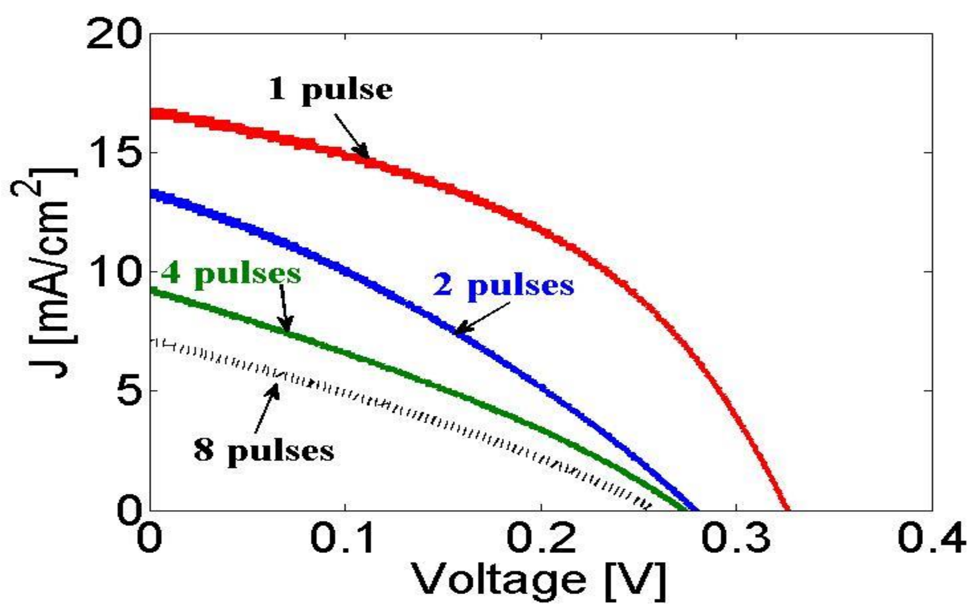

Figure 4.11 Measured J-V characteristics of a SiC/Si photovoltaic cell fabricated using different number of laser pulses

The measured internal quantum efficiency (IQE) spectra for a SiC/Si (1 pulse) based photovoltaic cell is also shown in Fig. 4.12 (right). The spectrally resolved IQE exhibits a peak at around 650 nm which coincides with peak of a SiC/Si photovoltaic cell previously reported in [156]. However, this process is simpler and requires few fabrication steps, and more importantly it does not require vacuum processing (an expensive fabrication step). These results clearly show that high quality SiC layer can be formed on Si substrate using laser processing. The overall performance of a photovoltaic cell depends on several factors such as the series resistance due to contacts and bulk resistance of the substrate. The low V_{oc} and relatively weaker response of IQE can be contributed to higher series resistance and recombination losses. The series resistance can also affect the fill factor, short circuit current and ultimately the efficiency of the device.

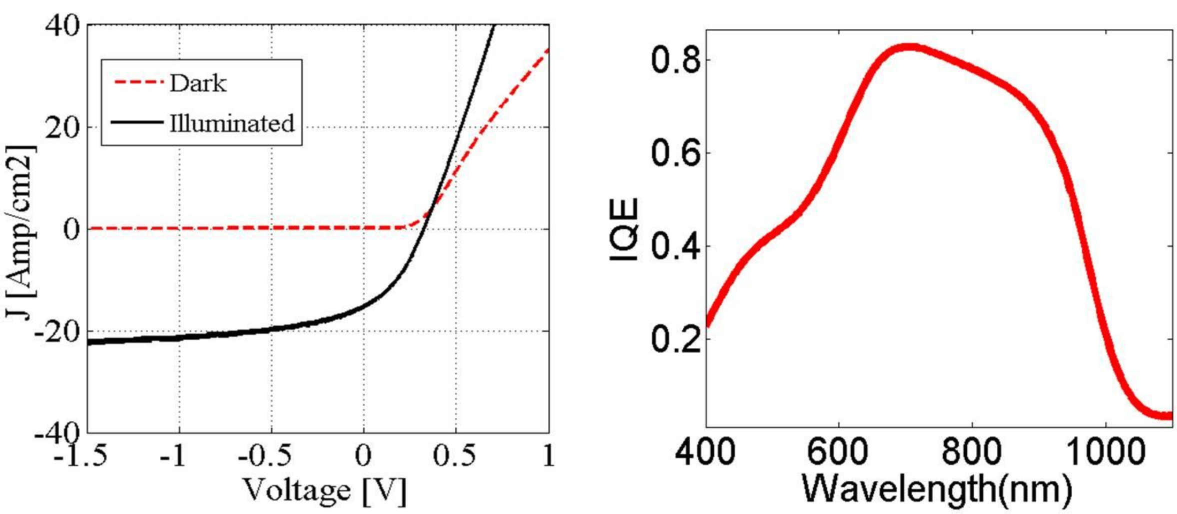

Figure 4.12 Dark and illuminated J-V curve for device made using single pulse (Left), IQE spectra of SiC/Si diode (Right)

The series resistance can be reduced by annealing the contacts near 400 ° C and by using a thinner Si substrate with higher doping. We also believe that by introducing a good buffer layer at the interface on both sides of Si Substrate prior to growth of emitter layer can help in improve open circuit voltage. The low open circuit voltage can also be attributed to carbon rich region on the edge of the device. This can be improved by edge termination. The weak spectral response may be due to high surface recombination and the device quality may further be improved but needs further investigation. Another benefit of this laser synthesis process is the in-built surface texturing of solar cells. Surface texturing is carried out to enhance light trapping and thus to improve efficiency. In high efficiency commercial photovoltaic cells this texturing is usually carried out through wet etching to increase the amount of light coupled into the cell. In our process it can be achieved during the formation of the SiC layer (Figure. 4.2(c)) without using any harsh chemicals.

4.8.4 Photovoltaic Characteristics: Unpolished Wafers

One of the major contributing expenses to manufacture of solar cells is the silicon substrate. Cutting, grinding, lapping and polishing is performed which can amount as much as 50% of the substrate cost. Thus, in the manufacture of solar cells, as-cut Si wafers/ unpolished wafers are desirable. As discussed earlier, excimer lasers have been used to transform thin layer of amorphous Si (50 – 200nm) into high quality polycrystalline Si with greatly enhanced electron mobility. In the formation of SiC layer in the process here, the surface of the Si undergoes melting and solidification, and it thus naturally reduces surface defects. Preliminary tests were carried out to determine the possibility of using an unpolished Si wafer in the formation of a Si-SiC heterojunction solar cell. Figure. 4.13 shows the micrograph of a device fabricated on an unpolished (as-cut) 250 µm thick silicon wafer (~ 10^{15}/cm3). There is a clear contrast between the SiC region formed from the silicon melt and the neighboring unpolished Si region. Figure 4.14 shows the J-V characteristics of this device under dark and illuminated conditions using single laser pulse The diodes shows J_{sc} of 15 mA/cm^2 and V_{oc} of 0.23 V. Measured J-V of different devices formed using different number of pulses is also shown in Figure. 4.15. These preliminary results clearly show that high quality Si-SiC heterojunction devices can be formed on low cost unpolished Si wafers. The excimer laser melts and improves the quality of the surface region while forming a SiC layer.

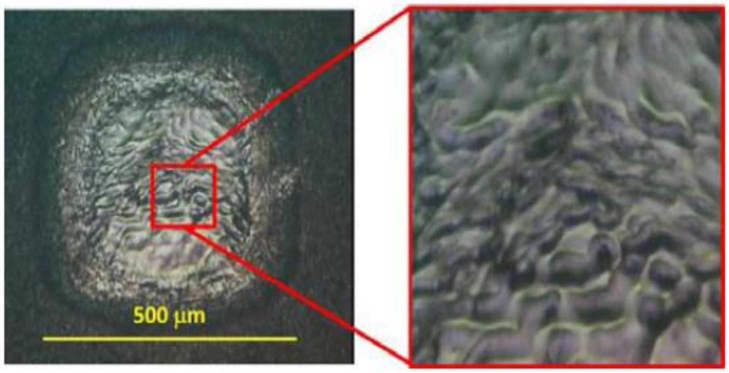

Figure 4.13 Optical micrograph of SiC/Si diodes fabricated on unpolished wafer

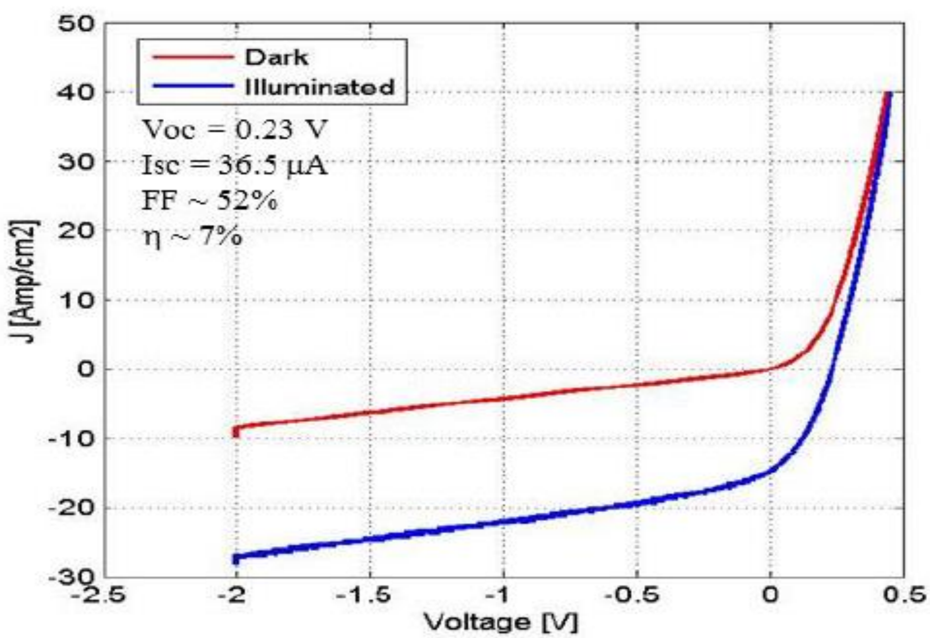

.

Figure 4.14 Measured J-V characteristics of the devices on unpolished wafer under dark and illuminated conditions with single laser pulse

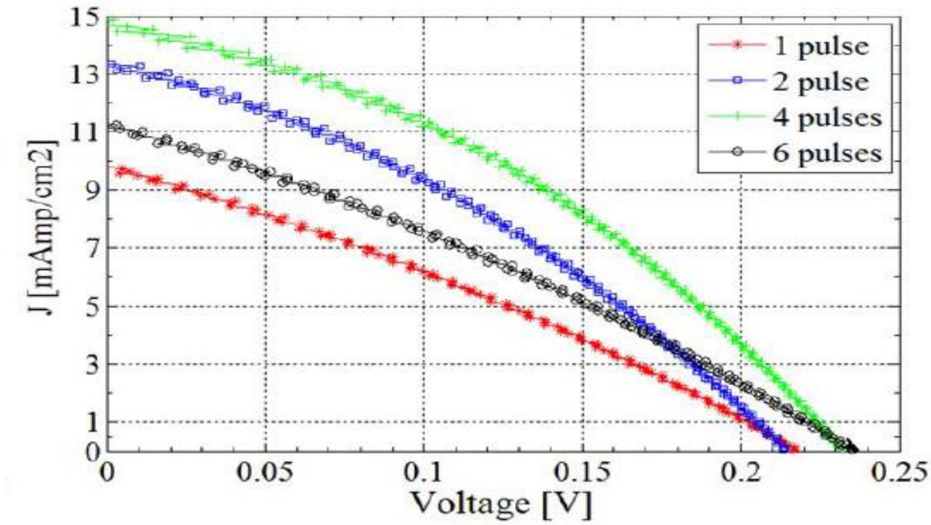

Figure 4.15 Measured I-V under illumination condition for devices fabricated using different number of laser pulses

CHAPTER 5: LASER ASSISTED GROWTH OF SIC/SI DIODES FOR MICROWAVE CIRCUIT APPLICATIONS

Low cost high power microwave devices are required for emerging applications in wireless communication systems. As discussed earlier, devices suffer from increased temperature of operation as they cannot handle high power densities. Wide gap materials like GaN and SiC. Recently, SiC has regain interest for power applications, due to higher thermal conductivity and can theoretically operate at higher power densities than GaN. The use of novel process for fabrication of SiC/Si heterojunction diodes as discussed in Chapter 4; allows ease of integration with Si which is very important to enable mass production of high power devices for commercial MMW applications. Most importantly this process allows direct growth of these materials on silicon which is very challenging. This chapter presents the high power microwave circuits using SiC/Si diode fabricated by excimer laser process. The diodes show good rectification characteristics with low leakage current and high breakdown voltage (>200 V). The preliminary results on microwave detection and frequency multiplication show good RF performance of SiC/Si diodes.

5.1 Device Fabrication

The SiC/Si diodes were fabricated on two different type of wafer, both are p-type but with different carrier concentration and thickness. Firstly the devices are made on medium doped wafer, the same as used in the Chapter 4 i.e. with carrier 4.3×10^{14} cm^{-3}, thickness = 250μm (Type I wafer). It was found that the devices made on low doped wafer have higher series resistance and thus doesn’t perform well at higher frequencies. To reduce the series resistance the wafer with higher doping ~$3 \times 10^{15} cm^{-3}$ and thickness of 150μm (Type II wafer) is selected. The silicon wafer was first prepared by removing the native oxide using buffered hydrofluoric acid (HF) solution followed by spin coating of a thin layer of PMMA (~400 nm). The sample was then irradiated with high power KrF excimer laser (λ = 248 nm, pulse duration of ~25 ns) (Figure 5.1 (a)). The details of the laser synthesis process as well as material characterization of SiC are explained in Chapter 4. The average area of grown SiC is 350 × 500 μm^2. To realize RF circuits with working frequencies in GHz range, the size of the active area needs to smaller [157]. The SiC/Si diodes are coupled with coplanar waveguide (CPW) feed network structures for on-wafer probing at high frequencies. The steps to fabricate small area diodes embedded in CPW structures are shown in Figure 5.1 (b-f). Following the formation of a SiC layer on Si, a 200nm layer of Nickel (Ni) and 200 nm layer of Aluminum (Al) are deposited using e-beam evaporation (Figure 5.1(b)). The bottom Ni forms the Ohmic contact to SiC while Al is used here as a hard mask for etching SiC by reactive ion etching (RIE) in an SF_6 / O_2 plasma. The metals were first patterned to open a window for RIE etching of the SiC. For all lithography steps, the positive Shipley resist S1813 is used. The Al mask was etched using H_3PO_4: HAc: HNO_3:H_2O (16:1:1:2) and Ni was etched using $FeCl_3$. Figure 5.2(a) shows the optical image of device, after 1st lithography step for patterning of Al hard mask to protect device area during the plasma etching in next step.

After patterning the first layer, SiC was etched using SF_6 and O_2 plasma (figure 5.1(c)). Here, different sets of flow rate of the SF_6/O_2, power and plasma time are tried in order to determine a recipe for etching SiC. Our experiments show that power of 120 W, plasma time of 2 min, SF_6 /O_2 flow of 15/5 sccm etches the SiC. The diode area achieved after RIE is ~ 70 x 70 μm^2. Next, 300nm of SiO_2 was deposited using PECVD process (Figure 5.1(d)) and patterned to open a window on Si area (Figure 5.1(e)). During the SiO_2 growth process the substrate was maintained at constant temperature of 300 ºC. In the next step SiO_2 is etched using buffer oxide etch (BOE). to open a window for forming Ohmic contacts to Si. The optical image of window opened in SiO_2 is shown in Figure 5.2(c). The top metal layer of Al is deposited to serve as an Ohmic contact to the Si side of the diode. In the final step, the Al was patterned to release the diode structures (Figure 1(f)). The fabricated CPW structure is shown in Figure 5.3 the ground (G) pad is the contact to Si and the signal(S) pad is the contact to SiC.

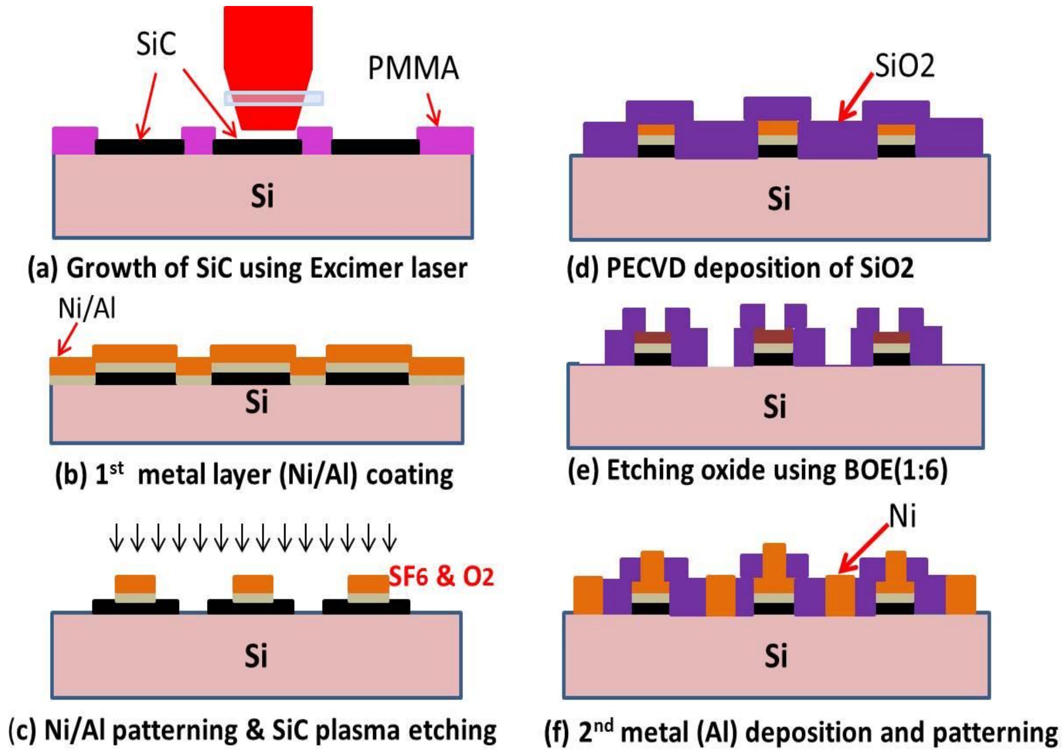

Figure 5.1 Fabrication steps for SiC/Si diodes for RF circuits

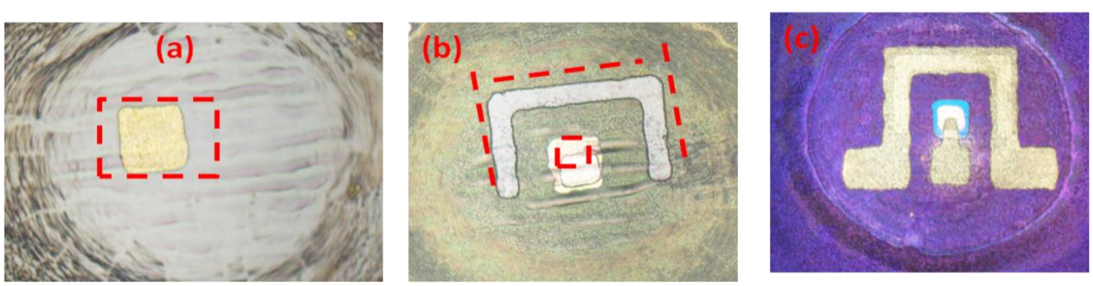

Figure 5.2 Optical pictures of fabricated diodes (a) After 1st layer patterning (b) 2nd layer patterning (c) 3rd layer patterning

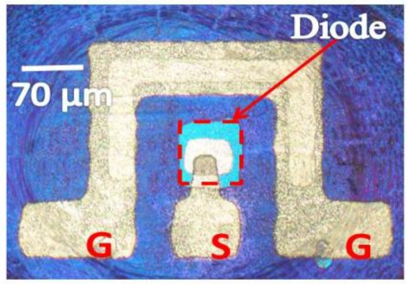

Figure 5.3 Fabricated CPW structure with SiC/Si diode

5.2 Experimental Results: Low doped wafer

5.2.1 Current – Voltage characteristics

Figure 3 shows the measured current -voltage (I-V) characteristics of the small are SiC/Si diode for low doped wafer at room temperature and under dark conditions. The measurements are shown for the best performing diode (2 laser pulses) and for optimum focus. The diode shows good rectification and a small leakage current of ~10nA (-1V).

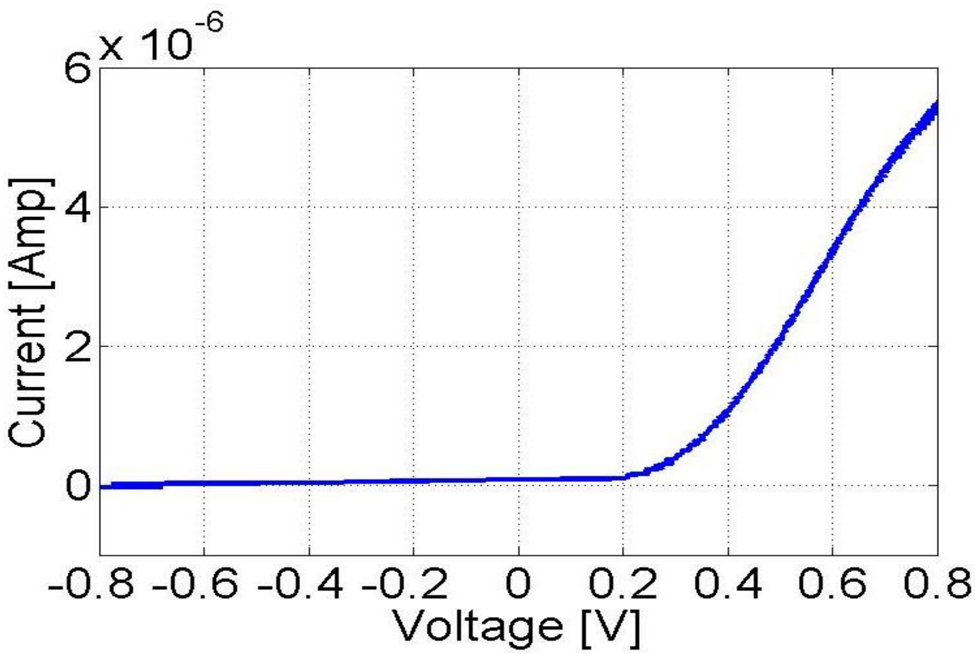

Figure 5.4 Measured J-V characteristics of a small area SiC/Si diode for low doped wafer (Type I)

5.2.2 Microwave rectification

Microwave or millimeter wave detectors are fundamental building blocks for applications such as wireless power transmission, concealed weapon detection, spectroscopy and medical imaging and energy recycling [158-161]. For high power rectification devices based on wide-bandgap semiconductors are required [162]. Here, performance of SiC/Si heterojunction diodes fabricated using laser process is investigated for microwave detection. All measurements were carried out at room temperature by probing the devices using a 50 Ω coplanar GSG probe.

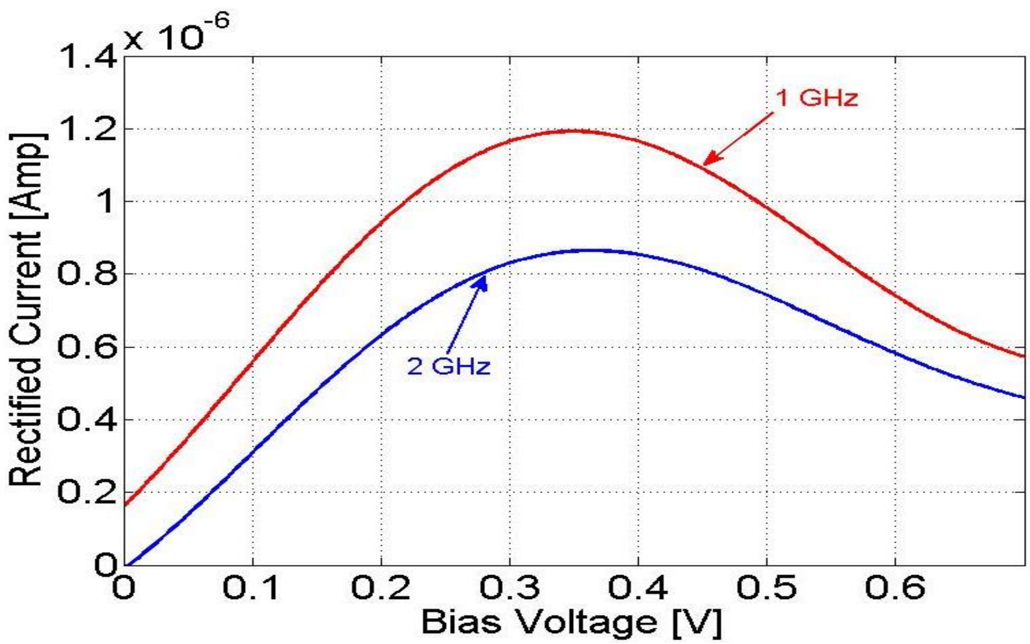

Figure 5.5 Measured rectified current vs applied bias at 1 and 2 GHz at input RF power of 5 dBm for low doped wafer (Type I)

For the measurement, the signal (RF +DC) is applied to the device through a CPW probe, T-Bias and via a directional coupler (HP87300B). The directional coupler is used to acquire incident and reflected waves from the device and is measured through a spectrum analyzer. The I-V characteristics are measured with RF on and off conditions and the delta current at a certain bias point is extracted. The high frequency losses are also measured in order to estimate the actual power delivered to the device. Figure 5.5 shows the measured rectified current as a function of applied DC bias for 1 and 2 GHz at fixed input RF power of ~ 5 dBm. The highest measured rectified voltage is near bias voltage of ~0.35V, which is close to the strongest non-linearity point of the diode. Figure 5.6 shows the rectified current as a function of frequency shows the rectified current as a function of frequency, and at a fixed bias of ~ 0.35 V and RF power of 5 dBm, which is close to the strongest non-linearity point of the diode.

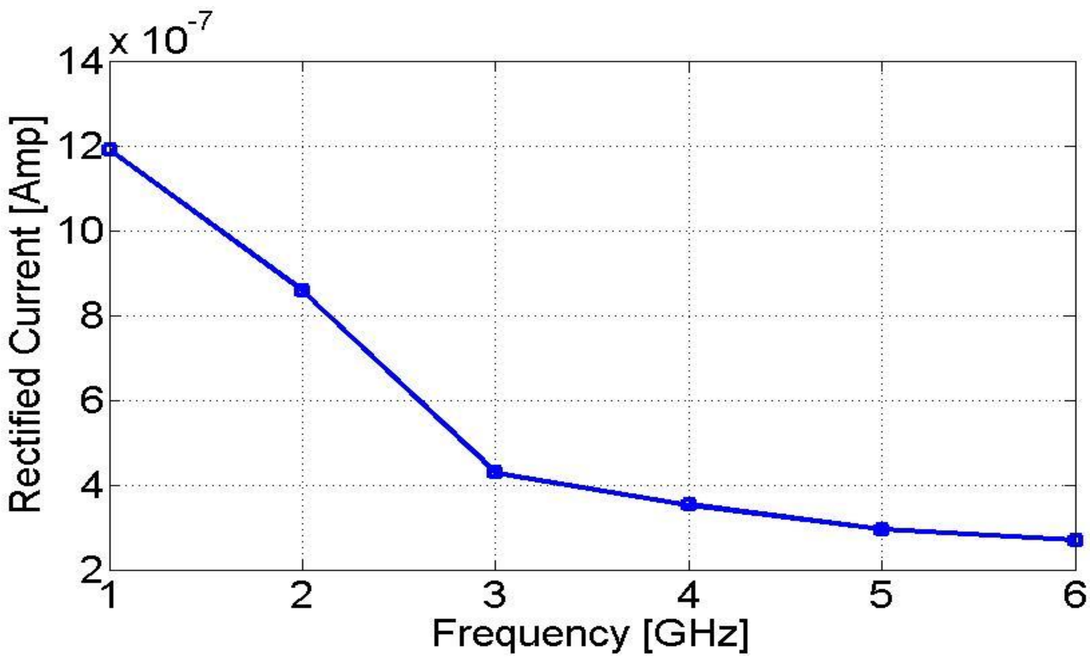

Figure 5.6 Rectified current vs Input frequency for SiC/Si RF diodes at a fixed bias of ~ 0.35 V and RF power of 5 dBm for low doped wafer

The results show the rectified current decrease as a function of frequency due to the parasitics associated with the diode. However current is in detectable microamp range were observed over a wide range of input frequencies of 1 – 6 GHz. For instance, diode shows rectified current of 1.2 µA and 0.43 µA at 1 and 3 GHz respectively and current remain above ~ 0.3 µA over the entire measured frequency range. Considering the large area of the device and low doping the device is performing well. However better performance with much higher rectified current is expected from wafer with higher doping (Type II) as presented in next section.

5.3 Experimental Results: Highly doped wafer

5.3.1 Current – Voltage characteristics

All the measurements presented in this section were carried at room temperature and under dark conditions. Figure 5.7 shows the measured current density-voltage (J-V) characteristics of the large area (500 x 350 μm^2) SiC/Si diode over a wide voltage range. The measurements are shown for the best performing diode made with 2 laser pulses. The diode shows a high reverse breakdown voltage of >200V (source limited) with very small leakage current of ~5μA/cm^2 (-5V). The small leakage current indicates fewer defects at the interface. The inset of Figure 3 shows plots of the measured log I vs. V and curve fitted to the diode equation at room temperature for a small area diode. A fit to diode equation gives ideality factor (n) = 3.2 and a series resistance (R_s) = 6 kΩ.

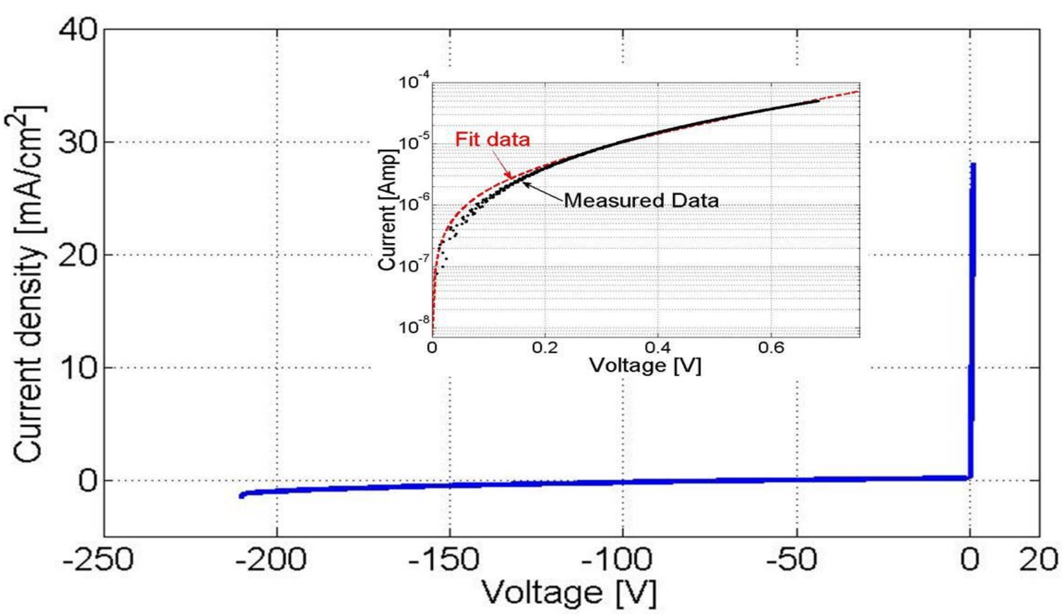

Figure 5.7 Measured J-V characteristics of a large SiC/Si diode, and the inset shows the I-V of a smaller device curve fitted to the diode equation

5.3.2 Microwave Rectification using SiC/Si Diode

The experimental set up is same as described in previous section. Figure 5.8 shows the measured rectified current as a function of applied DC bias for 5 and 6 GHz at input RF power of ~ 4 dBm. The highest measured rectified voltage is near bias voltage of ~0.35V, which is close to the strongest non-linearity point of the diode, as shown in Figure inset of figure 5.7.

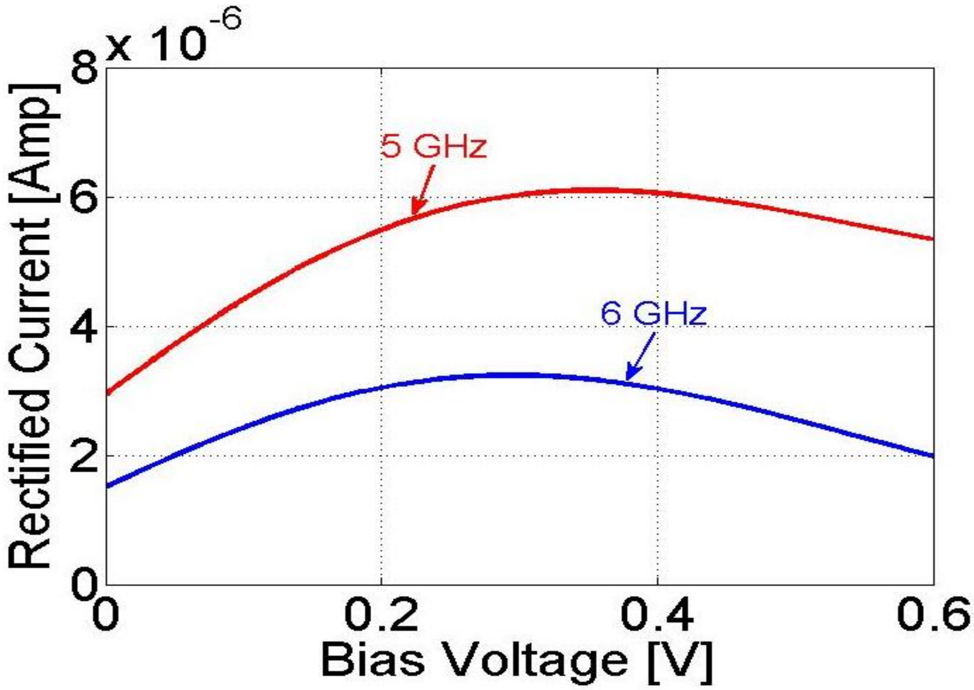

Figure 5.8 Rectified current vs applied bias at 5 and 6 GHz at input RF power of 4 dBm for wafer with higher doping (type II)

The diodes are performing well as microwave detection with high sensitivity. Considering the large area of the device and low doping the device is performing well. Figure 5.9 shows the rectified current as a function of frequency, and at a fixed bias of 0.35 V. The measured result shows reasonably high detected current of 35 µA for 2 GHz and 12 µA for 4 GHz and current remain above ~ 1 µA over the entire measured frequency range (2-7 GHz). Diode is performing better with much higher rectified current than wafer with lower doping (Type I) as expected.

For example, diodes made on wafer type II shows rectified current of 35 μA at 2 GHz while diodes made on low doped wafer shows current of 0.86 μA. deviation.

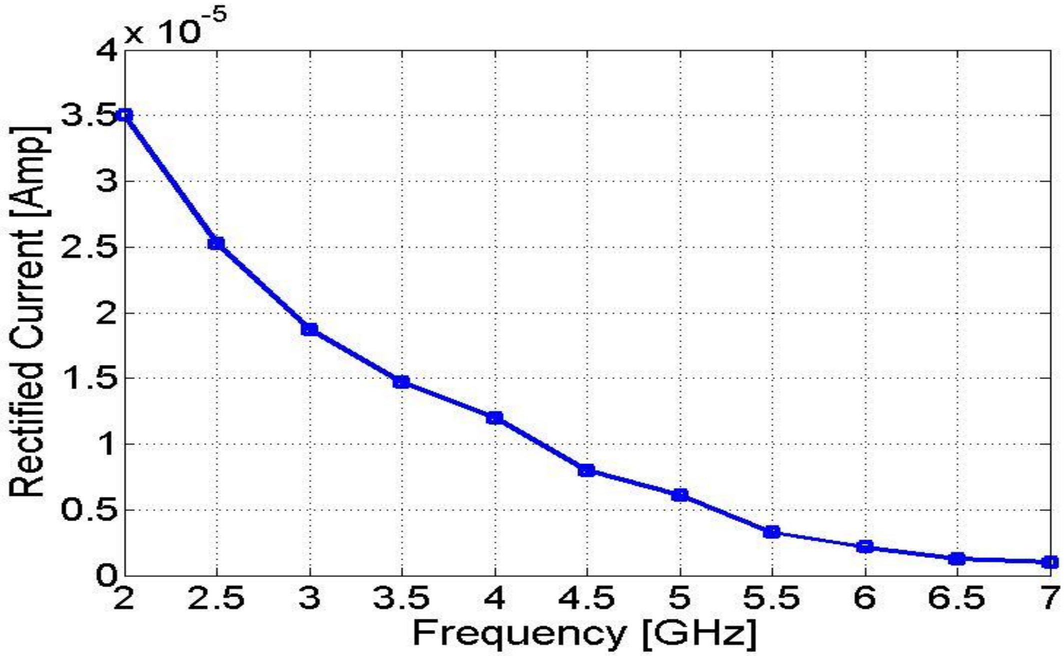

Figure 5.9 Rectified current vs Input frequency for SiC/Si RF diodes at a fixed bias of ~ 0.3 V and RF power of 4 dBm

The detected current decreases with increasing frequency as expected, due to higher impedance mismatch at higher frequencies. The higher frequency performance of the device is limited by transit time and can be further improved by lowering the series resistance and capacitance. The lower series resistance can be achieved by annealing the contacts in order to reduce the contact resistance, while diodes with smaller area can be used to achieve lower capacitance. Figure 5.10 shows measured detected current as a function of input power for 3, 5 and 6 GHz and at a fixed bias of 0.35 V. From the slope of Figure 5.10 it can be verified that the detected current response is linear (log scale) over a wide power range (-10 dBm to 4 dBm) and follows the square law detection with slight The diodes were measured multiple times to make sure it can withstand cycle of high power level and same results are achieved every time. The maximum

RF power applied to the diode is limited by source, but it is expected that higher detected current can be achieved at even higher power level without breaking down. The measured result shows that device has sensitivity of ~ 8.4mA/W for 3 GHZ signal in the measured power range.

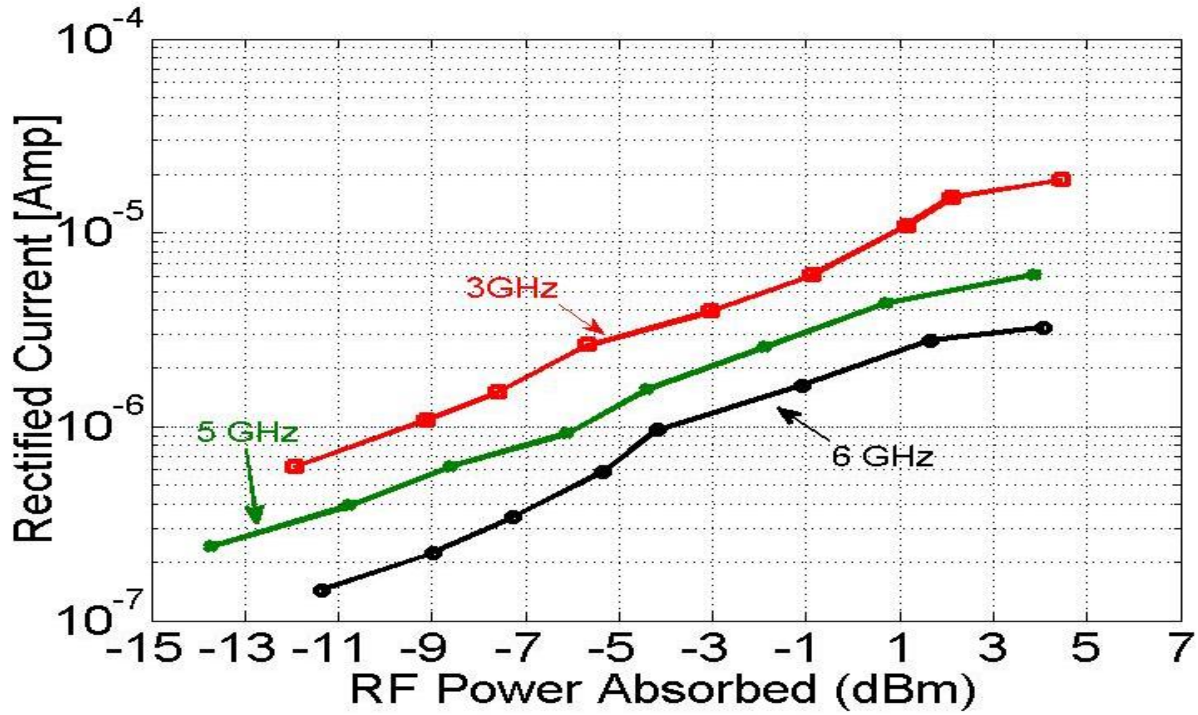

Figure 5.10 Measured rectified current vs. input RF power for SiC/Si diodes diode at 3, 5 and 6 GHz with applied bias of 0.35 V

5.3.3 SiC/Si Diode based Frequency Doubler

High power frequency multipliers are an essential part of the communications systems, as they are required to generate high frequency signals in the MMW to terahertz (THz) frequency range. Frequency multipliers are often used in a variety of applications such as frequency synthesizers, transceivers, down converters [163-165] and recently finding applications in future 60 GHz broadband wireless systems and 77 GHz automotive radar [101]. Any nonlinear component such as diodes, varactors or transistors can be used to generate harmonics. Frequency multiplier based on different semiconductor technologies such as GaAs metamorphic

HEMT (mHEMT), SiGe BiCMOS and AlGaN/GaN HEMTs h8as been demonstrated in past [166, 167]. GaN on SiC based HEMTs has led to the highest power levels achieved so far. Recently, there is great interest in developing low cost frequency multipliers for commercial (Monolithic Microwave Integrated Circuit) MMIC transceivers. Si-based technologies offer low-cost and high volume commercialization for single-chip transceivers, however for power applications, the mostly hybrids GaN on SiC based multipliers are still prominent [168]. Here we report a frequency multipliers based on SiC/Si diodes. Second order harmonics were observed over a wide range of fundamental frequencies (f_{in}) of 2 – 6.5 GHz with input power level of -3 dBm (Figure 5.11).

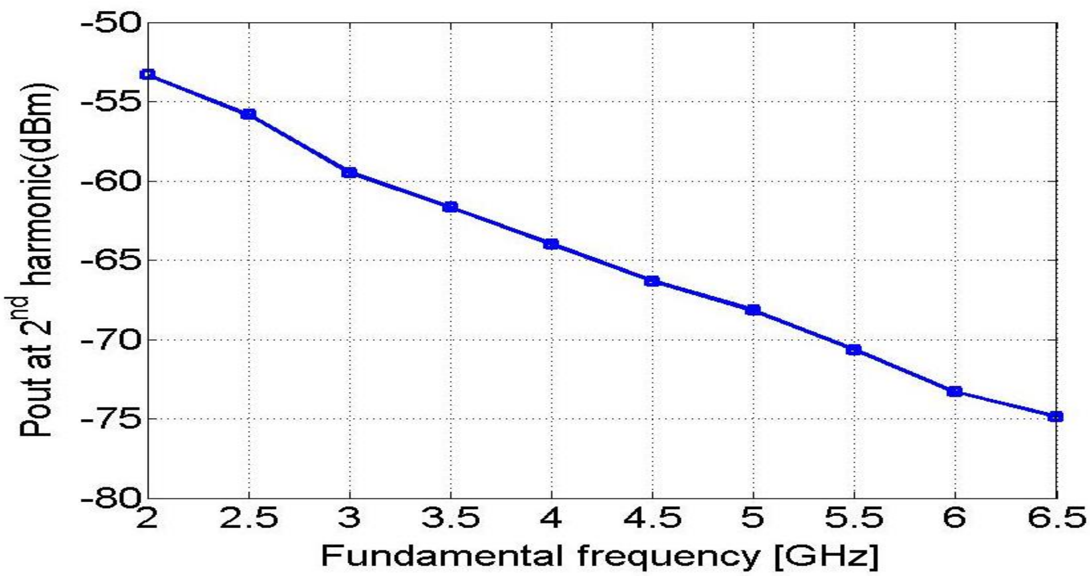

Figure 5.11 Measured output power of 2nd harmonic versus fundamental frequency of a SiC/Si device at a fixed input power of approximately -3 dBm

The diode shows an output power - 53 dBm for 2 x f_{in} = 4 GHz, and the highest measured output power remains above -72 dBm for frequencies up to 2 x f_{in} = 12 GHz. Considering the large area of the device, good conversion efficiency is achieved in the high frequency region. The output power decreases at higher frequencies due to transit time loss and impedance mismatch. Figure 5.12 shows the output power of the 2nd harmonic as a function of input power at f_{in} = 2 and 4 GHz. The output power increases linearly with input power over the entire input power range, demonstrating a stable operation of the diode. Higher input power levels are not used here due to presence of harmonics in the source used for the measurement. It is anticipated that higher output power can be achieved with more RF input power. This is clear from detection results where comparatively higher power is used. In future the results can be further improved by employing an impedance matching circuit and bandpass filter to filter the desired harmonic and suppress unwanted frequencies.

Figure 5.12 Measured output power of 2nd harmonic for SiC/Si at fundamental frequencies of 2, 4 GHz

5.4 Preliminary 100 GHz Detection Measurements

The measurement setup for characterizing the RF response of a detector is shown in Fig. 5.13. A W-band (75-110GHz) Backward Wave Oscillator (BWO) was used as the source. The transmitting antenna is a horn antenna which send signal to dipole antenna. The power coupled from horn to dipole antenna depends on the area ratio of two antennas. Since the radius of the dipole antenna is very small, very small power is coupled into the antenna and thus to the diode. Here, the dipole antenna is also acting as contact to the diode. The rectified voltage generated from the detector was measured using a Keithley nano-voltmeter. Measurements were carried out by fixing the wave frequency and power while changing the forward bias. The power received by the dipole (wire) antenna was measured, by calculating the area differences between horn antenna and device log-periodic antenna. Figure. 5.14 show the measured rectified output voltage at different DC forward bias points. The RF frequency on the detector is 100 GHz. A maximum rectified voltage of 7mV is measured near a DC bias of 0.3V. The diode detector shows highest detection at strongest non-linearity. The set up used here for getting preliminary results purposes and proof of concept purposes. In future, planar antenna/waveguides would be fabricated on the wafer with diodes embedded in between them. In conclusion, SiC/Si diodes fabricated by a novel excimer laser process have been investigated for high power microwave circuit applications.

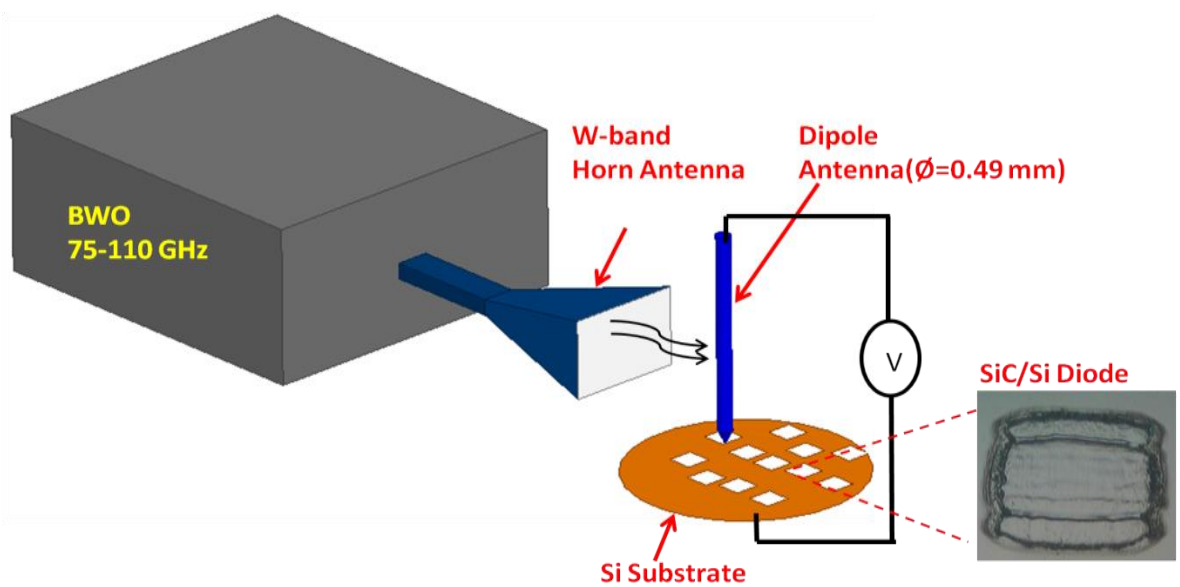

Figure 5.13 Experimental set up to measure detection measurement at 100 GHz

The diodes show strong non-linear I-V characteristics with small leakage current and high breakdown voltage. Successful demonstration of microwave rectification and frequency multiplication in the frequency range has been achieved. These results clearly attest to the viability of high-performance SiC based microwave devices on low-cost, large diameter Si substrates. This technology can potentially reduce manufacturing cost associated with high-high power high frequency devices, and also provide a path to directly integrate SiC/Si devices along with CMOS circuitry.

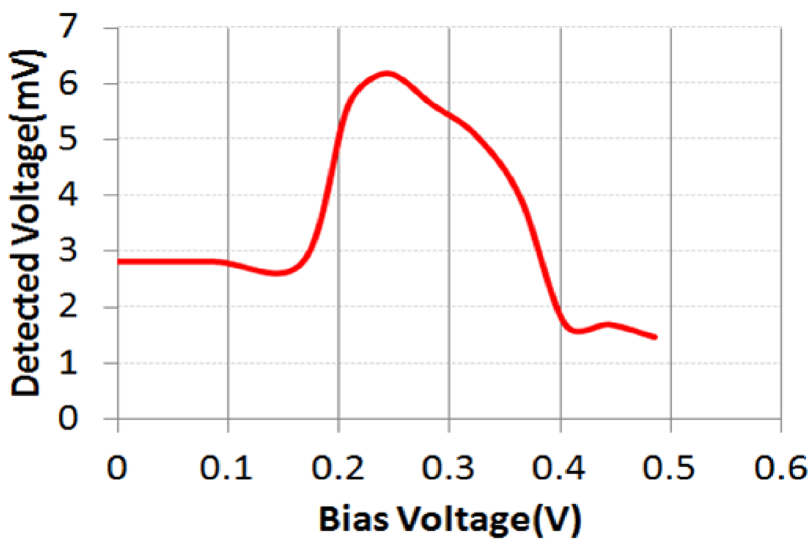

Figure 5.14 Measured detection/ rectification at 100 GHz for SiC/Si diode using point contact

CHAPTER 6: CONCLUSION AND FUTURE WORK

6.1 Conclusion

Starting from the introduction of MMW and its unique properties for different applications, the thesis first introduced the importance of heterogeneous integration of different device technologies for MMW circuit applications. Based on the literature and the need for future microwave and MMW systems two key challenges that needs to be solved includes: 1) integration of active devices on flex substrates for low power RF applications, and 2) integration of high power high frequency devices on silicon substrates. In particular, two terminal high frequency devices are needed to meet most of the application needs. Thus, this thesis focuses on diodes for high frequency applications, one for low-power applications and the other for high power applications. This work focuses on three types of diodes: Reduced graphene oxide based Schottky diodes, Metal-Insulator-Metal (MIM) tunneling diode and excimer laser synthesized Silicon Carbide/ Silicon (SiC/Si) heterojunction diodes. The use of these diodes allows to meet the need of fully integrated high frequency systems, i.e. Antennas, RF, Analog and Digital components, on a common substrate (e.g., a single chip).

The reduced graphene oxide based Schottky diodes have been implemented on high frequency compatible flexible substrate (PEEK) using asymmetrical metal contacts. The undercut self-alignment process used for fabrication allows the use of conventional optical-lithography to achieve small feature size. The diodes show strong non-linear I-V characteristics with forward current achieved on the order of µA and low series resistances. The diodes show zero-bias RF to DC rectification higher detection sensitivity of 30 V/Watt (at 22 GHz). Higher zero bias rectification sensitivity shows the potential of r-GO diodes in energy harvesting and transfer RF energy in smart sensors applications. In addition, these diodes show 3rd order frequency multiplication in the frequency range of 6 – 18 GHz. The devices demonstrated here allows for separate control of device size and band gap opening through chemical reduction. This work will motivate further research on realization of high-performance low power GHz circuits on flexible substrates.

MIM diodes is proposed as a non-semiconductor solution for MMW circuits on flexible substrate. Thin film MIM diodes with asymmetrical electrodes (Ti-TiO_2-Pd and Ni-Ni-NiO-Mo) were designed and demonstrated. The insulator layers, tunneling region, are obtained using two different techniques: in-situ oxidation for TiO_2 and plasma oxidation for NiO. Both of these diode designs show strong non-linearity with asymmetric I-V characteristics. The NiO based diodes shows higher current densities and higher ideality factor in comparison to TiO_2 based diodes. This can be attributed to growth of thin and high quality NiO using plasma oxidation. High frequency characterization of MIM diode was carried out using the following: (1) S-parameters measurement and equivalent modeling (2) Microwave to DC rectification (3) Frequency multiplication and mixing. To the best of our knowledge, this is the first time a detailed characterization of MIM diodes for high frequency applications have been carried out. The presented results of extracted diode resistances and capacitances can be useful in the calculating the area required for operation of MIM diodes in THz range. The diodes provide good rectification with measured sensitivity of 18 V/Watt and 70 V/Watt for TiO_2 and NiO based diode, respectively. The diodes also were determined to work efficiently at zero bias. NiO based diodes show higher detection sensitivity due to lower capacitance and better impedance matching than TiO_2 diodes. This can be attributed to lower dielectric constant value of NiO as compared to TiO_2. The nonlinearity of the diodes was also characterized by measuring multiplication characteristics and the diodes show 2^{nd} and 3^{rd} order frequency multiplication.

The TiO_2 based devices shows multiplication in the frequency range of 1 - 4 GHz, while the NiO based diode shows multiplication at even higher fundamental frequency range of 2-10 GHz. Diodes with different area are also fabricated and their performances are compared. The area required for the diodes operating at millimeter wave and beyond can be estimated using equivalent model (extracted from S-Parameter results).

A novel technique was proposed to selectively grow wide bandgap SiC material on Si for high power microwave applications. This low cost technique allows for direct and selective growth of SiC on Si under ambient conditions which is very challenging to achieve using conventional methods. The fabrication of SiC/Si heterojunction diodes is done using a high power KrF excimer laser. The electrical performances show that the devices with very high breakdown voltages (>200V) can be fabricated using this approach. The diodes show a good rectification ratio of 1.0×10^4 at ±1.0 V and low leakage current density of 6 $\mu A/cm^2$ (−1 V). As a first test of this new process for device applications, a photovoltaic cell with efficiency of approximately 8% is demonstrated. The device quality may further be improved by reducing series resistance and further optimizing the laser pulse power. The fabricated SiC/Si diodes were investigated for high power microwave circuit applications. Successful demonstration of microwave rectification with current in range of 18.72 µA for 3 GHz and frequency multiplication in the frequency range of 4-12 GHz (2^{nd} harmonic) has been achieved. These results clearly attest to the viability of high-performance SiC based microwave devices on low-cost, large diameter Si substrates. This technology can potentially reduce manufacturing cost associated with high-high power high frequency devices, and also provide a path to directly integrate SiC/Si devices along with CMOS circuitry. Furthermore, the results indicate that high frequency optical devices can be designed and fabricated using the process demonstrated under this work.

6.2 Future work

Graphene based diodes:

1. In the graphene based diodes presented here the band gap opening is achieve using chemical modification , but in future other energy gap opening mechanisms such as plasma oxidation of CVD grown graphene film can be investigated for microwave and MMW diodes.

2. Oxidation process generates various types of defects in the graphene lattice, which limits transport. At a low oxidation levels the band gap is small which gives GO the characteristics of a semiconductor. Different oxidation/reduction level of graphene/GO leads to different number of defects. Thus, a further study is needed to analyze the surface chemical composition and bonding of samples with different reduction times or levels. X-ray photoelectron spectroscopy (XPS) can be used to achieve this in future.

3. We used dielectrophoresis (DEP) as the deposition technique for graphene convenient way to evaluate the performance of the studied. But, in future other deposition techniques which are compatible with future printed electronics can be used. In particular, fabrication of multiple devices in parallel will be necessary to reduce fabrication costs and to improve throughput.

MIM DIODES

1. High frequency rectification measurements and imaging: The microwave rectification measurements were carried out by directly connecting the source to the diode and the rectified voltage was measured using a millimeter. Future work in this area could explore the integration of MIM diodes with antennas to actually show case zero-bias microwave and MMW rectification using ambient energy. Additionally, multiple MIM diodes can be implemented in rectification configuration to achieve better efficiency. Another possibility is to use the multiple insulator diodes Metal–Insulator-Insulator-Metal diode (MIIM), and integrate them with

antennas to achieve better efficiency. Multi-insulator diodes can be engineered to provide both low resistance and nonlinearity. An imaging system can be designed and demonstrated working in the THz spectral region.

2. Roll to Roll fabrication: The thesis presents the fabrication of MIM diodes on flexible substrate using conventional lithography techniques. However, the eventual goal should be to fabricate MIM diodes using a large-scale printing process which could offer the advantage of roll to roll printing of diodes that can be integrated with antennas and can be used for a range of applications requiring large substrate area (e.g., energy harvesting). Printing should be targeted on flexible and low-cost substrates which could lead to commercialization of MIM diodes for RF application- using the advantage of zero-bias operation over semiconductor based diodes.

Laser synthesized SiC/Si diodes

1. Doping of SiC: Laser has been successfully used in the doping of CVD grown SiC. In future this laser process can be advanced by introducing dopants during the SiC growth through Si melt. Dopants can be introduced with the polymer material (PMMA) to simultaneously dope and form SiC films. Laser can be used to assist doping of SiC with nitrogen, aluminum, phosphorous and boron. Laser process offers the advantage of locally increasing the temperature without heating the whole substrate. Moreover both doping and activation of dopant can be achieved in a single process. P-type doping of SiC can be achieved by boron spin-on dopant solution and irradiation with high power excimer laser pulse. The thickness of the doped layer depends on the absorption of laser energy by SiC. As SiC has higher absorption at 248 nm, it will results in thinner doped layers. This also causes concentrated localized temperature rise which also help in diffusion of boron. Due to localized heating, the temperature drops down

quickly and thus the dopant gets trapped in the film. The doping profile may be controlled by energy density of pulse which needs further study.

2. Graded bandgap structure: Devices with graded bandgap structure are of interest for variety of application. A detailed study can be carried in future to control the laser power density to achieve graded bandgap SiC film. The substrate can be exposed to different power levels during laser melting of Si to form SiC films. The forbidden energy bandgap (Eg) is dictated by the Si to C ratio in SiC films and this will be controlled as a function of depth to achieve desired band grading.

3. Device measurement and modeling: In order to validate the developed process and to understand the underlying physics, detailed modeling and characterization of the devices needs to be carried out. Device modeling includes barrier height, understanding of mid-level and surface traps if present, carrier lifetime, carrier mobility, etc. Understanding of these and other key device parameters will allow us to improve the efficiency of the devices.

4. Fabrication of devices on large area for photovoltaic applications and high frequency optical applications: For preliminary experiments, Si-SiC devices with approximate area of 500µm X 400µm were fabricated. For applications devices that are significantly large needs to be fabricated and characterized. The preliminary measurements here have shown that high speed optical devices can be designed using SiC on Si. This should be further explored for direct RF to optical conversion and vice versa. This will become an important area of research in particular with growing interest in internet of things (IOT).

APPENDICES

Appendix A: Reduced Graphene oxide based diode

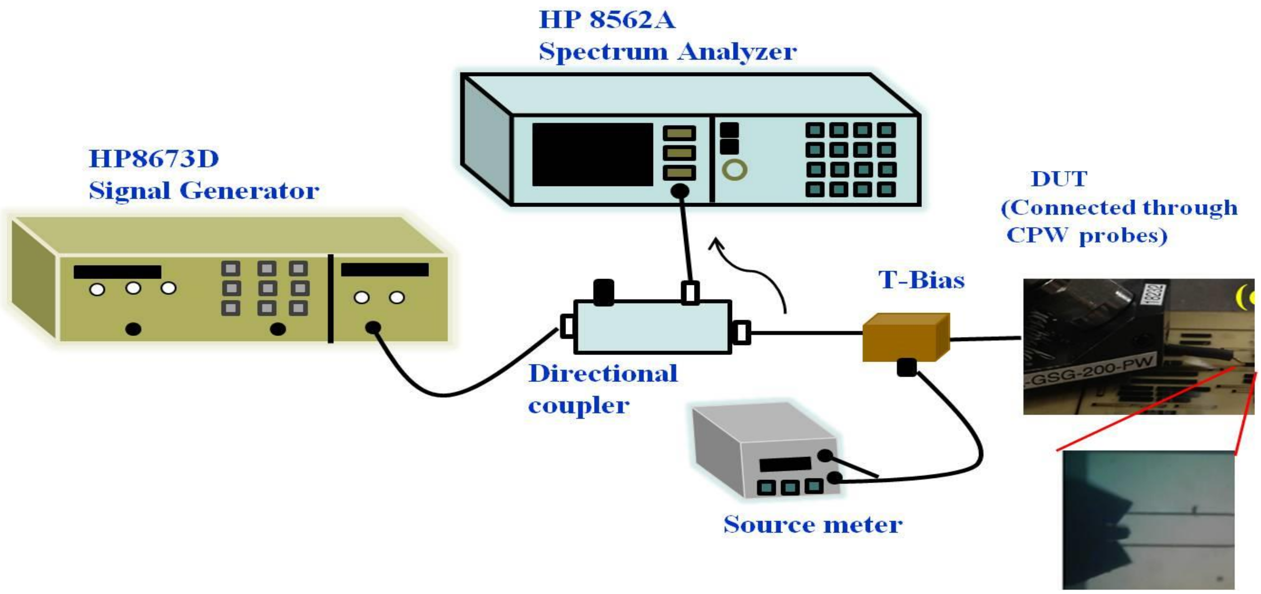

Figure A.1 Measurement set up for microwave rectification/ frequency multiplication

1) Frequency mixing :Top contact Ti-RGO-Pd diode

- Deviation from linearity - self-biasing
- IF($f_{IF} = f_{RF} - f_{LO}$) signal power vs. the input RF power at fixed LO power = -10 dBm

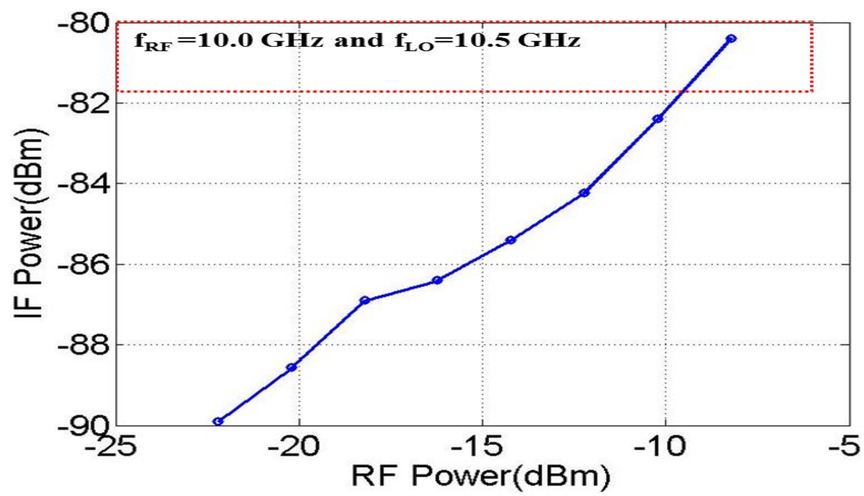

Figure A.2 Frequency mixing for Ti-RGO-Pd diode fRF =10.0 GHz and fLO=10.5 GHz

2) **I-V characteristics of RGO Ti-RGO-Pd Schottky diode (side metal contact)**

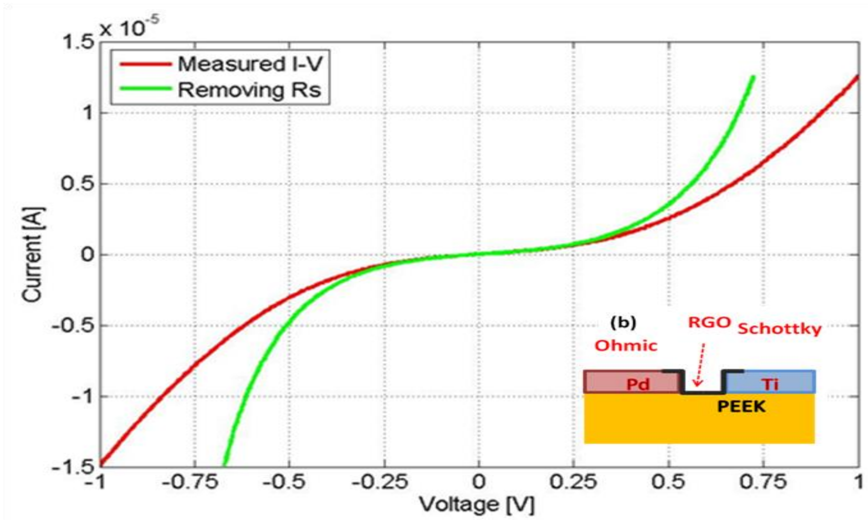

Figure A.3 Measured I-V characteristics of Ti-RGO-Pd Schottky diode (side metal contact) before and after removing series

3) **Microwave rectification for side metal contact Ti-RGO-Pd RGO diode**

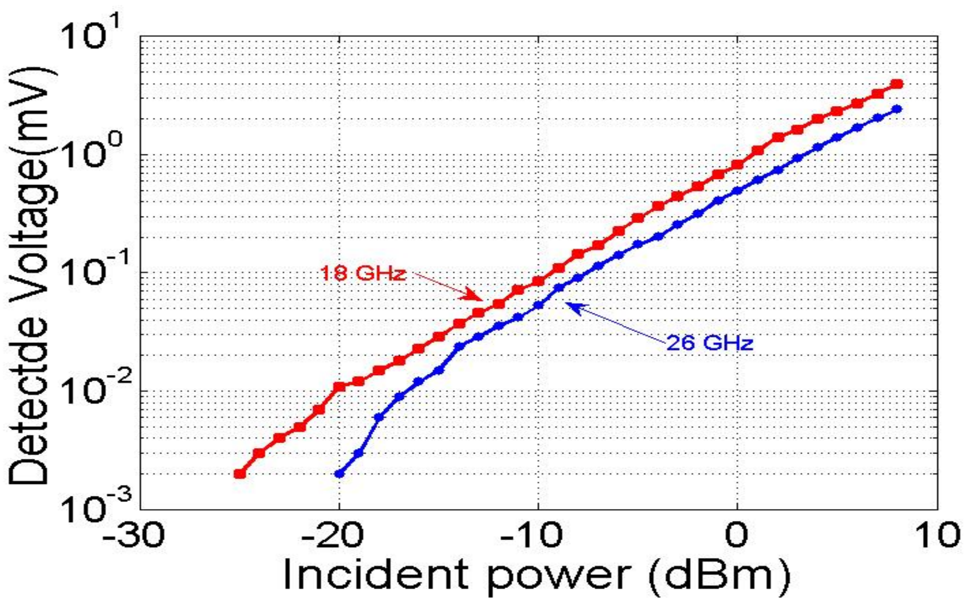

Figure A.4 Measured dc output voltage versus input power for side metal contact Ti-RGO-Pd RGO diode at 18 and 26 GHz under zero bias conditions

4) Frequency multiplication: Side contact Ti-RGO-Pd RGO based diode.

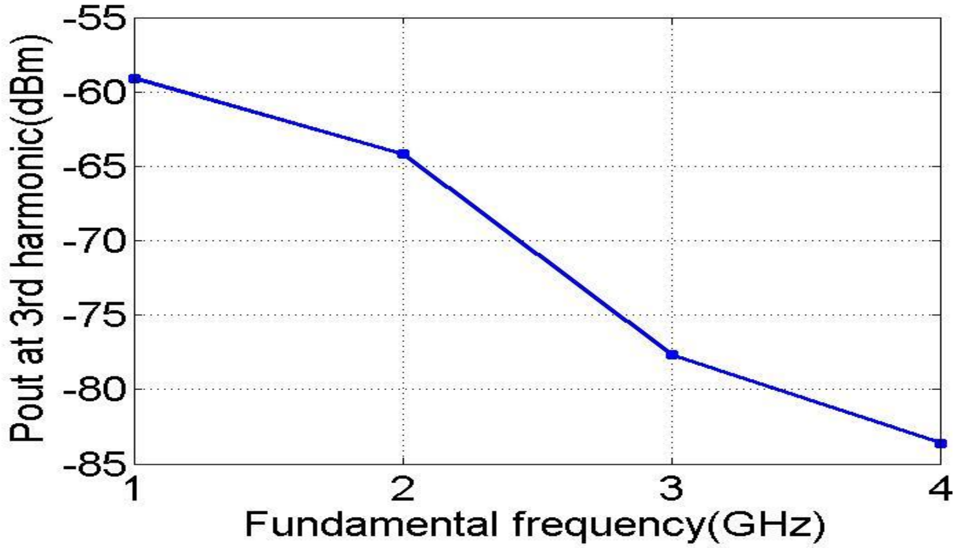

Figure A.5 Measured output power of 3rd harmonic versus fundamental frequency for side contact Ti-RGO-Pd RGO based diode.

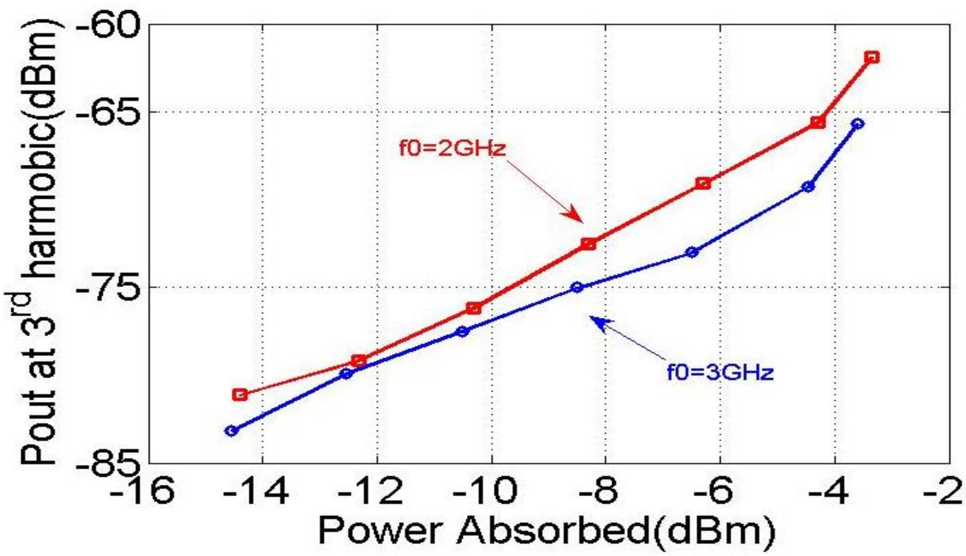

Figure A.6 Measured output power of 3rd harmonic versus input power for side contact Ti-RGO-Pd RGO diode

5) Measured I-V characteristics : Ti-RGO-Cu diode

6)

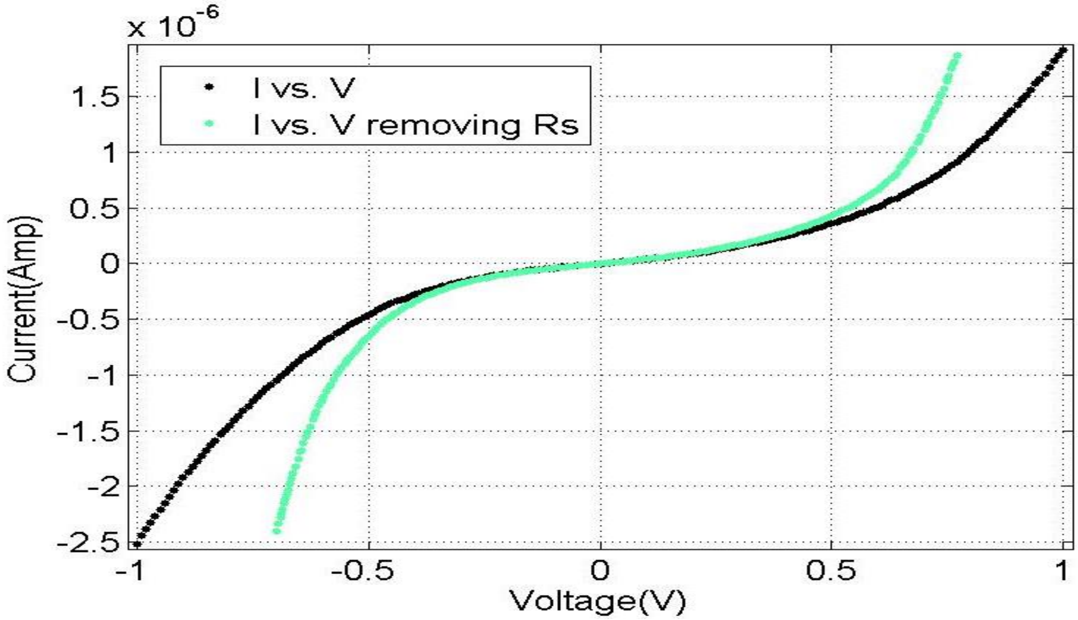

Figure A.7 Measured I-V characteristics of Ti-RGO-Cu before and after removing series resistance

Appendix B: MIM Diodes Ni-NiO-Ti based MIM Diodes

1) Microwave Rectification

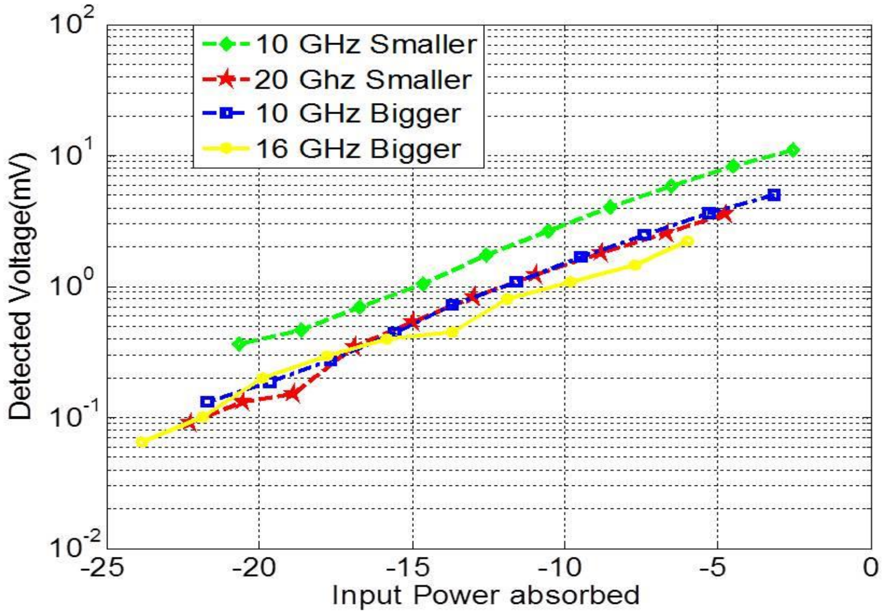

Figure B.1 Rectified voltage vs. Input RF power for Ni/NiO/Ti based MIM diode at fixed Bias

2) Frequency Multiplication: Ni/NiO/Ti based MIM diode

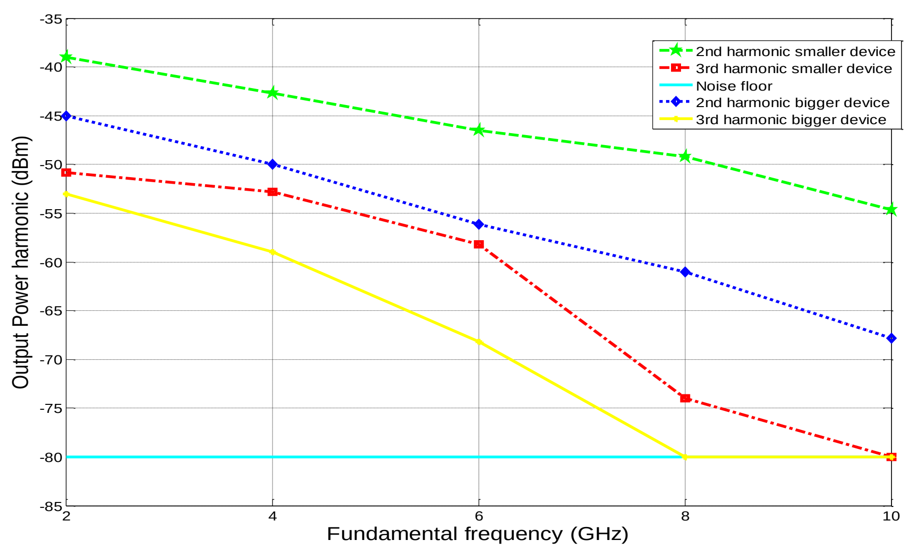

Figure B.2 Output power at 2nd harmonic vs. fundamental frequency for Ni/NiO/Ti based MIM diode at fixed Bias

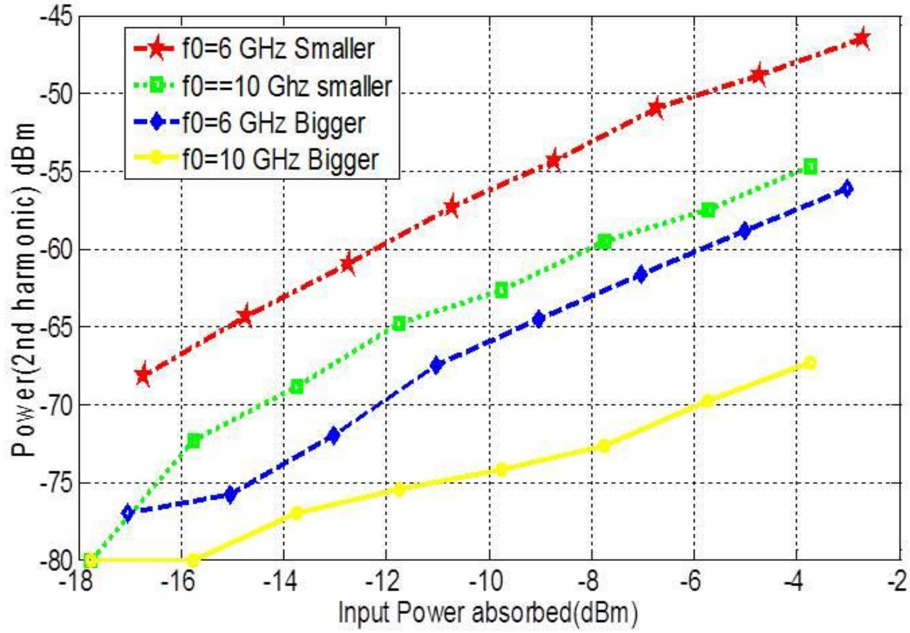

Figure B.3 Output power at 2nd harmonic vs. Input RF power for Ni/NiO/Ti based MIM diode at fixed Bias

Appendix C: SiC/Si diodes

Graded SiC on Si heterostructure are desired as they provider faster switching capabilities and high voltage operation. When semiconductor of different band gaps, work functions, and electron affinities are brought together to form a junction. In an abrupt junction the discontinuities in the energy bands is formed as the Fermi levels line up at equilibrium. The discontinuities in the conduction band ΔE_c and the valence band ΔE_v accommodate the difference in band gap between the two semiconductors ΔE_g.

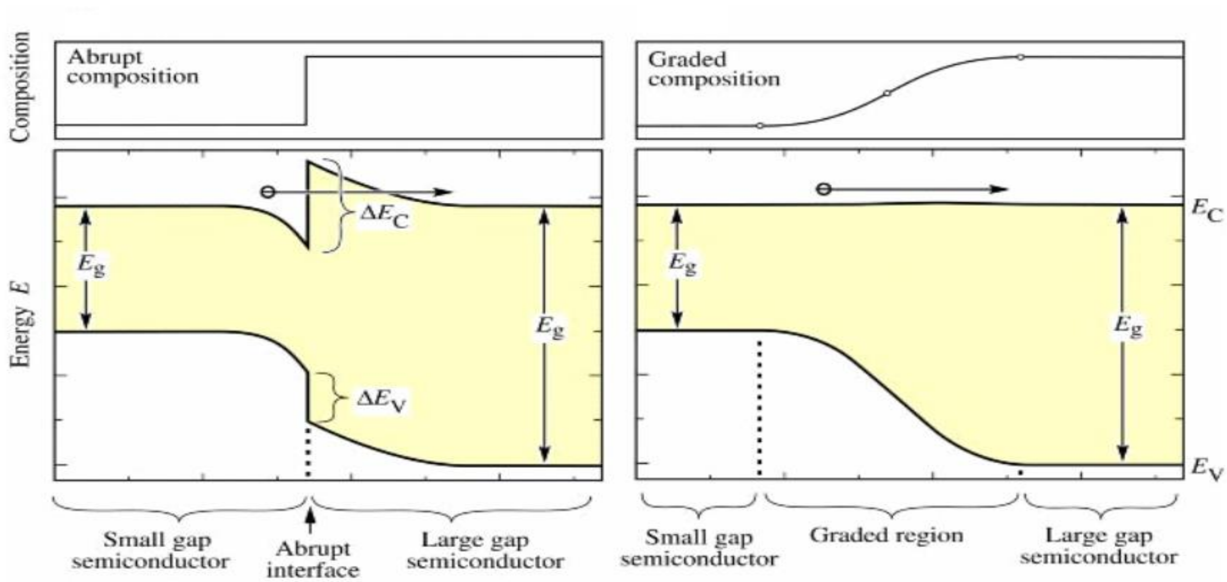

Figure C.1 Abrupt band gap and graded bandgap SiC/Si diodes

1) Graded SiC Bandgap: $Si_{(1-x)}C_x$: Indirect This is similar to the Vagard's Law

$Eg(x) = 1.1(1-x) + 3.8x$

$Eg(x) = 1.12+0.70x+3.68x^2$

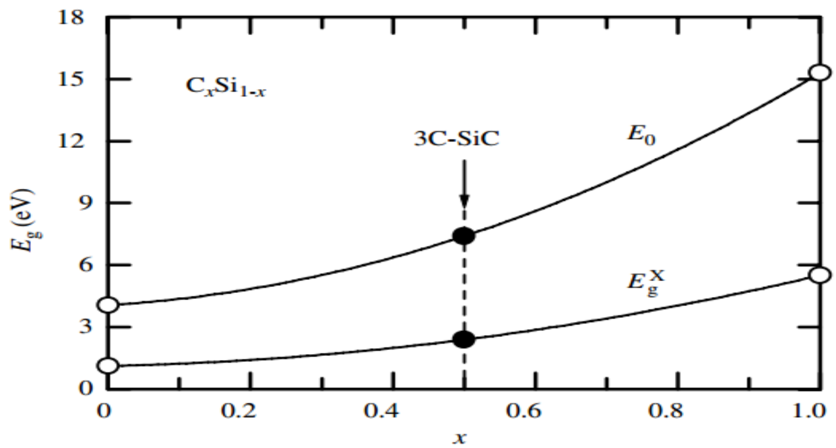

Figure C.2 Graded SiC Bandgap: Si (1-x)Cx

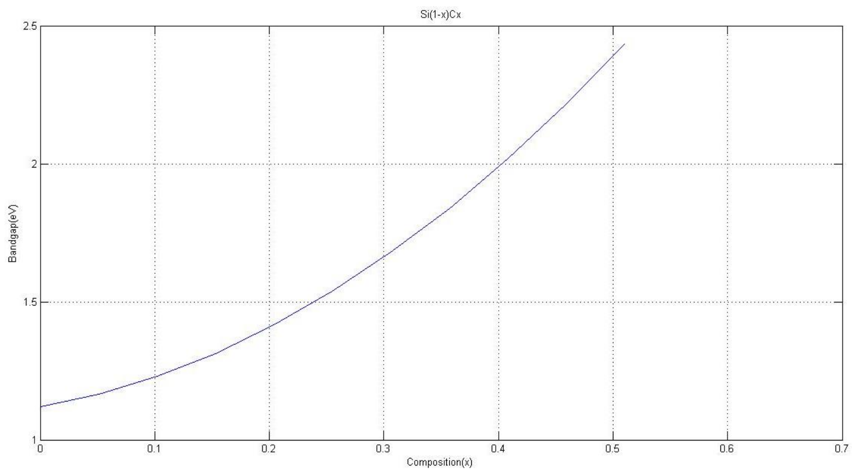

Figure C.3 Bandgap for $Si_{1-x}C_x$ as a function of Composition Ratio (x)

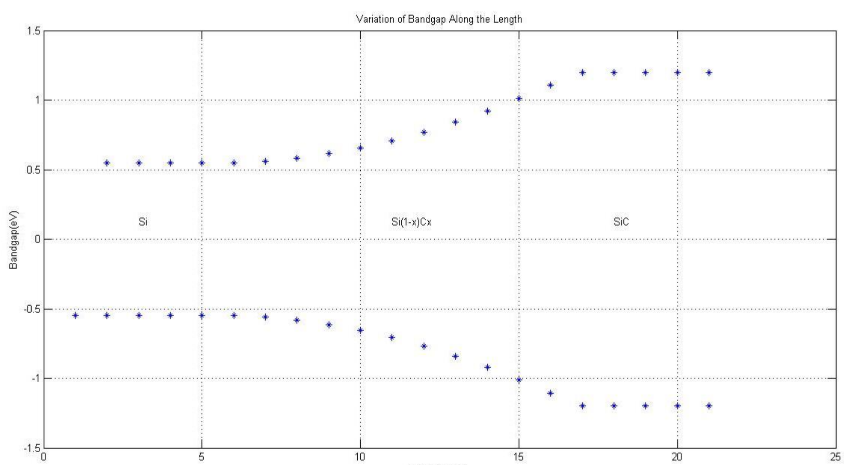

Figure C.4 Bandgap for $Si_{1-x}C_x$ –SiC along length of the device with no doping

2) Permittivity- $\mathcal{E}(x)=11.68(1-x)+9.75x$

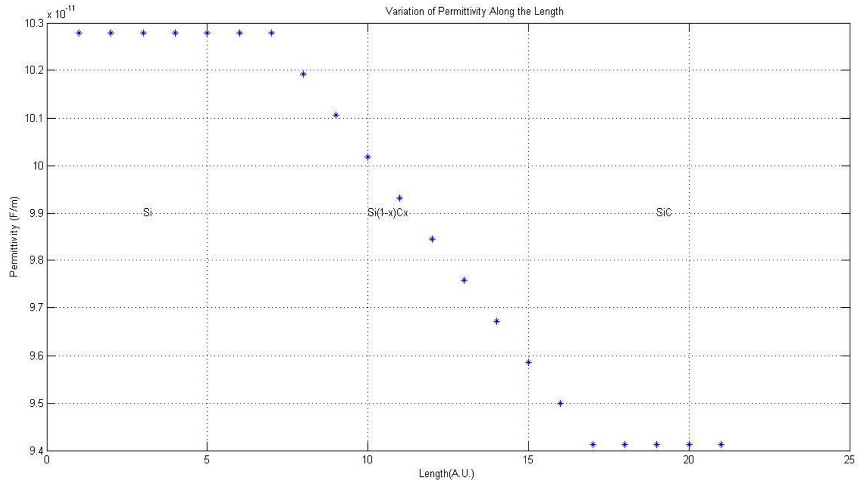

Figure C.5 Permittivity variation along length

3) Temperature Dependence

E_{gSiC} (T)=2.4-6x10^{-4} $\frac{T^2}{T+1200}$

E_{gSi} (T)=1.12-4.73x10^{-4} $\frac{T^2}{T+1200}$

E_{gC} (T)=3.68-2x10$^{-4}T^2$ $\frac{1.27T-1860}{(T+1200)(T+636)}$

4) Schottky Barrier

$\varphi_{BO}=(\varphi_m-\chi)$, where φ_m=Metal work function and χ=Electron affinity of Semiconductor

This is the barrier seen from the metal side.

Built in Potential- $Vbi= (\varphi_{BO}-\varphi_n)$ where $\varphi_n=\frac{KT}{q}\ln\frac{N_c}{N_d}$

This is the barrier seen from the semiconductor side

Depletion Width of heterostructure

$$W=\sqrt{\frac{V_{bi}2\varepsilon n\varepsilon p(Ndn+Nap)^2}{eNdnNap(\varepsilon nNdn+\varepsilon pNap)}}$$

Junction Capacitance

$$W=\sqrt{\frac{e\varepsilon n\varepsilon pNdnNap}{2(Vbi+VR)(\varepsilon nNdn+\varepsilon pNap)}}$$

$$C = \frac{\text{Co}}{(1 + \text{Vr VT})\eta} \qquad \text{where } \frac{\text{C0}}{\text{A}} = \sqrt{\frac{q\epsilon_0\epsilon_a\epsilon_d N_a N_d}{2(N_a\epsilon_a+\epsilon_{d_a}N_d)(V_{bi}-V)}}$$

5) Lattice Constant- C=3.5670 Å and Si=5.4310Å

Due to huge lattice mismatch between C and Si a small amount of substantially incorporated C induces a substantial tensile strain in pseudomorphic CxSi1-x layers on Si.

a (x)=5.4310-2.4239x+0.5705x^2 Å

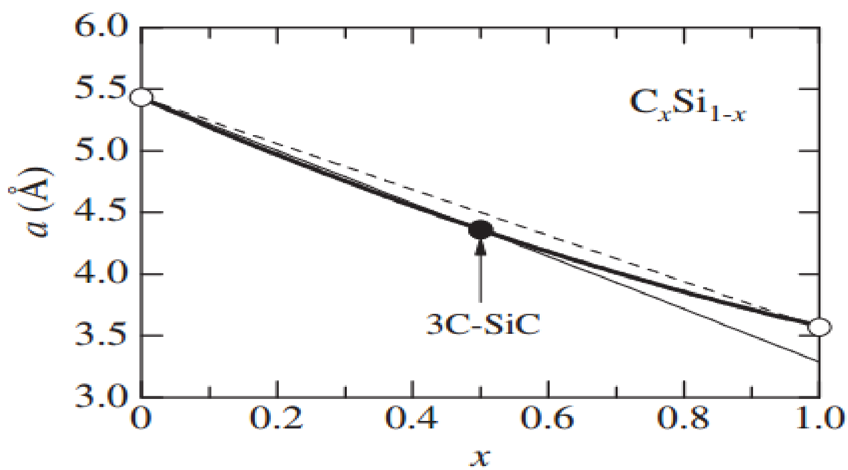

Figure C.6 Lattice constant variation along the length

6) Mobility

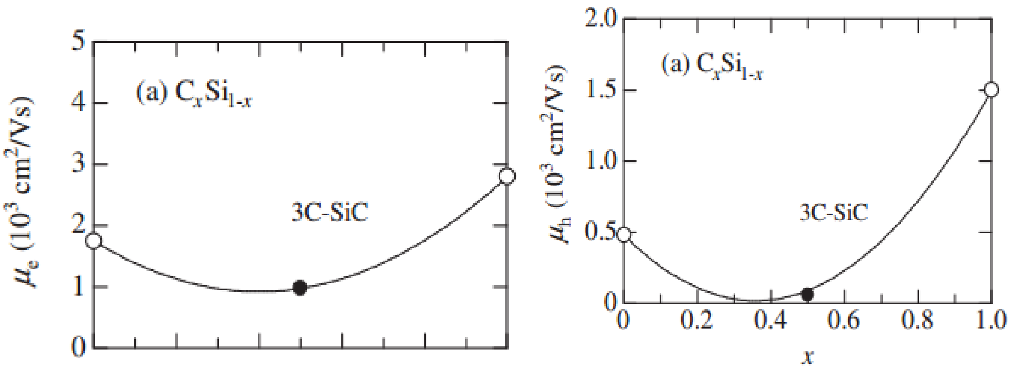

Figure C.7 Bowing parameters for the mobility

7) Current –Voltage characteristics: Experiment vs. simulation

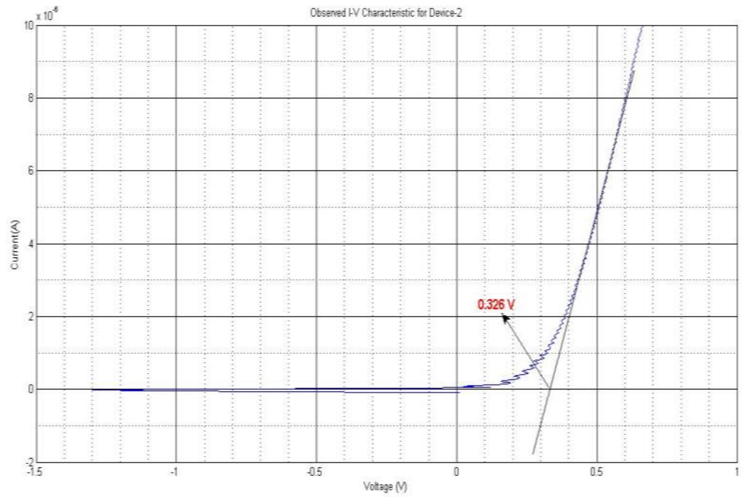

Figure C.8 Current –Voltage characteristics: Experiment

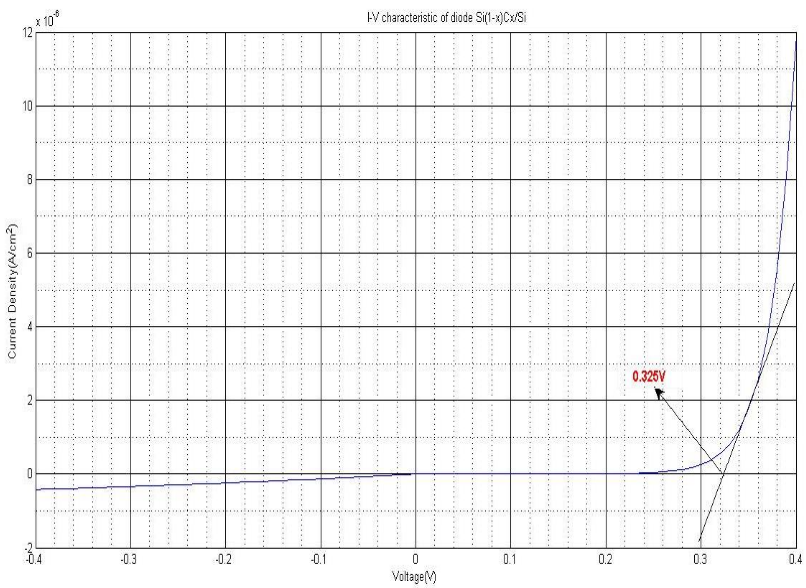

Figure C.9 Current –Voltage characteristics: Simulation

8) Capacitance –Voltage characteristics: Experiment vs. simulation

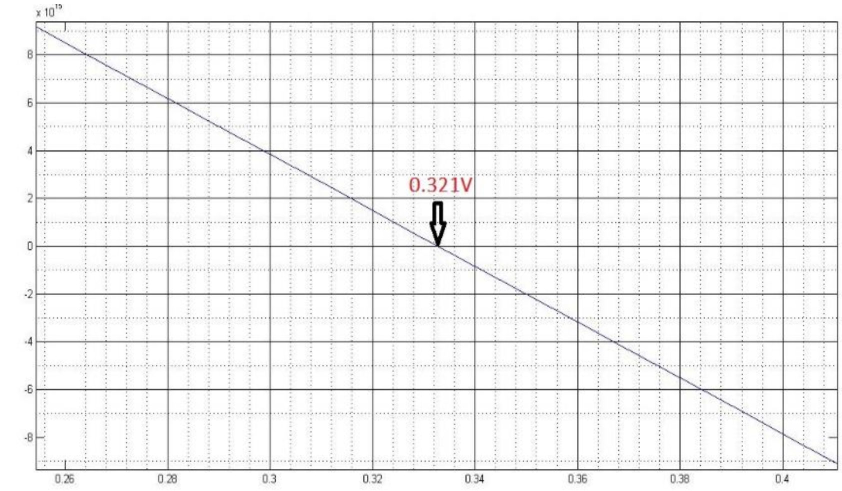

Figure C.10 Capacitance –Voltage characteristics: Experiment

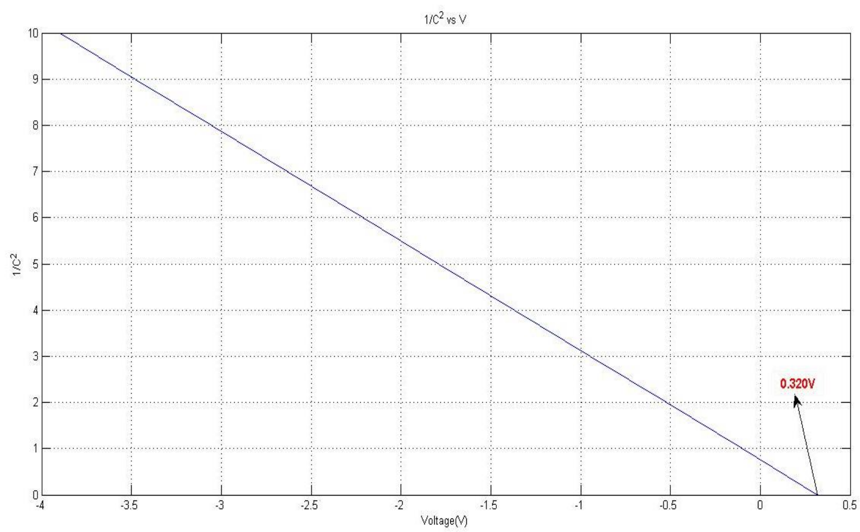

Figure C.11 Capacitance –Voltage characteristics: Simulation

9) Measured S-Parameters for SiC/Si RF

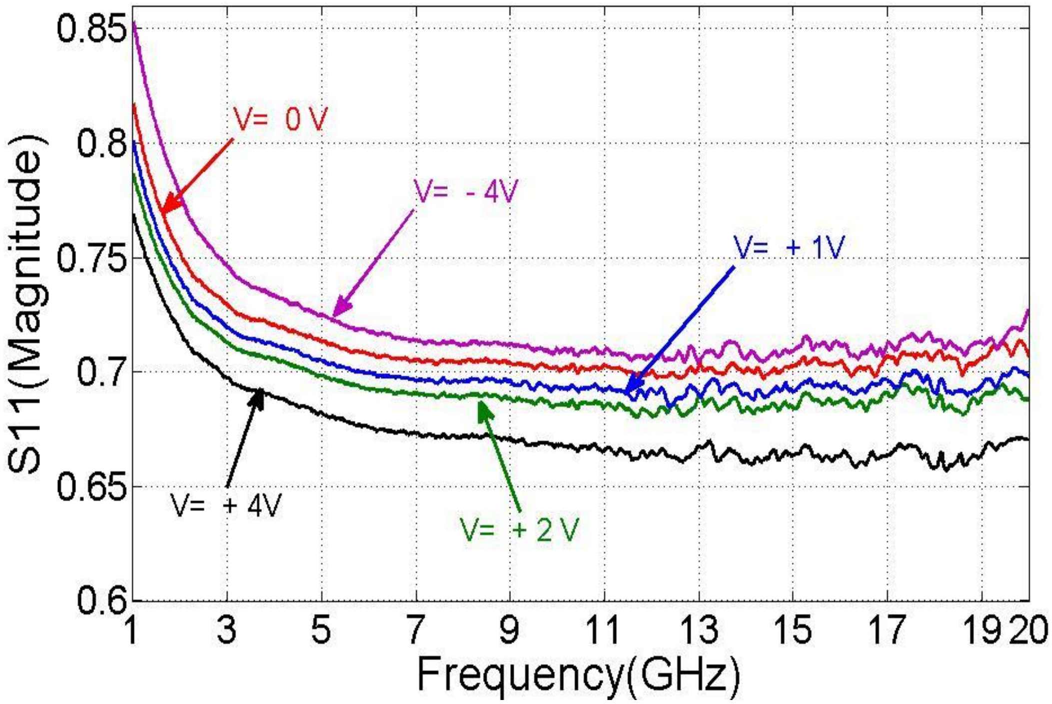

Figure C.12 Measured S-Parameters for SiC/Si RF diodes over frequency range of 1-20 GHz under different applied bias voltage)

10) Profilometer for 12 pulse device (in focus)

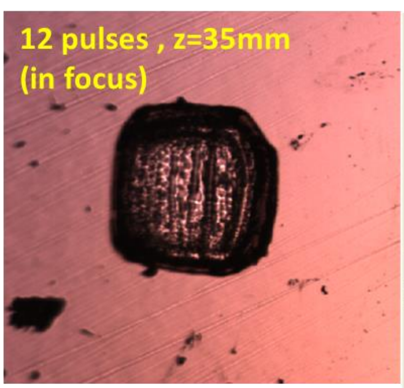

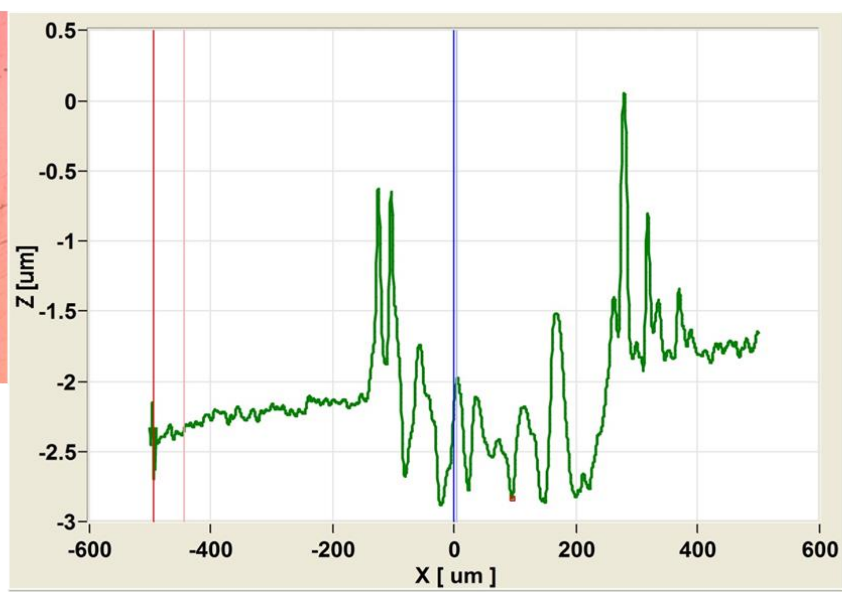

Figure C.13 Profilometer for 12 pulse device (in focus)

11) Optical images of SiC/Si diode: Unpolished wafer

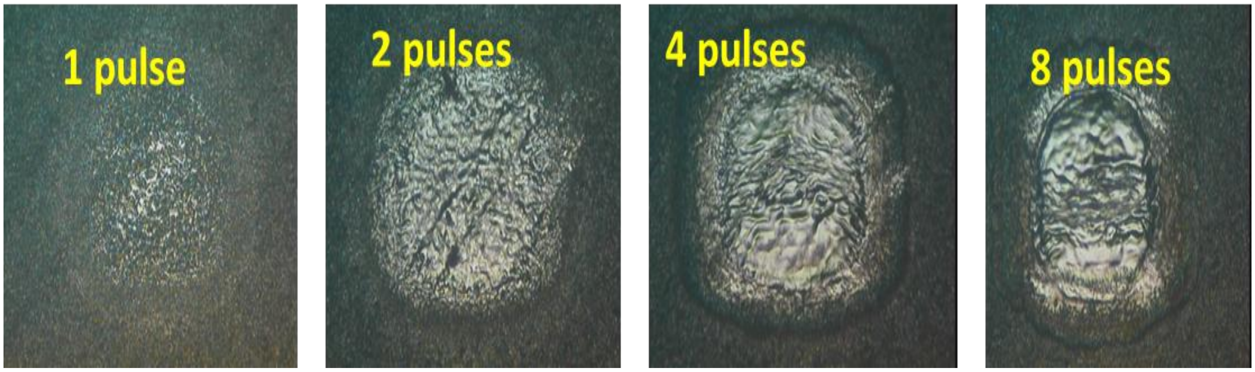

Figure C.14 Optical images of SiC/Si diode fabricated using laser process on unpolished wafer: Different number of pulses

12) SiC/Si Devices made using 100% Glycerin as carbon source

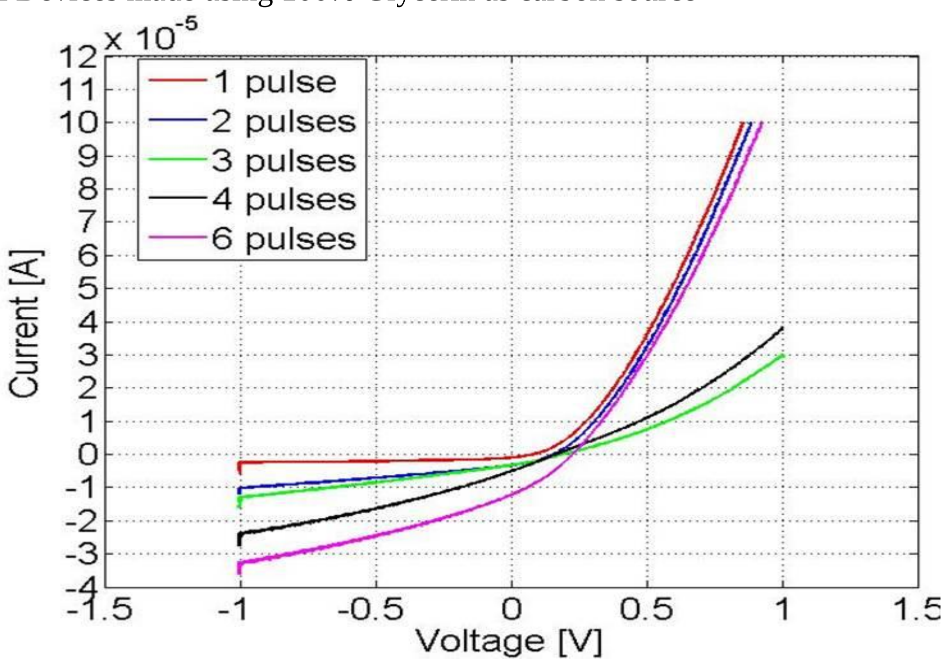

Figure C.15 SiC/Si Devices made using 100% Glycerin as carbon source: Measured I_V with Light on

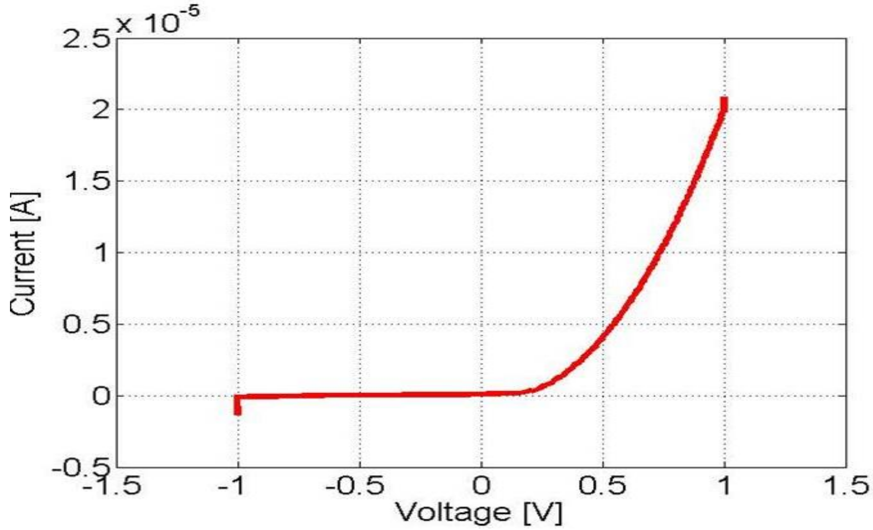

Figure C.16 SiC/Si Devices made using 100% Glycerin as carbon source: Measured I_V with Light off

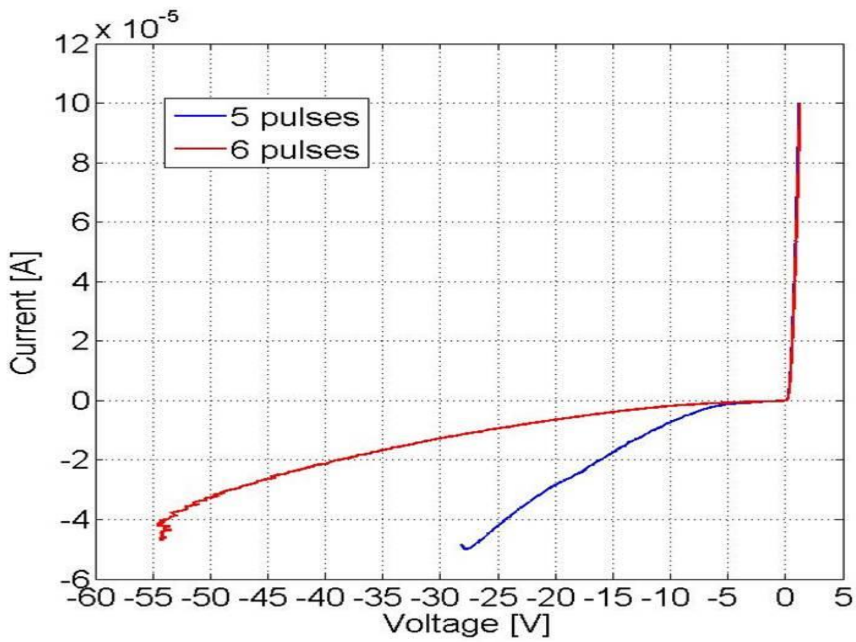

Figure C.17 SiC/Si Devices made using 100% Glycerin as carbon source: Measured I_V

BIBLIOGRAPHY

BIBLIOGRAPHY

[1] Cisco, "Cisco Visual Networking Index: Global Mobile Data Traffic Forecast Update, 2015–2020 White Paper", Cisco, 2016. [Online]. Available at http://www.cisco.com/c/en/us/solutions/collateral/service-provider/visual-networking-index-vni/mobile-white-paper-c11-520862.html. [Accessed: 02- May- 2016].

[2] R. Emrick, S. Franson, J. Holmes, B. Bosco, and S. Rockwell, "Technology for emerging commercial applications at millimeter-wave frequencies," in Wireless Communications and Applied Computational Electromagnetics, 2005. IEEE/ACES International Conference on, 2005, pp. 425-429.

[3] J. Powell and D. Bannister, "Business prospects for commercial mm-wave MMICs," Microwave Magazine, IEEE, vol. 6, pp. 34-43, 2005.

[4] J. Laskar, S. Pinel, D. Dawn, S. Sarkar, B. Perumana, and P. Sen, "The next wireless wave is a millimeter wave," Microwave Journal, vol. 50, p. 22, 2007.

[5] P. Smulders, "Exploiting the 60 GHz band for local wireless multimedia access: prospects and future directions," Communications Magazine, IEEE, vol. 40, pp. 140-147, 2002.

[6] J. Lee, Y.-A. Li, M.-H. Hung, and S.-J. Huang, "A fully-integrated 77-GHz FMCW radar transceiver in 65-nm CMOS technology," Solid-State Circuits, IEEE Journal of, vol. 45, pp. 2746-2756, 2010.

[7] M. C. Ziskin, "Physiological mechanisms underlying millimeter wave therapy," in BIOELECTROMAGNETICS Current Concepts, ed: Springer, 2006, pp. 241-251.

[8] V. N. Skresanov, I. V. Kas, E. A. Okhryamkina, V. P. Palamarchuk, and L. D. Tondy, "Complex treatment cardiovascular disease with a low power millimeter-wave radiation," in Physics and Engineering of Millimeter and Sub-Millimeter Waves, 2001. The Fourth International Kharkov Symposium on, 2001, pp. 939-940.

[9] L. Yujiri, "Passive millimeter wave imaging," in Microwave Symposium Digest, 2006. IEEE MTT-S International, 2006, pp. 98-101.

[10] D. Nötel, J. Huck, S. Neubert, S. Wirtz, and A. Tessmann, "A compact mmW imaging radiometer for concealed weapon detection," in Infrared and Millimeter Waves, 2007 and the 2007 15th International Conference on Terahertz Electronics. IRMMW-THz. Joint 32nd International Conference on, 2007, pp. 269-270.

[11] E. D. Cohen, "The MIMIC Program—A Retrospective," Microwave Magazine, IEEE, vol. 13, pp. 77-88, 2012.

[12] U. K. Mishra, L. Shen, T. E. Kazior, and Y.-F. Wu, “GaN-based RF power devices and amplifiers,” Proceedings of the IEEE, vol. 96, pp. 287-305, 2008.

[13] R. Lai, W. Deal, X. Mei, W. Yoshida, J. Lee, L. Dang, et al., "Fabrication of InP HEMT devices with extremely high Fmax," in Indium Phosphide and Related Materials, 2008. IPRM 2008. 20th International Conference on, 2008, pp. 1-3.

[14] J. Nah, H. Fang, C. Wang, K. Takei, M. H. Lee, E. Plis, et al., "III–V Complementary metal–oxide–semiconductor electronics on silicon substrates," Nano letters, vol. 12, pp. 3592-3595, 2012.GaN-Based RF Power Devices and Amplifiers

[15] D. S. Green, C. L. Dohrman, and T.-H. Chang, "The DARPA Diverse Accessible Heterogeneous Integration (DAHI) Program: Status and Future Directions," in 2014 Compound Semiconductor Manufacturing Technology conference (CS MANTECH), 2014.

[16] X. Du, I. Skachko, A. Barker, and E. Y. Andrei, “Approaching ballistic transport in suspended graphene,” Nat Nano, vol. 3, pp. 491-495, 08//print 2008.

[17] T. Dürkop, S. Getty, E. Cobas, and M. Fuhrer, “Extraordinary mobility in semiconducting carbon nanotubes,” Nano letters, vol. 4, pp. 35-39, 2004.

[18] R. H. Reuss, B. R. Chalamala, A. Moussessian, M. G. Kane, A. Kumar, D. C. Zhang, et al., "Macroelectronics: Perspectives on technology and applications," Proceedings of the IEEE, vol. 93, pp. 1239-1256, 2005.

[19] A. Kaur, X. Yang, K. Y. Park, and P. Chahal, “Reduced graphene oxide based Schottky diode on flex substrate for microwave circuit applications,” in Electronic Components and Technology Conference (ECTC), 2013 IEEE 63rd, 2013, pp. 1037-1042.

[20] M. Nagae, “Response time of metal-insulator-metal tunnel junctions,” Japanese Journal of Applied Physics, vol. 11, p. 1611, 1972.

[21] A.Kaur, Y. Xianbo and P. Chahal, "Study of Microwave circuits based on Metal-Insulator-Metal (MIM) diodes on flex substrates ," in Electronic Components and Technology Conference (ECTC), 2014 IEEE 64th, 2014, pp. 2158-2164.

[22] R. Trew, “Wide bandgap semiconductor transistors for microwave power amplifiers,” Microwave Magazine, IEEE, vol. 1, pp. 46-54, 2000.

[23] R. S. Pengelly, S. M. Wood, J. W. Milligan, S. T. Sheppard, and W. L. Pribble, “A review of GaN on SiC high electron-mobility power transistors and MMICs,” Microwave Theory and Techniques, IEEE Transactions on, vol. 60, pp. 1764-1783, 2012.

[24] I. F. Akyildiz, W. Su, Y. Sankarasubramaniam, and E. Cayirci, "Wireless sensor networks: a survey," Computer networks, vol. 38, pp. 393-422, 2002.

[25] H. Kudo, T.Sawada, E. Kazawa, H. Yoshida, Y. Iwasaki and K. Mitsubayashi, “A flexible and wearable glucose sensor based on functional polymers with Soft-MEMS techniques,” Biosensors and Bioelectronics, Vol. 22, Issue 4, , pp. 558-562, 15 October 2006.

[26] Y. Chen, J. Au, P. Kazlas, A. Ritenour, H. Gates and M. McCreary," Electronic paper: Flexible active-matrix electronic ink display", Nature 423, pp.136-137, 8 May 2003.

[27] S. R. Forrest, "The path to ubiquitous and low-cost organic electronic appliances on plastic," Nature, vol. 428, pp. 911-918, 2004.

[28] L. Sun, G. Qin, H. Huang, H. Zhou, N. Behdad, W. Zhou and Z. Ma, "Flexible high-frequency microwave inductors and capacitors integrated on a polyethylene terephthalate substrate", Appl. Phys. Lett. Issue 96, No. 013509, 2010.

[29] H.C. Yuan and Z. Ma, "Microwave thin-film transistors using Si nanomembranes on flexible polymer substrate", Appl. Phys. Lett., Issue 89, No.212105, 2006.

[30] F. Greuter and G. Blatter, "Electrical properties of grain boundaries in polycrystalline compound semiconductors," Semiconductor Science and Technology, vol. 5, p. 111, 1990.

[31] K. Myny, S. Steudel, P. Vicca, J. Genoe, and P. Heremans, "An integrated double half-wave organic Schottky diode rectifier on foil operating at 13.56 MHz," Applied physics letters, vol. 93, p. 093305, 2008.

[32] E. Cantatore, T. C. Geuns, G. H. Gelinck, E. Van Veenendaal, A. F. Gruijthuijsen, L. Schrijnemakers, et al., "A 13.56-MHz RFID system based on organic transponders," Solid-State Circuits, IEEE Journal of, vol. 42, pp. 84-92, 2007.

[33] E. Menard, R. G. Nuzzo, and J. A. Rogers, "Bendable single crystal silicon thin film transistors formed by printing on plastic substrates," Applied Physics Letters, vol. 86, p. 093507, 2005.

[34] H.-C. Yuan, Z. Ma, M. M. Roberts, D. E. Savage, and M. G. Lagally, "High-speed strained-single-crystal-silicon thin-film transistors on flexible polymers," Journal of applied physics, vol. 100, p. 013708, 2006.

[35] Y. Sun, E. Menard, J. A. Rogers, H.-S. Kim, S. Kim, G. Chen, et al., "Gigahertz operation in flexible transistors on plastic substrates," Applied physics letters, vol. 88, p. 183509, 2006.

[36] T. Takahashi, K. Takei, E. Adabi, Z. Fan, A. M. Niknejad, and A. Javey, "Parallel array InAs nanowire transistors for mechanically bendable, ultrahigh frequency electronics," ACS nano, vol. 4, pp. 5855-5860, 2010.

[37] D. Jariwala, V. K. Sangwan, L. J. Lauhon, T. J. Marks, and M. C. Hersam, "Carbon nanomaterials for electronics, optoelectronics, photovoltaics, and sensing," Chemical Society Reviews, vol. 42, pp. 2824-2860, 2013.

[38] Y.-M. Lin, K. A. Jenkins, A. Valdes-Garcia, J. P. Small, D. B. Farmer, and P. Avouris, "Operation of Graphene Transistors at Gigahertz Frequencies,"Nano Letters, vol. 9, pp. 422-426, 2009/01/14 2008.

[39] L. Yu-Ming, C. Hsin-Ying, K. A. Jenkins, D. B. Farmer, P. Avouris, and A. Valdes-Garcia, "Dual-Gate Graphene FETs With f_t of 50 GHz," Electron Device Letters, IEEE, vol. 31, pp. 68-70, 2010.

[40] Y.-M. Lin, C. Dimitrakopoulos, K. A. Jenkins, D. B. Farmer, H.-Y. Chiu, A. Grill, et al.,"100-GHz Transistors from Wafer-Scale Epitaxial Graphene," Science, vol. 327, p. 662, February 5, 2010.

[41] B. N. Szafranek, G. Fiori, D. Schall, D. Neumaier, and H. Kurz, "Current Saturation and Voltage Gain in Bilayer Graphene Field Effect Transistors," Nano Letters, vol. 12, pp. 1324-1328, 2012/03/14 2012.

[42] H. Wang, D. Nezich, J. Kong, and T. Palacios, "Graphene Frequency Multipliers, "Electron Device Letters, IEEE, vol. 30, pp. 547-549, 2009.

[43] T. Palacios, A. Hsu, and H. Wang, “Applications of graphene devices in RF communications,” Communications Magazine, IEEE, vol. 48, pp. 122-128, 2010.

[44] H. Wang, A. Hsu, B. Mailly, K. K. Kim, L. Kong, and T. Palacios, “Towards ubiquitous RF electronics based on graphene,” in Microwave Symposium Digest (MTT), 2012 IEEE MTT-S International, 2012, pp. 1-3.

[45] H. Wang, A. Hsu, J. Wu, J. Kong, and T. Palacios, “Graphene-based ambipolar RF mixers,” Electron Device Letters, IEEE, vol. 31, pp. 906-908, 2010.

[46] Y.-M. Lin, A. Valdes-Garcia, S.-J. Han, D. B. Farmer, I. Meric, Y. Sun, et al., “Wafer-scale graphene integrated circuit,” Science, vol. 332, pp. 1294-1297, 2011.

[47] G. Deligeorgis, F. Coccetti, G. Konstantinidis, and R. Plana, “Radio frequency signal detection by ballistic transport in Y-shaped graphene nanoribbons,” Applied Physics Letters, vol. 101, p. 013502, 2012.

[48] J. Lee, T.-J. Ha, K. N. Parrish, S. F. Chowdhury, L. Tao, A. Dodabalapur, et al., “High-performance current saturating graphene field-effect transistor with hexagonal boron nitride dielectric on flexible polymeric substrates,”Electron Device Letters, IEEE, vol. 34, pp. 172-174, 2013.

[49] X. Liang, Y. Liang, Z. Zhang, W. Li, X. Huo, and L.-M. Peng, “High mobility flexible graphene field-effect transistors and ambipolar radio-frequency circuits,” Nanoscale, 2015.

[50] M. Jung, J. Kim, J. Noh, N. Lim, C. Lim, G. Lee, et al., "All-printed and roll-to-roll-printable 13.56-MHz-operated 1-bit RF tag on plastic foils," Electron Devices, IEEE Transactions on, vol. 57, pp. 571-580, 2010.

[51] M. R. Islam, D. Joung, and S. I. Khondaker, “Schottky diode via dielectrophoretic assembly of reduced graphene oxide sheets between dissimilar metal contacts,” New Journal of Physics, vol. 13, p. 035021, 2011.

[52] Nourbakhsh, M. Cantoro, A. Hadipour, T. Vosch, M. H. van der Veen, M. M. Heyns, et al., “Modified semiconducting graphene in contact with a metal: Characterization of the Schottky diode,”Applied Physics Letters, vol. 97, pp. -, 2010.

[53] R. Stratton, “Volt-current characteristics for tunneling through insulating films,” Journal of Physics and Chemistry of Solids, vol. 23, pp. 1177-1190, 1962.

[54] A.Hoofring, V. Kapoor, and W. Krawczonek, "Submicron nickel-oxide-gold tunnel diode detectors for rectennas," Journal of applied Physics, vol. 66, pp. 430-437, 1989.

[55] M. J. Estes, "Metal-insulator varactor devices," ed: Google Patents, 2008.

[56] M. J. Estes and B. J. Eliasson, “Thin-film transistors based on tunneling structures and applications,” ed: Google Patents, 2007.

[57] S. Grover, O. Dmitriyeva, M. J. Estes, and G. Moddel, “Traveling-wave metal/insulator/metal diodes for improved infrared bandwidth and efficiency of antenna-coupled rectifiers,” Nanotechnology, IEEE Transactions on, vol. 9, pp. 716-722, 2010.

[58] I. Wilke, Y. Oppliger, W. Herrmann, and F. Kneubühl, "Nanometer thin-film Ni-NiO-Ni diodes for 30 THz radiation," Applied Physics A, vol. 58, pp. 329-341, 1994.

[59] S. Krishnan, H. La Rosa, E. Stefanakos, S. Bhansali, and K. Buckle, "Design and development of batch fabricatable metal–insulator–metal diode and microstrip slot antenna as rectenna elements," Sensors and Actuators A: Physical, vol. 142, pp. 40-47, 3/10/ 2008.

[60] J. Bean, A. Weeks, and G. D. Boreman, "Performance optimization of antenna-coupled tunnel diode infrared detectors," Quantum Electronics, IEEE Journal of, vol. 47, pp. 126-135, 2011.

[61] S. Krishnan, E. Stefanakos, and S. Bhansali, "Effects of dielectric thickness and contact area on current–voltage characteristics of thin film metal–insulator–metal diodes," Thin Solid Films, vol. 516, pp. 2244-2250, 2008.

[62] S. Grover and G. Moddel, “Applicability of metal/insulator/metal (MIM) diodes to solar rectennas,” Photovoltaics, IEEE Journal of, vol. 1, pp. 78-83, 2011.

[63] R. Waser and M. Aono, “Nanoionics-based resistive switching memories,” Nature materials, vol. 6, pp. 833-840, 2007.

[64] A. Osseiran, F. Boccardi, V. Braun, K. Kusume, P. Marsch, M. Maternia, et al., “Scenarios for 5G mobile and wireless communications: the vision of the METIS project,” Communications Magazine, IEEE, vol. 52, pp. 26-35, 2014.

[65] F. H. Raab, P. Asbeck, S. Cripps, P. B. Kenington, Z. B. Popović, N. Pothecary, et al., “Power amplifiers and transmitters for RF and microwave,” Microwave Theory and Techniques, IEEE Transactions on, vol. 50, pp. 814-826, 2002.

[66] G. Chattopadhyay, "Technology, capabilities, and performance of low power terahertz sources," Terahertz Science and Technology, IEEE Transactions on, vol. 1, pp. 33-53, 2011.

[67] A. Jones, J. Jewell, J. Mabon, E. Reuter, S. Bishop, S. Roh, et al., "Long-wavelength InGaAs quantum wells grown without strain-induced warping on InGaAs compliant membranes above a GaAs substrate," Applied physics letters, vol. 74, 1999.

[68] C. Pei, J. Héroux, J. Sweet, W. Wang, J. Chen, and M. Chang, "High quality GaAs grown on Si-on-insulator compliant substrates," Journal of Vacuum Science & Technology B, vol. 20, pp. 1196-1199, 2002.

[69] A. Gutierrez-Aitken, P. Chang-Chien, D. Scott, K. Hennig, E. Kaneshiro, P. Nam, et al., "Advanced heterogeneous integration of InP HBT and CMOS Si technologies," in Compound Semiconductor Integrated Circuit Symposium (CSICS), 2010 IEEE, 2010, pp. 1-4.

[70] H. J. Oh, K. J. Choi, W. Y. Loh, T. Htoo, S. J. Chua, and B. J. Cho, "Integration of GaAs epitaxial layer to Si-based substrate using Ge condensation and low-temperature migration enhanced epitaxy techniques," Journal of Applied Physics, vol. 102, p. 054306, 2007.

[71] S. Lee, L. Dawson, S. Brueck, and A. Stintz, "Heteroepitaxial selective growth of $In_xGa_{1-x}As$ on SiO2-patterned GaAs (001) by molecular beam epitaxy," Journal of applied physics, vol. 96, pp. 4856-4865, 2004.

[72] T. Kazior, J. LaRoche, D. Lubyshev, J. Fastenau, W. Liu, M. Urteaga, et al., "A high performance differential amplifier through the direct monolithic integration of InP HBTs and Si CMOS on silicon substrates," in Microwave Symposium Digest, 2009. MTT'09. IEEE MTT-S International, 2009, pp. 1113-1116.

[73] J. W. Chung, E. L. Piner, and T. Palacios, "N-face GaN/AlGaN HEMTs fabricated through layer transfer technology," Electron Device Letters, IEEE, vol. 30, pp. 113-116, 2009.

[74] D. Pasquariello and K. Hjort, "Plasma-assisted InP-to-Si low temperature wafer bonding," Selected Topics in Quantum Electronics, IEEE Journal of, vol. 8, pp. 118-131, 2002

[75] M. Lapisa, G. Stemme, and F. Niklaus, "Wafer-level heterogeneous integration for MOEMS, MEMS, and NEMS," Selected Topics in Quantum Electronics, IEEE Journal of, vol. 17, pp. 629-644, 2011.

[76] J. Pernot, W. Zawadzki, S. Contreras, J. Robert, E. Neyret, and L. Di Cioccio, “Electrical transport in n-type 4H silicon carbide,” Journal of Applied Physics, vol. 90, pp. 1869-1878, 2001.

[77] A. Schöner, M. Krieger, G. Pensl, M. Abe, and H. Nagasawa, “Fabrication and Characterization of 3C-SiC-Based MOSFETs,” Chemical Vapor Deposition, vol. 12, pp. 523-530, 2006.

[78] P. H. Yih, J. P. Li, and A. J. Steckl, "SiC/Si heterojunction diodes fabricated by self-selective and by blanket rapid thermal chemical vapor deposition," Electron Devices, IEEE Transactions on, vol. 41, pp. 281-287, 1994.

[79] V. Zakhvalinskii, E. Piliuk, I. Goncharov, A. Simashkevich, D. Sherban, L. Bruc, N. Curmei and M. Rusu, "Silicon carbide nanolayers as a solar cell constituent," physica status solidi (a), vol. 212, pp. 184-188, 2015.

[80] D. Gao, M. B. J. Wijesundara, C. Carraro, R. T. Howe, and R. Maboudian, “Characterization of residual strain in SiC films deposited using 1,3-disilabutane for MEMS application,” J. Micro/ Nanolithograph., MEMS, MOEMS, vol. 2, no. 4, pp. 259–264, 2003.

[81] M. Capano, B. Kim, A. Smith, E. Kvam, S. Tsoi, and A. Ramdas, "Residual strains in cubic silicon carbide measured by Raman spectroscopy correlated with x-ray diffraction and transmission electron microscopy," Journal of applied physics, vol. 100, p. 083514, 2006.

[82] H. Nagasawa and K. Yagi, "3C-SiC Single-Crystal Films Grown on 6-Inch Si Substrates," physica status solidi (b), vol. 202, pp. 335-358, 1997.

[83] T. Hatayama, Y. Tarui, T. Fuyuki, and H. Matsunami, "Low-temperature heteroepitaxial growth of cubic SiC on Si using hydrocarbon radicals by gas source molecular beam epitaxy," Journal of crystal growth, vol. 150, pp. 934-938, 1995.

[84] Q. Cheng, S. Xu, J. Long, and K. Ostrikov, "Low-Temperature PECVD of Nanodevice-Grade nc-3C-SiC," Chemical Vapor Deposition, vol. 13, pp. 561-566, 2007.

[85] L. Moro, A. Paul, D. Lorents, R. Malhotra, R. Ruoff, P. Lazzeri, et al., "Silicon carbide formation by annealing C60 films on silicon," Journal of applied physics, vol. 81, pp. 6141-6146, 1997.

[86] B. Wu, C. Chung, and C. Peng, "Rapid thermal annealing enhanced crystalline SiC particles at lower formation temperature," in Nano/Micro Engineered and Molecular Systems, 2008. NEMS 2008. 3rd IEEE International Conference on, 2008, pp. 1181-1184.

[87] S. Krishnan, G. D'Couto, M. Chaudhry, and S. Babu, "Excimer laser-induced doping of crystalline silicon carbide films," Journal of materials research, vol. 10, pp. 2723-2727, 1995.

[88] P. Smith, P. Carey, and T. Sigmon, "Excimer laser crystallization and doping of silicon films on plastic substrates," Applied physics letters, vol. 70, pp. 342-344, 1997.

[89] D. Wei, J. I. Mitchell, C. Tansarawiput, W. Nam, M. Qi, P. D. Ye and X. Xu,"Laser direct synthesis of graphene on quartz," Carbon, vol. 53, pp. 374-379, 3// 2013.

[90] H. Castro Neto, F. Guinea, N. M. R. Peres, K. S. Novoselov, and A. K. Geim, "The electronic properties of graphene," Reviews of Modern Physics, vol. 81, pp. 109-162, 01/14/ 2009.

[91] R. Saito, M.S. Dresselhaus, G. Dresselhaus Physical Properties of Carbon Nanotubes (Imperial College Press, London, 1998

[92] P. R. Wallace, "The Band Theory of Graphite," Physical Review, vol. 71, pp. 622-634, 05/01/ 1947.

[93] S. Das Sarma, S. Adam, E. H. Hwang, and E. Rossi, "Electronic transport in two-dimensional graphene," Reviews of Modern Physics, vol. 83, pp. 407-470, 05/16/ 2011.

[94] P. Blake, E. W. Hill, A. H. Castro Neto, K. S. Novoselov, D. Jiang, R. Yang, et al., "Making graphene visible," Applied Physics Letters, vol. 91, pp. -, 2007.

[95] T. Stauber, N. M. R. Peres, and A. K. Geim, "Optical conductivity of graphene in the Visible region of the spectrum," Physical Review B, vol. 78, p. 085432, 08/26/ 2008.

[96] E. Moreau, S. Godey, F. J. Ferrer, D. Vignaud, X. Wallart, J. Avila, et al., "Graphene growth by molecular beam epitaxy on the carbon-face of SiC," Applied Physics Letters, vol. 97, pp. 241907-241907-3, 2010.

[97] Y. Lee, S. Bae, H. Jang, S. Jang, S.-E. Zhu, S. H. Sim, et al., "Wafer-Scale Synthesis and Transfer of Graphene Films," Nano Letters, vol. 10, pp. 490-493, 2010/02/10 2010.

[98] Bae, S., Kim, H., Lee, Y., Xu, X., Park, J. S., Zheng, Y., ... & Iijima, S. (2010). Roll-to-Roll production of 30-inch graphene films for transparent electrodes. Nature nanotechnology, 5(8), 574-578.

[99] J. W. Suk, A. Kitt, C. W. Magnuson, Y. Hao, S. Ahmed, J. An, et al., "Transfer of CVD-Grown Monolayer Graphene onto Arbitrary Substrates," ACS Nano, vol. 5, pp. 6916-6924, 2011/09/27 2011.

[100] M. Alfè, V. Gargiulo, R. Di Capua, F. Chiarella, J.-N. Rouzaud, A. Vergara, et al., "Wet Chemical Method for Making Graphene-like Films from Carbon Black,"ACS Applied Materials & Interfaces, vol. 4, pp. 4491-4498, 2012/09/26 2012.

[101] X. Li, H. Wang, J. T. Robinson, H. Sanchez, G. Diankov, and H. Dai, "Simultaneous Nitrogen Doping and Reduction of Graphene Oxide," Journal of the American Chemical Society, vol. 131, pp. 15939-15944, 2009/11/04 2009.

[102] M. Y. Han, B. Özyilmaz, Y. Zhang, and P. Kim, "Energy Band-Gap Engineering of Graphene Nanoribbons," Physical Review Letters, vol. 98, p. 206805, 05/16/ 2007.

[103] Y. Yinxiao and R. Murali, "Impact of Size Effect on Graphene Nanoribbon Transport, "Electron Device Letters, IEEE, vol. 31, pp. 237-239, 2010.

[104] J. Bai, X. Duan, and Y. Huang, "Rational Fabrication of Graphene Nanoribbons Using a Nanowire Etch Mask," Nano Letters, vol. 9, pp. 2083-2087, 2009/05/13 2009.

[105] A. Lerf, H. He, M. Forster, and J. Klinowski, "Structure of Graphite Oxide Revisited, The Journal of Physical Chemistry B, vol. 102, pp. 4477-4482, 1998/06/01 1998.

[106] W. S. Hummers and R. E. Offeman, "Preparation of Graphitic Oxide," Journal of the American Chemical Society, vol. 80, pp. 1339-1339, 1958/03/01 1958.

[107] G. Eda, C. Mattevi, H. Yamaguchi, H. Kim, and M. Chhowalla, "Insulator to Semimetal Transition in Graphene Oxide," The Journal of Physical Chemistry C, vol. 113, pp. 15768-15771, 2009/09/03 2009.

[108] G. Eda, G. Fanchini, and M. Chhowalla, "Large-area ultrathin films of reduced graphene Oxide as a transparent and flexible electronic material," Nat Nano, vol. 3, pp. 270-274, 05//print 2008.

[109] J. Wu, H. A. Becerril, Z. Bao, Z. Liu, Y. Chen, and P. Peumans, "Organic solar cells with solution-processed graphene transparent electrodes," Applied Physics Letters, vol. 92, pp. 263302-3, 06/30/ 2008.

[110] D. Joung, A. Chunder, L. Zhai, and S. I. Khondaker, "High yield fabrication of chemically reduced graphene oxide field effect transistors by dielectrophoresis," Nanotechnology, vol. 21, p. 165202, 2010.

[111] J. T. Robinson, F. K. Perkins, E. S. Snow, Z. Wei, and P. E. Sheehan, "Reduced Graphene Oxide Molecular Sensors," Nano Letters, vol. 8, pp. 3137-3140, 2008/10/08 2008.

[112] D. R. Dreyer, S. Park, C. W. Bielawski, and R. S. Ruoff, "The chemistry of graphene oxide," Chemical Society Reviews, vol. 39, pp. 228-240, 2010.

[113] J. A. Hejase, P. R. Paladhi, and P. Chahal, "Terahertz Characterization of Dielectric Substrates for Component Design and Nondestructive Evaluation of Packages, "Components, Packaging and Manufacturing Technology, IEEE Transactions on, vol. 1, pp. 1685-1694, 2011.

[114] D. Xu, A. Subramanian, L. Dong, and B. J. Nelson, “Shaping nanoelectrodes for high-precision dielectrophoretic assembly of carbon nanotubes,” Nanotechnology, IEEE Transactions on, vol. 8, pp. 449-456, 2009.

[115] S. Stankovich, D. A. Dikin, R. D. Piner, K. A. Kohlhaas, A. Kleinhammes, Y. Jia, et al., “Synthesis of graphene-based nanosheets via chemical reduction of exfoliated graphite oxide,” Carbon, vol. 45, pp. 1558-1565, 2007.

[116] K. N. Kudin, B. Ozbas, H. C. Schniepp, R. K. Prud'Homme, I. A. Aksay, and R. Car, “Raman spectra of graphite oxide and functionalized graphene sheets,” Nano letters, vol. 8, pp. 36-41, 2008.

[117] W. Liu, J. Wei, X. Sun, and H. Yu, “A study on graphene-metal contact,” Crystals, vol. 3, pp. 257-274, 2013.

[118] C. Malec, B. Elkus, and D. Davidović, “Vacuum-annealed Cu contacts for graphene electronics,” Solid State Communications, vol. 151, pp. 1791-1793, 2011.

[119] S. A. Mikhailov, “Non-linear electromagnetic response of graphene,” EPL (Europhysics Letters), vol. 79, p.27002, 2007.

[120] J. Simmons, "Conduction in thin dielectric films," Journal of Physics D: Applied Physics, vol. 4, p. 613, 1971.

[121] J. G. Simmons, "Electric tunnel effect between dissimilar electrodes separated by a thin insulating film," Journal of Applied Physics, vol. 34, pp. 2581-2590, 1963.

[122] J. G. Simmons, "Generalized formula for the electric tunnel effect between similar electrodes separated by a thin insulating film," Journal of Applied Physics, vol. 34, pp. 1793-1803, 1963.

[123] Sanchez, C. Davis Jr, K. Liu, and A. Javan, "The MOM tunneling diode: theoretical estimate of its performance at microwave and infrared frequencies," Journal of Applied Physics, vol. 49, pp. 5270-5277, 1978.

[124] T. E. Hartman, "Tunneling through asymmetric barriers," Journal of Applied Physics, vol. 35, pp. 3283-3294, 1964.

[125] G. D. Wilk, R. M. Wallace, and J. Anthony, "High-κ gate dielectrics: Current status and materials properties considerations," Journal of applied physics, vol. 89, pp. 5243-5275, 2001.

[126] M. D. Stamate, "Dielectric properties of TiO_2 thin films deposited by a DC magnetron sputtering system," Thin Solid Films, vol. 372, pp. 246-249, 2000.

[127] Y. Rawal, S. Ganguly, and M. S. Baghini, “Fabrication and Characterization of New Ti-TiO_2-Al and Ti-TiO_2-Pt Tunnel Diodes,” Active and Passive Electronic Components Vol.2012, Article ID 694105, 2012.

[128] L. Hoey, J. B. Carlson, R. M. Osgood, B. Kimball, and W. Buchwald, "rf plasma oxidation of Ni thin films sputter deposited to generate thin nickel oxide layers," Applied Physics Letters, vol. 97, pp. 153104-153104-3, 2010.

[129] A. Konno, Y. Narita, T. Itoh, K. Yasui, H. Nakzawa, T. Endoh, et al., "Low-temperature Heteroepitaxial Growth of 3C-SiC (111) on Si (110) Substrate Using Monomethylsilane," ECS Transactions, vol. 3, pp. 449-455, 2006.

[130] M. Reyes, Y. Shishkin, S. Harvey, and S. E. Saddow, "Development of a high-growth rate 3C-SiC on Si CVD process," in MRS Proceedings, 2006, pp. 0911-B08-01.

[131] C. Cheng, T. Pi, C. Ouyang, and J. Wen, "SiC formation by C60 molecules as a precursor: A synchrotron-radiation photoemission study of the carbonization process," Journal of Vacuum Scienece and Technology A Vacuums Surfaces and Films, vol. 24, p. 70, 2006.

[132] N. Tomozeiu and M. De Seta, "Some properties of SiC layers obtained from C 60 precursors," in Semiconductor Conference, 2000. CAS 2000 Proceedings. International, 2000, pp. 197-200.

[133] M. De Seta, D. Sanvitto, and F. Evangelisti, "Direct evidence of C 60 chemical bonding on Si (100)," Physical Review B, vol. 59, p. 9878, 1999.

[134] C. Cepek, P. Schiavuta, M. Sancrotti, and M. Pedio, "Photoemission study of C 60/Si (111) adsorption as a function of coverage and annealing temperature," Physical Review B, vol. 60, p. 2068, 1999.

[135] C. W. Hu, A. Kasuya, S. Suto, A. Wawro, and Y. Nishina, "Surface structure of 3C-SiC (111) grown on Si (111) surface by C60 precursor," Applied physics letters, vol. 68, pp. 1253-1255, 1996.

[136] C.-K. Chung and B.-H. Wu, "Thermally induced formation of SiC nanoparticles from Si/C/Si multilayers deposited by ultra-high-vacuum ion beam sputtering," Nanotechnology, vol. 17, p. 3129, 2006.

[137] R. Delmdahl and B. Fechner, "Large-area microprocessing with excimer lasers, " Applied Physics A, vol. 101, pp. 283-286, 2010.

[138] S. Zhang, Y. Ren, and G. Lüpke, "Ultrashort laser pulse beam shaping," Applied optics, vol. 42, pp. 715-718, 2003.

[139] M. S. Brown and C. B. Arnold, "Fundamentals of laser-material interaction and application to multiscale surface modification," in Laser Precision Microfabrication, ed: Springer, 2010, pp. 91-120.

[140] J. Ion, Laser processing of engineering materials: principles, procedure and industrial application: Butterworth-Heinemann, 2005.

[141] A.Simchi, "Direct laser sintering of metal powders: Mechanism, kinetics and microstructural features," Materials Science and Engineering: A, vol. 428, pp. 148-158, 2006.

[142] W. Staudt, S. Borneis, and K. D. Pippert, "TFT Annealing with Excimer Laser. Technology and Market Outlook," physica status solidi (a), vol. 166, pp. 743-749, 1998.

[143] G. Račiukaitis, M. Brikas, V. Kazlauskienė, and J. Miškinis, "Doping of silicon with carbon during laser ablation process," Applied Physics A, vol. 85, pp. 445-450, 2006.

[144] J. K. Seo, Y.-H. Joung, Y. Park, and W. S. Choi, "Substrate temperature effect on the SiC passivation layer synthesized by an RF magnetron sputtering method," Thin Solid Films, vol. 519, pp. 6654-6657, 8/1/ 2011

[145] Z. C. Feng, A. J. Mascarenhas, W. J. Choyke, and J. A. Powell, "Raman scattering studies of chemical-vapor-deposited cubic SiC films of (100) Si," Journal of Applied Physics, vol. 64, pp. 3176-3186, 1988.

[146] J. Wasyluk, T. S. Perova, S. A. Kukushkin, A. V. Osipov, N. A. Feoktistov, and S. A. Grudinkin, "Raman investigation of different polytypes in SiC thin films grown by solid-gas phase epitaxy on Si (111) and 6H-SiC substrates," in Materials Science Forum, 2010, pp. 359-362.

[147] J. Zhu, S. Liu, and J. Liang, "Raman study on residual strains in thin 3C-SiC epitaxial layers grown on Si (001)," Thin Solid Films, vol. 368, pp. 307-311, 2000.

[148] V. George, A. Das, M. Roy, A. Dua, P. Raj, and D. Zahn, "Bias enhanced deposition of highly oriented β-SiC thin films using low pressure hot filament chemical vapour deposition technique," Thin Solid Films, vol. 419, pp. 114-117, 2002.

[149] Avila, I. Montero, L. Galan, J. M. Ripalda, and R. Levy, "Behavior of oxygen doped SiC thin films: An x-ray photoelectron spectroscopy study," Journal of Applied Physics, vol. 89, pp. 212-216, 2001.

[150] S. Kerdiles, A. Berthelot, R. Rizk, and L. Pichon, "Fabrication and properties of low-temperature (⩽ 600° C) processed n-type nanocrystalline SiC/p-type crystalline Si heterojunction diodes," Applied physics letters, vol. 80, pp. 3772-3774, 2002. http://dx.doi.org/10.1063/1.1480474

[151] J. Hwang, Y. Fang, K. Wu, and S. Chou, "Improving breakdown voltage of SiC/Si heterojunction with graded structure by rapid thermal CVD technology," Electron Devices, IEEE Transactions on, vol. 44, pp. 2029-2031, 1997. http://dx.doi.org/10.1109/16.641376

[152] Q. Wahab, M. Karlsteen, O. Nur, L. Hultman, M. Willander, and J.-E. Sundgren, "Heterojunction diodes in 3C-SiC/Si system grown by reactive magnetron sputtering: Effects of growth temperature on diode rectification and breakdown," Journal of electronic materials, vol. 25, pp. 1495-1500, 1996.

[153] J. Freitas Jr, S. Bishop, P. Nordquist Jr, and M. Gipe, "Donor binding energies determined from temperature dependence of photoluminescence spectra in undoped and aluminum-doped beta SiC films," Applied physics letters, vol. 52, pp. 1695-1697, 1988.

[154] C. Liu and J. Sturm, "Low temperature chemical vapor deposition growth of β-SiC on (100) Si using methylsilane and device characteristics," Journal of applied physics, vol. 82, pp. 4558-4565, 1997.

[155] M. A. Fraga, M. Massi, I. C. Oliveira, H. S. Maciel, S. G. dos Santos Filho, and R. D. Mansano, "Nitrogen doping of SiC thin films deposited by RF magnetron sputtering," Journal of Materials Science: Materials in Electronics, vol. 19, pp. 835-840, 2008.

[156] T. Azizi, A. Torchani, M. Ben Karoui, R. Gharbi, M. Fathallah, and E. Tresso, "Effect of defects on the efficiency of a-SiC: H p-i-n based solar cells," in Electrical Engineering and Software Applications (ICEESA), 2013 International Conference on, 2013, pp. 1-5.

[157] R. Han, Y. Zhang, D. Coquillat, H. Videlier, W. Knap, and E. Brown, "A 280-GHz Schottky diode detector in 130-nm digital CMOS," Solid-State Circuits, IEEE Journal of, vol. 46, pp. 2602-2612, 2011

[158] J. A. Hagerty, F. B. Helmbrecht, W. H. McCalpin, R. Zane, and Z. B. Popović, "Recycling ambient microwave energy with broad-band rectenna arrays," Microwave Theory and Techniques, IEEE Transactions on, vol. 52, pp. 1014-1024, 2004.

[159] A. Costanzo, M. Fabiani, A. Romani, D. Masotti, and V. Rizzoli, "Co-design of ultra-low power RF/Microwave receivers and converters for RFID and energy harvesting applications," in Microwave Symposium Digest (MTT), 2010 IEEE MTT-S International, 2010, pp. 856-859.

[160] J. O. McSpadden, L. Fan, and K. Chang, "Design and experiments of a high-conversion-efficiency 5.8-GHz rectenna," Microwave Theory and Techniques, IEEE Transactions on, vol. 46, pp. 2053-2060, 1998.

[161] Y. Kobayashi, M. Hori, H. Noji, G. Fukuda, and S. Kawasaki, "The S-band GaN-based high power amplifier and rectenna for space energy transfer applications," in Microwave Workshop Series on Innovative Wireless Power Transmission: Technologies, Systems, and Applications (IMWS), 2012 IEEE MTT-S International, 2012, pp. 271-274.

[162] M. Coffey, S. Schafer, and Z. Popovic, "Two-stage high-efficiency X-Band GaN MMIC PA/rectifier," in Microwave Symposium (IMS), 2015 IEEE MTT-S International, 2015, pp. 1-4.

[163] T. Baras and A. F. Jacob, "K-band frequency synthesizer with subharmonic signal generation and LTCC frequency tripler," in Microwave Integrated Circuit Conference, 2008. EuMIC 2008. European, 2008, pp. 466-469.

[164] S. E. Gunnarsson, C. Kärnfelt, H. Zirath, R. Kozhuharov, D. Kuylenstierna, A. Alping, et al., "Highly integrated 60 GHz transmitter and receiver MMICs in a GaAs pHEMT technology," Solid-State Circuits, IEEE Journal of, vol. 40, pp. 2174-2186, 2005.

[165] J. Udomoto, T. Matsuzuka, S. Chaki, K. Kanaya, T. Katoh, Y. Notani, et al., "A 38/77 GHz MMIC transmitter chip set for automotive applications," in Microwave Symposium Digest, 2003 IEEE MTT-S International, 2003, pp. 2229-2232.

[166] Y. Campos-Roca, C. Schwörer, A. Leuther, M. Seelmann-Eggebert, and H. Massler, "A D-band frequency doubler MMIC based on a 100-nm metamorphic HEMT technology," Microwave and Wireless Components Letters, IEEE, vol. 15, pp. 466-468, 2005.

[167] K. Yuk, G. Branner, and C. Wong, "High power, high conversion gain frequency doublers using SiC MESFETs and AlGaN/GaN HEMTs," in Microwave Symposium Digest (MTT), 2010 IEEE MTT-S International, 2010, pp. 1008-1011.

[168] K. Yuk and G. Branner, "Advances in active microwave frequency multipliers," in Circuits and Systems (MWSCAS), 2011 IEEE 54th International Midwest Symposium on, 2011, pp. 1-4.